İSTANBUL TECHNICAL UNIVERSITY ★ INSTITUTE OF SCIENCE AND TECHNOLOGY

SPEED SENSORLESS DIRECT VECTOR CONTROL OF SQUIRREL CAGE INDUCTION MACHINES

Msc. Thesis by
Eşref Emre ÖZSOY , Eng.
(504051127)

Date of submission : 22 July 2008

Date of defence examination: 1 August 2008

Supervisor (Chairman): Prof. Dr. Metin GÖKAŞAN

Members of the Examining Committee Prof.Dr. Hakan TEMELTAŞ(İTÜ)

Assoc.Prof.Dr. Osman Kaan EROL (İTÜ)

AUGUST 2008

ACKNOWLEDGEMENTS

I would like to thank to my supervisor Prof. Dr. Metin GÖKAŞAN for his great support and guidance in my thesis.

I wish to thank to my chief engineers at ERDEMİR Vedat BEKTAŞ and Mr. Metin BAŞTAŞ and all my managers for their valuable encouragement.

I am grateful to ERDEMIR Electronic Workshop Staff Mehmet İBRAHİMBAŞ, Necat YILMAZ, Halkan ÖZCAN, Musa AYNACI and all other technicians for their technical assistance and support for PCB circuit design and manufacture.

I would also thank to ABB/ISTANBUL Service Engineers Levent BÜTÜN, Sabri DEMİRYÜREK and Hüseyin DEMİR who sponsored the ACS 300 inverter.

I would also thank to my wife and whole my family for their patience.

May 2008 E.Emre ÖZSOY

CONTENTS

ABBREVIATIONS

SCIM	: Squirrel Cage Induction Machine
EKF	: Extended Kalman Filter
DSP	: Digital Signal Processor
FPGA	: Field Programmable Gate Array
PWM	: Pulse Width Modulation
SVPWMM	: Space Vector Pulse Width Modulation
VSI	: Voltage Source Inverter
CSI	: Current Source Inverter
DC	: Direct Current
IGBT	: Insulated Gate Bipolar Transistor
IGCT	: Insulated Gate Commutated Thyristor
GTO	: Gate Turn off Thyristor
VGE	: Gate-Emitter Voltage
VCE	: Collector-Emitter Voltage
RG	**:** Gate Resistance

TABLE LIST

FIGURE LIST

SYMBOL LIST

R_E : Electrical Equivalent Resistance
R_s : Stator Resistance
R_r : Rotor Resistance
L_m : Mutual Inductance
L_r : Rotor Inductance
б : Leakage Factor
T_e : Electrical Torque
w : Motor angular velocity in rad/s
B : Viscous Friction constant
J : Inertia Constant
T_L : Mechanical Torque
$i_{s\alpha}$: α Component of stator current
$i_{s\beta}$: β Component of stator current
$\psi_{r\alpha}$: α Component of rotor flux
$\psi_{r\beta}$: β Component of rotor flux
i_{sd} : d Component of stator current
i_{sq} : q Component of stator current
ψ_{rd} : d Component of rotor flux
ψ_{rq} : q Component of rotor flux
A : System Matrix (Mathematical Model of System)
B : Input Matrix
H : Measurement Matrix
x : State Vector
z : Measurement Vector
u : Control Input Vector
P : Error Covariance Matrix
K_k : Kalman Gain
f: Fundamental Frequency
T_z: Switching Time
m: Modulation index

SPEED SENSORLESS DIRECT VECTOR CONTROL OF SQUIREL CAGE INDUCTION MACHINES

SUMMARY

Squirrel cage induction machines (SCIM) are the workhorses of the industry due to its ruggedness, low cost and free maintenance properties. In spite of its well-known usage, there are some constraints in their control. So, in 1969 and 1972 flux oriented vector control techniques are innovated in order to let SCIM control as a DC machine control. In the following years, SCIM high performance control has another prospect with the innovation of Direct Torque Control.

Speed and flux data are needed in order to achieve these new challenging techniques. But, getting flux and speed feedbacks increase the cost or in same cases it is impossible to get the speed feedback because of physical difficulties. Flux feedback usage is not preferred due to requirement of the changes in the construction of the machine. When sensorless high performance SCIM control is considered, there are many constraints in the fifth order, recurrent, nonlinear and parameter varying SCIM dynamic model. Sensorless high performance control can be mentioned in a wide speed range, if model uncertainties are estimated in a high resolution.

When parameter uncertainties of an electrical machine are considered, there are two basic uncertainties: mechanical and electrical. When SCIM is considered, it is known the negative effects in variations in the rotor and stator resistances as well as motor fluxes. Rotor resistance is especially affected from skin effect with the variations in the frequency. Stator resistance is also affected from motor temperature. On the other hand, mechanical uncertainties as friction and load are another affects that are making sensorless high performance control difficult.

There are many methods to achieve these problems. Model Reference Systems, Luenberger Observer, Sliding Mode Observer, Artificial Intelligence based methods and Extended Kalman Filter are very commonly used. EKF based observer is a very appropriate method for SCIM dynamic model due to its stochastic behavior in spite of its computational complexity.

In this study, uncertainties of SCIM as load, rotor and stator resistances of SCIM are estimated by using an EKF based observer in order to get accurate speed and flux feedback. On the other hand, different than previous schemes, order of EKF is increased and an eight order EKF is designed in order to estimate rotor and stator resistances simultaneously. Besides, electrical and mechanical uncertainties are estimated experimentally by combining a digital signal processor and an open loop voltage source inverter.

After the introduction section in the first chapter, dynamic model of SCIM is introduced in alfa- beta and d-q axis and dynamic model is obtained which is used in the experiments. In the third chapter of this study, direct vector control technique is examined and Luenberger observer is introduced due to its basic observer property. In the fourth chapter of this study, EKF based observer design is explained in detail and a sixth, seventh and eighth order EKF algortihms are designed in order to

estimate load, rotor and stator resistances respectively as well as rotor flux and speed. In the fifth chapter, electrical drive circuits used in SCIM control are introduced and space vector modulation pulse witdth modulation technique is explained in detail which is widely used in the electrical drives. In the sixth chapter, practical knowledge about preparing the experimental test bed are given. In the seventh chapter simulation and experimental results are given in detail. In the last chapter, concluding and future comments are explained.

SİNCAP KAFESLİ ASENKRON MAKİNALARIN ALGILAYICISIZ DOĞRUDAN VEKTÖR KONTROLÜ

ÖZET

Sincap kafesli asenkron makinalar(SKAM) sağlamlıkları, düşük maliyetleri ve bakım gerektirmemeleri gibi nedenlerle endüstride en çok kullanılan makina tipidir. Yaygın kullanılmalarına rağmen kontrolünde güçlükler bulunmaktadır. Bu sebeple ilk defa 1969 ve 1972 yıllarında asenkron makinaların DC makinalar gibi kontrol edilmesini sağlayan alan yönlendirmeli vektör kontrol yöntemleri geliştirilmiştir. Daha sonraki yıllarda da doğrudan moment kontrolünün geliştirilmesiyle yüksek performanslı asenkron makina kontrolü yeni bir bakış açısı kazanmıştır.

Bu kontrol yöntemlerinin gerçeklenmesi için hız ve akı bilgisine ihtiyaç duyulmaktadır. Ancak hız ve akı bilgisinin alınması maliyetleri arttırmakta veya bazı ortamlarda hız geri beslemesinin alınması fiziksel güçlükler nedeniyle mümkün olamamaktadır. Akı geri beslemesinin alınması ise motorun konstrüksiyonuna direk müdahale gerektirdiği için tercih edilmemektedir. Algılayıcısız yüksek performanslı kontrolün gerçeklenebilirliği düşünüldüğünde beşinci derece, geri beslemeli, nonlineer ve parametreleri zamanla değişen SKAM modeli için bir çok zorluk bulunmaktadır. Ancak yüksek doğrulukta paremetrelerin kestrildiği durumlarda geniş hız ve yük aralığında yüksek performanslı algılayıcısız kontrolden bahsedilebilir.

Bir elektrik makinasında parametre belirsizlikleri gözönüne alındığında elektriksel ve mekanik olmak üzere iki temel belirsizlikten söz edilebilir. SKAM göz önüne alındığında ise elektriksel belirsizlik olarak rotor akılarının yanı sıra rotor ve stator direncinin çalışma koşullarının değişiminden etkilenerek bozucu etkilere neden olduğu bilinmektedir. Rotor direnci özellikle deri olayının etkisiyle frekans değişimlerinden etkilenmektedir. Stator direnci de özelikle motor sıcaklığından etkilenmektedir. Diğer taraftan sürtünme ve yük gibi mekanik yana ilişkin belirsizlikler de yüksek performanslı algılayıcısız kontrolü güçleştiren diğer etkenlerdir.

Yukarıda belirtilen problemlerin aşılması amacıyla literatürde bir çok yöntem geliştirilmiştir. Model uyarlamalı sistemler, Luenbeger Gözlemleyicisi, Kayan Kipli Kontrol ve yapay zeka yöntemleri ve genişletilmiş kalman filtresi(GKF) gibi bir çok yöntem mevcuttur. GKF olasıl bir yöntem olması sebebiyle çok fazla işlem gerektirmesine rağmen SKAM'nin dinamik modeli için son derece uygun bir yaklaşımdır.

Bu çalışmada GKF tabanlı gözlemleyici tasarlanarak makinanın yük momenti, rotor ve stator dirençleri gibi belirsizlikleri kestirilerek geniş hız aralığında yüksek doğrulukta akı ve hız bilgisine ulaşılmaya çalışılmıştır. Ayrıca önceki çalışmalardan farklı olarak GKF mertebesi arttırılarak sekizinci derecede GKF algoritması tasarlanmış ve rotor ve stator dirençleri eş zamanlı olarak kestirilmeye çalışılmıştır. Benzetim çalışmalarının yanı sıra dijital işaret işleyici ve açık çevrim bir gerilim kaynaklı bir evirici birleştirilerek elektriksel ve mekanik yana ilişkin belirsizlikler deneysel olarak kestirimeye çalışılmıştır.

Bu çalışmanın ilk bölümündeki girişten sonra ikinci bölümde SKAM'nin dinamik modeli alfa-beta ve d-q eksen takımında verilerek benzetim çalışmalarında kullanılacak alfa-beta dinamik modeli elde edilmiştir. Çalışmanın üçüncü bölümünde doğrudan vektör kontrol yöntemi incelenmiş ve temel bir gözlemleyici olması nedeniyle Luenberger gözlemleyicisi tanıtılmıştır. Çalışmanın dördüncü bölümünde GKF tabanlı gözlemleyici tasarımı detayları ile birlikte anlatılmış ve sırasıyla altıncı, yedinci ve sekizinci derece GKF algoritmaları tasarlanarak makinanın hız ve akı bilgilerinin yanı sıra yük, rotor ve stator dirençlerinin kestirimi yapılmıştır. Beşinci bölümde SKAM kontrolünde kullanılan elektrik sürücü devreleri detayları ile birlikte verilmiş Darbe Genişlik modülasyonu yöntemleri arasında en yaygın olarak kullanılan uzay vektörleri darbe genişlik modülasyonu ile ilgili detaylı bilgiler verilmişitir. Çalışmanın altıncı bölümünde deney çalışmalarının yapılabilmesi için gerekli olan deney setinin hazırlanması ile ilgili pratik bilgiler verilmiştir. Çalışmanın yedinci bölümünde benzetim ve deney çalışmalarının sonuçları detayları ile birlikte verilmiştir. Son bölümde ise çalışmaya ait sonuçlar değerlendirilmiş ve gelecek yönlendirmeler sıralanmıştır.

1. INTRODUCTION

Squirrel Cage Induction Machine (SCIM) is the most popular electrical machine due to its ruggedness, cheapness and free maintenance properties. Historically, they were only used in many uncontrolled applications due to its 6% to 10% speed drop from no load to full load and difficulties in changing its speed by the last few decades of 20^{th} century. DC machines were popularly used in speed and/or torque control applications due to its controllability. Speed and/or torque control of SCIM is very complex compared to DC machines. However, DC machines are not suitable for explosive areas due to its carbon brush structure conducting the armature current to the rotor causing sparks and frequent maintenance requirements in the brushes. Besides, DC machine construction is very expensive compared to the SCIM construction.

Because of the disadvantages of DC machines, SCIM have always been wanted to take over because of its low cost, high efficiency, ruggedness and free maintenance. In recent years, with the innovations in the processor technology and variety of power semiconductor devices, made high performance SCIM control possible. Electrical drive circuits used in SCIM control change frequency and/or voltage into a specified value. Voltage Source Inverter (VSI) is popularly used in SCIM control in open loop V/Hz operation. So, SCIM has started to take over the DC machines in the industry where high performance control is not required. However, scalar control methods are not adequate for a wide speed and torque range. In transient conditions, speed and torque control of SCIM is not adequate to use in high performance applications such as mills, cranes electrical cars etc. Besides, SCIM could not be used in position control applications because of uncontrollability in transient conditions. Control algorithms which overcome these difficulties in SCIM control are called high performance control (Bose, 1997).

In order to achieve high performance control of SCIM, field oriented or vector control methods are used. Indirect vector control by Hasse in 1969 and direct vector

control method by Blaschke in 1972 were first proposed. The idea of field oriented method is basically imitating DC machine control into SCIM. Classical DC motors have field and armature current components. Field current controls the flux required, while armature current controls the torque. These two components are physically different and can be controlled independently. SCIM does not have a separate field circuit. So, torque producing component of current (I_q) and flux producing component of current (I_d) should mathematically be separated. Park transformations are used to separate these components.

Dynamic model of SCIM is a 5^{th} order, parameter varying, recurrent and nonlinear equation (Bose, 2002 and others). SCIM electrical parameters are vulnerable to vary with operating conditions. Rotor and stator resistances are easily to change with frequency and temperature variances. 5 dynamic equations of SCIM should also be calculated and derivations of these equations increase the computational complexity. These computational complexities and Park and/or Clarke transformations applied to motor voltages and motor feedback currents required high level processors such as DSP (Digital signal Processor) or FPGA (Field Programmable Gate Array). Therefore, developed vector control algorithms could practically be used in SCIM control in 1980s with the innovations in the processor technologies.

Indirect vector control algorithms assume machine parameters constant (Sarıoğlu, 2003). However, machine parameters such as rotor and stator resistances are vulnerable to change easily in the variation of frequency, load and temperature. This problem makes the flux calculations mistaken for some conditions. Therefore, this method is not examined in this study.

Direct vector control algorithms require additional flux sensors installed to the motor in order to correctly measure rotor flux. This requires additional cost to the motors and in some applications installation of these sensors and cabling are not possible. Besides, feedback of these sensors is not reliable in low speed operation and causes torque pulsations at lower speeds.

Vector control algorithms also require a correct speed feedback in order to operate correctly. Installation of speed encoder is sometimes impossible in some applications. These encoders are expensive and increase the cost. Because of these

difficulties, additional alternatives to these control methods are required. These methods use calculations instead of measurements. Observers are used in the estimation of motor parameters and variables. Luenberger observer with its linear property can calculate rotor fluxes correctly. So, Luenberger Observer (Luenberger, 1971) based direct vector control algorithms can be applied to the motor. But, this method is not sufficient to calculate motor speed correctly and sensor noises are not taken into consideration in this deterministic approach.

Kalman Filter (Kalman, 1960) which is a stochastic approach was first proposed in 1960. Kalman filter has found many application areas in the literature. Extended kalman filters (EKF) which are used in nonlinear systems are also popular for satellite tracking, global position systems, radars etc. to estimate any parameter uncertainties.

Voltages of the motor applied by inverters have harmonics and noises. Parameter variations in SCIM, harmonics and noises in the electrical components make EKF algorithms applicable. In spite of the computational complexity of EKF algorithm, innovations in the processor technologies make it applicable to use in high performance control of SCIM. Besides, EKF algorithm not only estimates the speed but also estimates other electrical and mechanical uncertainties of SCIM such as rotor and stator resistances and the load applied.

Historically, electrical drive circuits also evolved in recent years. Cycloconverters were used in high power applications of SCIM control. But, their complexity, low power factor and harmonic effects make it impossible to use for every applications. Current source inverters (CSI) were also used in SCIM control. However, poverty of their dynamic performance, impossibility of usage without closed loop, and impossibility of usage in multimotor applications decreased its popularity in SCIM control.

Voltage Source Inverters (VSI) are the correct choice for SCIM control applications because of its high dynamic performance, no current feedback requirements and availability of usage with asymmetric power electronic devices such as IGBTs (Insulated Gate Bipolar Transistors) for low power applications, GTOs (Gate Turn off Thyristors), and IGCTs (Integrated Gate Commutating Thyristors) for high power

applications. The evolution of power semiconductor devices continues that IGBTs which are more advantageous are tried to be used in state of IGCTs and GTOs in high power applications. Maximum medium voltage level for asymmetric power electronic devices is 6600V which limits the motor nominal voltage.

Evolutions of PWM methods are also important in high performance control of SCIM. Conventionally, sine triangle PWM methods have commonly been used for many years. But Space Vector Modulation Pulse Width Modulation (SVPWM) techniques are more advantageous because of lower harmonics and higher modulation indexes compared to the other methods. There are also linearization methods for operating in overmodulation regions which increases the voltage of the inverter. In spite of its computational complexity, SVPWM is applicable with a high level processor.

In the second chapter of this study, dynamic model of SCIM which is fifth order, nonlinear, recurrent and parameter varying is introduced in alfa-beta and d-q reference frame. Alfa-beta model is simulated and this model is used as a reference in the next chapters.

In the third chapter of this study, direct vector control algorithms are introduced. Direct vector control algorithms with the flux sensors are simulated in Matlab/Simulink. This method is not feasible to use because of the flux sensors installed to the motor. So, Luenberger observer which is a deterministic approach is also simulated with direct vector control algorithm in Matlab/Simulink.

In the fourth chapter of this study, kalman filter which is a stochastic approach for parameter estimation is introduced. Extended Kalman Filter (EKF) based observer is designed for parameter and state estimation of SCIM. Rotor and stator resistance variations of SCIM due to frequency and temperature affect sensorless high performance control in a wide speed range. A 7^{th} order EKF algorithm which estimates rotor or stator resistance as well as load torque, speed and flux is designed. In addition, a novel 8^{th} order EKF which estimates stator and rotor resistances in a single EKF as well as load torque, speed and flux is designed.

In the fifth chapter, power electronic circuits used in SCIM control are explained in detail. Cycloconverters, CSIs and VSI are compared. PWM techniques used in VSIs are also compared and SVPWM technique is simulated in Matlab/Simulink.

In the sixth chapter, design criteria of IGBT gate drive circuits are explained in detail. In order to get experimental results, an intelligent gate drive circuit with HCPL-316 integrated circuit is designed. The designed circuit is capable of operating with DSPACE DS1104 controller board PWM outputs. Besides, this gate drive circuit is capable of operating with ABB ACS 300 VSI.

In the seventh chapter, simulation and experimental results of the studies are explained in detail. In the 8^{th} chapter, conclusion comments are given to the reader comparing the results. Also new proposals to control and estimation techniques of SCIM are given.

2. DYNAMIC MODEL OF SQUIRREL CAGE INDUCTION MACHINES

In order to design a vector control algorithm based induction machine drive, dynamic model of induction machines must be learned. This model must require transient and steady state conditions of Squirrel Cage Induction Machine (SCIM) for any instantaneous value of current and voltage. Before introducing the dynamic model of induction machines, assumptions given below should be considered. (Sarıoğlu, 2003)

- Stator windings are distributed to stator surface normally and air gap flux changes sinusoidal.
- 3 Phase stator windings will be distributed to surface with 120 degrees electrical angle correctly.
- Saturation is neglected.
- Hysterisis and Foucault Losses are neglected.
- Conduction of magnetic surfaces is considered to be infinitive.
- Skin effect is neglected.
- Changes of resistances and inductances with temperature and frequency changes are neglected.
- Rotor bars are installed symmetrically.
- Every bar of rotor is assumed to be a rotor phase winding.

SCIM Dynamic Model must be expressed in stationary $\alpha - \beta$ axis or synchronously rotating dq coordinate system in order to be used in control algorithms.

All symbols in equations are;

$R_E =$ Electrical Equivalent Resistance

$R_s =$ Stator Resistance

$R_r^{'} =$ Rotor Resistance

$L_m =$ Mutual Inductance

$L_r^{'} =$ Rotor Inductance

$\sigma =$ Leakage Factor

$T_e =$ Electrical Torque

w = Motor angular velocity in rad/s

B = Viscous Friction constant

J = Inertia Constant

$T_L =$ Mechanical Torque

$i_{s\alpha} =$ α Component of stator current

$i_{s\beta} =$ β Component of stator current

$\psi_{r\alpha} =$ α Component of rotor flux

$\psi_{r\beta} =$ β Component of rotor flux

$i_{sd} =$ d Component of stator current

$i_{sq} =$ q Component of stator current

$\psi_{rd} =$ d Component of rotor flux

$\psi_{rq} =$ q Component of rotor flux

2.1 $\alpha - \beta$ Model of Induction Machines

Voltage vectors V_a, V_b, and V_c values have 120 electrical degrees phase differences. These phase differences are represented in $\alpha - \beta$ axis. With this representation, electrical values are converted to two phase values. This transformation is called Clarke Transformation.

$$\begin{bmatrix} V_0 \\ V_\alpha \\ V_\beta \end{bmatrix} = \sqrt{\frac{2}{3}} \begin{bmatrix} \frac{\sqrt{2}}{2} & \frac{\sqrt{2}}{2} & \frac{\sqrt{2}}{2} \\ 1 & -\frac{1}{2} & -\frac{1}{2} \\ 0 & \frac{\sqrt{3}}{2} & -\frac{\sqrt{3}}{2} \end{bmatrix} \begin{bmatrix} V_{sa} \\ V_{sb} \\ V_{sc} \end{bmatrix} \quad \textbf{(2.1)}$$

$$V_0 = \frac{1}{\sqrt{3}}(V_{sa} + V_{sb} + V_{sc}) \quad \textbf{(2.2)}$$

V_0 is zero for balanced systems.

$$V_{sa} = V_m \sin\theta_s \tag{2.3}$$

$$V_{sb} = V_m \sin(\theta_s + \frac{2\pi}{3}) \tag{2.4}$$

$$V_{sc} = V_m \sin(\theta_s - \frac{2\pi}{3}) \tag{2.5}$$

$$\theta = \int_0^t w_s dt = 2\pi \int_0^t f_s dt \tag{2.6}$$

f_s is the stator frequency or supply voltage frequency. So, $\alpha - \beta$ voltages are sinusoidal.

$$V_\alpha = \frac{\sqrt{3}}{\sqrt{2}} V_m \sin\theta_s \tag{2.7}$$

$$V_\beta = \frac{\sqrt{3}}{\sqrt{2}} V_m \sin\theta_s \tag{2.8}$$

Voltage transformations written above can be reproduced for different electrical components such as current, flux etc. $\alpha - \beta$ model squirrel cage induction machine dynamic equations are;

$$\frac{di_{s\alpha}}{dt} = \frac{1}{\sigma L_s}\left\{\frac{L_m}{L_r^{'}}\left(\frac{R_r^{'}}{L_r^{'}}\psi_{r\alpha} + pw\psi_{r\beta}\right) - R_E i_{s\alpha} + V_{s\alpha}\right\} \tag{2.9}$$

$$\frac{di_{s\beta}}{dt} = \frac{1}{\sigma L_s}\left\{\frac{L_m}{L_r^{'}}\left(\frac{R_r^{'}}{L_r^{'}}\psi_{r\beta} - pw\psi_{r\alpha}\right) - R_E i_{s\alpha} + V_{s\beta}\right\} \tag{2.10}$$

$$\frac{d\psi_{r\alpha}}{dt} = -\frac{R_r^{'}}{L_r^{'}}\psi_{r\alpha} - pw\psi_{r\beta} + \frac{R_r^{'} L_m}{L_r^{'}} i_{s\alpha} \tag{2.11}$$

$$\frac{d\psi_{r\beta}}{dt} = -\frac{R_r^{'}}{L_r^{'}}\psi_{r\beta} + pw\psi_{r\beta} + \frac{R_r^{'} L_m}{L_r^{'}} i_{s\beta} \tag{2.12}$$

$$\frac{dw}{dt} = \frac{p}{j}\frac{L_m}{L_r}(\psi_{r\alpha} i_{s\beta} - \psi_{r\beta} i_{s\alpha}) - \frac{B}{J}w + \frac{1}{J}T_L \tag{2.13}$$

$$T_e = p\frac{L_m}{L_r^{'}}(i_{s\beta}\psi_{r\alpha} - i_{s\alpha}\psi_{r\beta}) \tag{2.14}$$

$$R_E = R_S + \frac{R_r^{'} L_m^2}{L_r^{'2}} \tag{2.15}$$

$$\sigma = 1 - \frac{L_m^2}{L_s L_r^{'}} \tag{2.16}$$

2.2 D-Q (Synchronously Rotating Reference Frame) Axis Model

DQ transformation is a transformation of coordinates from three phase stationary coordinate system to the two phase dq rotating coordinate system. DQ axis is a rotating coordinate that turns at synchronous speed. Park transformation equations are;

$$\begin{bmatrix} V_{s0} \\ V_{sd} \\ V_{sq} \end{bmatrix} = \frac{2}{3}\begin{bmatrix} \frac{1}{\sqrt{2}} & \frac{1}{\sqrt{2}} & \frac{1}{\sqrt{2}} \\ Cos\theta_s & Cos(\theta_s - \frac{2\pi}{3}) & Cos(\theta_s + \frac{2\pi}{3}) \\ -\sin\theta_s & -\sin(\theta_s - \frac{2\pi}{3} & -\sin(\theta_s + \frac{2\pi}{3}) \end{bmatrix}\begin{bmatrix} V_{as} \\ V_{bs} \\ V_{cs} \end{bmatrix} \tag{2.17}$$

$$\begin{bmatrix} i_a \\ i_b \\ i_c \end{bmatrix} = \sqrt{\frac{2}{3}}\begin{bmatrix} \frac{1}{\sqrt{2}} & Cos\theta_s & Sin\theta_s \\ \frac{1}{\sqrt{2}} & Cos(\theta_s - \frac{2\pi}{3}) & Sin(\theta_s - \frac{2\pi}{3}) \\ \frac{1}{\sqrt{2}} & Cos(\theta_s + \frac{2\pi}{3}) & Sin(\theta_s + \frac{2\pi}{3}) \end{bmatrix}\begin{bmatrix} i_{so} \\ i_{sd} \\ i_{sq} \end{bmatrix} \tag{2.18}$$

Park transformation is bi-directional and can be applied to any electrical magnitude. According to Park transformation equations, dq component of any electrical magnitude is a DC magnitude in steady state. DQ model squirrel cage induction machines dynamic equations are;

$$\frac{di_{sd}}{dt} = \frac{1}{\sigma Ls}\left[- R_E i_{sd} + \sigma L_s w_s i_{sq} + \frac{L_m R_r^{'}}{L_r^{'2}}\psi_{rd} + pw\frac{L_m}{L_r^{'}}\psi_{rq} + V_{sd} \right] \quad \textbf{(2.19)}$$

$$\frac{di_{sq}}{dt} = \frac{1}{\sigma Ls}\left[- R_E i_{sq} - \sigma L_s w_s i_{sd} - pw\frac{L_m}{L_r^{'}}\psi_{rq} + \frac{L_m R_r^{'}}{L_r^{'2}}\psi_{rq} + V_{sq} \right] \quad \textbf{(2.20)}$$

$$\frac{d\psi_{rd}}{dt} = \frac{R_r^{'} L_m}{L_r^{'}} i_{sd} - \frac{R_r^{'}}{L_r^{'}}\psi_{rd} + w_r \psi_{rq} \quad \textbf{(2.21)}$$

$$\frac{d\psi_{rq}}{dt} = \frac{R_r^{'} L_m}{L_r^{'}} i_{sq} - w_r \psi_{rd} - \frac{R_r^{'}}{L_r^{'}}\psi_{rq} \quad \textbf{(2.22)}$$

Motor Torque can be expressed in different types of current or flux.

$$T_e = \frac{3}{2} p \frac{L_m}{L_r^{'}}(i_{sq}\psi_{rd} - i_{sd}\psi_{rq}) \quad \textbf{(1.23 a)}$$

$$T_e = \frac{3}{2} p(i_{sq}\psi_{sd} - i_{sd}\psi_{sq}) \quad \textbf{(1.23 b)}$$

$$T_e = \frac{3}{2} p(i_{rd}\psi_{rq} - i_{rd}\psi_{rd}) \quad \textbf{(1.23 c)}$$

SCIM dynamic model has different properties that make the control system complicated (Barut, 2005a).

- Differentiation operation means **dynamic** property of SCIM.
- Multiplications between states of the machine mean **nonlinear** property of SCIM.
- Requirement of the rotor speed in order to calculate all the states of the machine means that system is **recurrent.**
- Model parameter values dependent on temperature and frequency means the property of parameter varying property with time.

In addition to properties written above unpredictable loading conditions make the control system design very difficult. Besides, parameter varying property has deteriorating effects on control algorithms. In conclusion, SCIM, of which

parameters change with time, recurrent and having nonlinear dynamic property with five equations can be defined as a benchmark control system (Barut, 2005a).

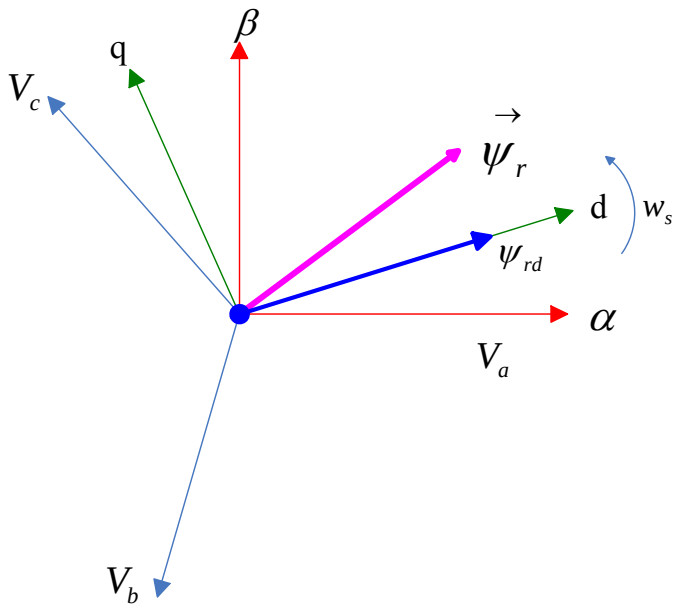

Figure 2.1 $\alpha - \beta$ and D-Q Axis Representation of Rotor Flux

3. VECTOR CONTROL TECHNIQUES OF SQUIREL CAGE INDUCTION MACHINES

Separately excited DC machines were commonly used because of the easiness of speed controllability and became unrivalled in speed control applications in the industry. But, maintenance requirements of brushes, unavailability of usage in flammable areas because of arcs occurring on brushes and collectors make these machines usage disadvantageous. Therefore, SCIM which is cheap in construction and no maintenance requirements has become advantageous by using voltage source inverters with vector control algorithms which provides high performance control (Bose, 1997). The aim of vector control is to run SCIM like a separately excited DC Machine.

A separately excited DC machine field current is perpendicular to armature flux produced by the armature current. These two vectors are decoupled and stationary with respect to each other. The aim of the armature current is to control the torque, while field current remains unaffected and constant.

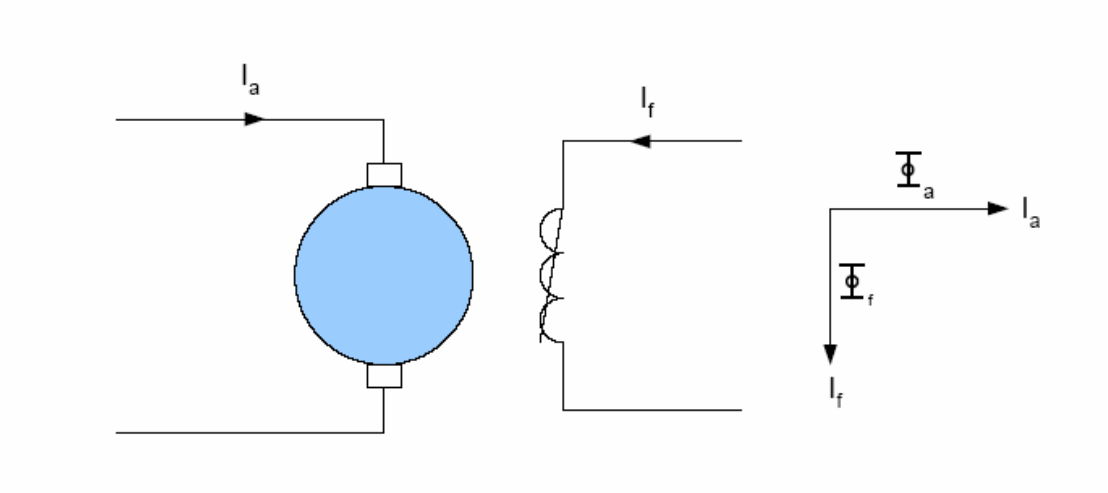

Figure 3.1 Separately Excited DC Machine

Vector control techniques, varying amounts of different types, search to create these orthogonal components in an AC Machine in order to control the torque producing

component of current and magnetic flux producing component of current so as to achieve the high performance response of separately excited DC Machine. But, SCIM does not physically have any current component that separately controls flux and torque. SCIM has only stator current which is sinusoidal.

3.1 Vector (Field Oriented) Control

In order to understand vector control concept better, first field orientation condition should be defined. This condition can be verified by zeroing the negative side of torque equation of SCIM given in Equation 2.23. So, the expression of torque consists of only two separate variables and these variables can be controlled separately. If the variable that is wanted to be zeroed is rotor flux, vector control method is called **rotor flux oriented vector control method**. If the variable that is wanted to be zeroed is stator flux, vector control method is called **stator flux oriented vector control method.** If the variable that is wanted to be zeroed is air gap flux, vector control method is called air **gap flux oriented vector control method** (Sarığlu, 2003).

$$T_e = \frac{3}{2} p \frac{L_m}{L_r'} (i_{sq}\psi_{rd} - \cancel{i_{sd}\psi_{rq}}) \qquad \textbf{(2.23.a)}$$

$$T_e = \frac{3}{2} p (i_{sq}\psi_{sd} - \cancel{i_{sd}\psi_{sq}}) \qquad \textbf{(2.23.b)}$$

$$T_e = \frac{3}{2} p (i_{rd}\psi_{rq} - \cancel{i_{rd}\psi_{rd}}) \qquad \textbf{(2.23.c)}$$

Common property of all vector control techniques is to separate flux producing current (I_{sd}) and torque producing current (I_{sq}) and adjusting torque by linearly changing torque producing current.

As mentioned in Chapter 2, SCIM dynamic model consists of 5 nonlinear equations. This nonlinearity not only comes from the speed and current multiplications in the equations, but also arises from the vulnerability of rotor parameters such as frequency and temperature effects.

In the d-q axis model, input of the machine (V_{sd} and V_{sq}) and all the states of the machine ($i_{sd}, i_{sq}, \psi_{rd}$ *and* ψ_{rq}) are defined in the d-q axis. These defined vectors;

$$\vec{V}_s = v_{sd} + jv_{sq} = \left|\vec{V}_s\right| e^{j\varphi} \tag{3.1}$$

$$\vec{I}_s = i_{sd} + ji_{sq} = \left|\vec{I}_s\right| e^{j\varphi} \tag{3.2}$$

$$\vec{\psi}_r = \psi_{rd} + j\psi_{rq} = \left|\vec{\psi}_r\right| e^{j\varphi} \tag{3.3}$$

$$\vec{\psi}_s = \sigma L_s \vec{i}_s + \frac{L_m}{L_r'} \vec{\psi}_r \tag{3.4}$$

$$T_e = p \frac{L_m}{L_r'} (\vec{i}_s \, x \, \vec{\psi}_r) \tag{3.5}$$

Selection of one variable in the motor model as a base and defining other variables according to selected variable are possible. These simplify the control algorithm and make control possible. The most appropriate variable is rotor flux when the torque equations (2.23) are observed. So, the appropriate vector control solution seems to be ***rotor flux oriented vector control***. If rotor flux is defined in d axis and all the variables of the SCIM are defined in d axis and quadrature q axis, stator current vector can be divided to d and q axis. So, d component of stator current (I_{sd}) is the component that controls the flux, and quadrature component of stator current (I_{sq}) is the component that controls the torque. So, the torque equation of the SCIM;

$$T_e = p \frac{L_m}{L_r'} i_{sq} \psi_{rd} \tag{3.6}$$

Stator flux oriented or air gap flux oriented control algorithms can also be applied. For example, Direct Torque Control (DTC) (Takahashi, 1986) is considered as a stator flux oriented vector control technique (Sarıoğlu, 2003), while it is sometimes considered as a high performance scalar technique (Bose, 1997). There are two kinds of these control techniques; indirect and direct control. Indirect vector control

techniques assume machine parameters constant. So, its performance is not sufficient for many applications. Therefore, it will not be explained in this study.

Main problem of rotor flux oriented control algorithms is that it is not possible to measure the rotor flux. Therefore, an additional flux sensor has to be installed on the machine or an observer has to be designed to calculate the rotor flux.

3.2 Direct Vector Control Techniques

It is a vector control method applied by Blaschke in Germany in 1972. This method requires measurement of rotor flux. For this reason, additional Hall Effect sensors are added to measure air gap rotor flux ($\psi_{m\alpha}$ *and* $\psi_{m\beta}$). System also needs current sensors to measure the phase current of the SCIM. These measured currents have to be transformed to $\alpha - \beta$ and d-q components with Clarke and Park transformations. Rotor flux is calculated with the equations below;

$$\psi_{r\alpha} = \frac{L_r^{'}}{L_m}\psi_{m\alpha} - L_{r\sigma}^{'} i_{s\alpha} \tag{3.7}$$

$$\psi_{r\beta} = \frac{L_r^{'}}{L_m}\psi_{m\beta} - L_{r\sigma}^{'} i_{s\beta} \tag{3.8}$$

Amplitude and phase of rotor flux are calculated with the equations below.

$$\left|\psi_r\right| = \sqrt{\psi_{r\alpha} + \psi_{r\beta}} = \psi_{rd} \tag{3.9}$$

$$\varphi_\psi = \tan^{-1}\left(\frac{\psi_{r\beta}}{\psi_{r\alpha}}\right) = \theta \tag{3.10}$$

Calculated phase angle is used in park transformations to transform current and voltage in d-q components. Block diagram of the system is shown in Figure 3.2

Main disadvantage of this method is the installation requirement of Hall Effect air gap flux sensors. This requires additional cost to new constructed motors and no any customer prefers this way. Because of this disadvantage, direct vector control techniques that are using observers to calculate rotor flux are preferred. It is possible

with the help of measured current and voltage that rotor flux amplitude, phase angle and/or speed can be calculated.

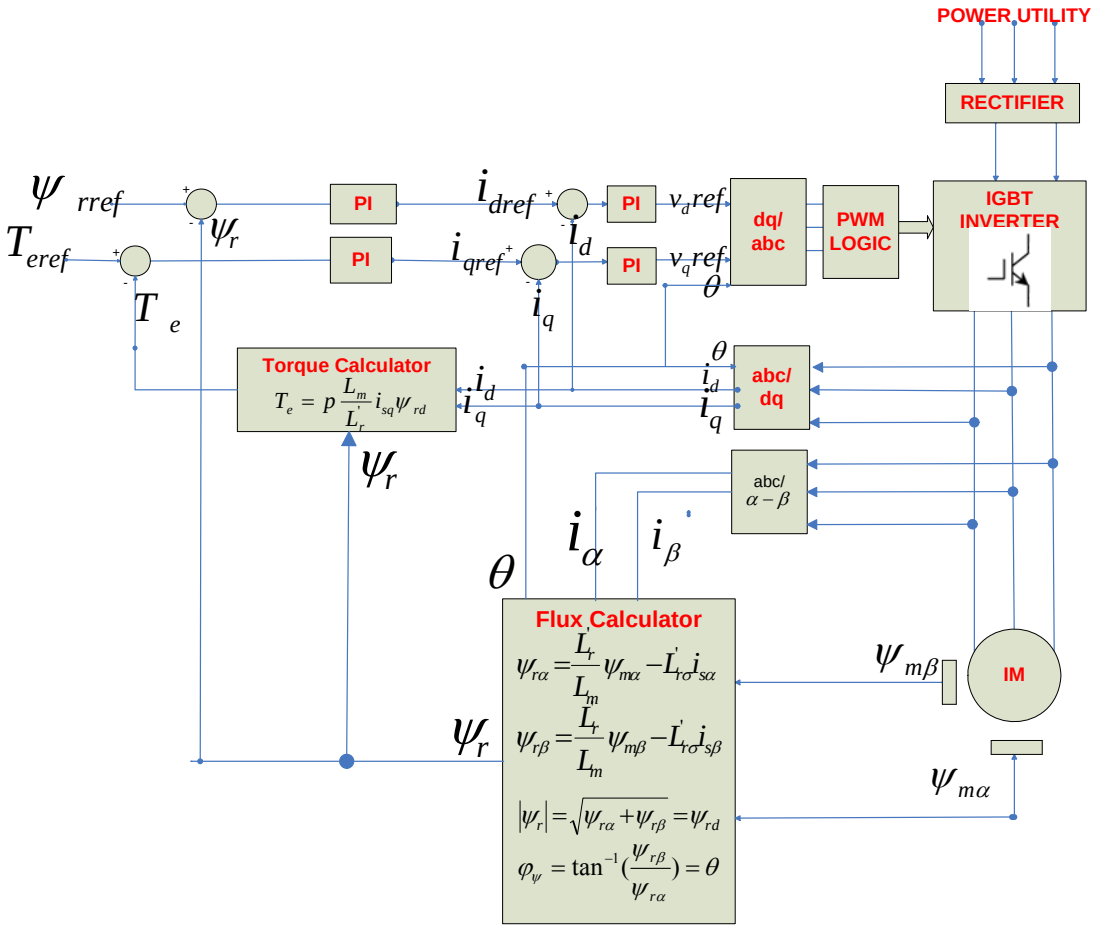

Figure 3.2 Direct Vector Control Block Diagram

Simulation results of Direct Vector Control Algorithm are in Appendix B1.

3.3 Observers

It is possible to calculate electrical or mechanical variables with the help of measured quantities such as stator currents and voltages. These observers use the voltages and currents of the motor and calculate the rotor fluxes, speed, load, stator or rotor resistances etc.

3.4 Luenberger Observer

A dynamic system is represented with the equations below.

$$\dot{x} = [A][x] + [B][u] \tag{3.10}$$

$$[y] = [C][x] \tag{3.11}$$

This system is imitated to SCIM model with the equation below.

$$\underbrace{\frac{d}{dt}\begin{bmatrix} \hat{i}_{s\alpha} \\ \hat{i}_{s\beta} \\ \hat{\psi}_{r\alpha} \\ \hat{\psi}_{r\beta} \end{bmatrix}}_{[\dot{\hat{x}}]} = \underbrace{\begin{bmatrix} \frac{R_E}{\sigma L_s} & 0 & \frac{L_m R_r'}{\sigma L_s L_r'^2} & pw\frac{L_m}{\sigma L_s L_r'} \\ 0 & \frac{R_E}{\sigma L_s} & -pw\frac{L_m}{\sigma L_s L_r'} & \frac{L_m R_r'}{\sigma L_s L_r'^2} \\ \frac{L_m R_r'}{L_r'} & 0 & \frac{R_r'}{L_r'} & -pw \\ 0 & \frac{L_m R_r'}{L_r'} & pw & \frac{R_r'}{L_r'} \end{bmatrix}}_{[A]} \underbrace{\begin{bmatrix} \hat{i}_{s\alpha} \\ \hat{i}_{s\beta} \\ \hat{\psi}_{r\alpha} \\ \hat{\psi}_{r\beta} \end{bmatrix}}_{\hat{x}} + \underbrace{\begin{bmatrix} \frac{1}{\sigma L_s} & 0 \\ 0 & \frac{1}{\sigma L_s} \\ 0 & 0 \\ 0 & 0 \end{bmatrix}}_{[B]} \underbrace{\begin{bmatrix} v_{s\alpha} \\ v_{s\beta} \end{bmatrix}}_{u} \tag{3.12}$$

$$\begin{bmatrix} i_{s\alpha} \\ i_{s\beta} \end{bmatrix} = \begin{bmatrix} 1 & 0 & 0 & 0 & 0 \\ 0 & 1 & 0 & 0 & 0 \end{bmatrix} \begin{bmatrix} i_{s\alpha} \\ i_{s\beta} \\ \psi_{r\alpha} \\ \psi_{r\beta} \end{bmatrix} \tag{3.13}$$

The input of this observer is the measured currents and voltages applied. Output of the observer is the rotor fluxes. Luenberger gain matrix is multiplied with the error e_1 and e_2 which are the differences of Luenberger observer currents and voltages and measured currents and voltages applied respectively. Block diagram of the Luenberger Observer Based Direct Vector Control algorithm is in the figure 3.4.

$$\underbrace{\frac{d}{dt}\begin{bmatrix}\hat{i}_{s\alpha}\\ \hat{i}_{s\beta}\\ \hat{\psi}_{r\alpha}\\ \hat{\psi}_{r\beta}\end{bmatrix}}_{\left[\dot{\hat{x}}\right]}=\underbrace{\begin{bmatrix}\frac{R_E}{\sigma L_s} & 0 & \frac{L_m R_r'}{\sigma L_s L_r'^2} & pw\frac{L_m}{\sigma L_s L_r'}\\ 0 & \frac{R_E}{\sigma L_s} & -pw\frac{L_m}{\sigma L_s L_r'} & \frac{L_m R_r'}{\sigma L_s L_r'^2}\\ \frac{L_m R_r'}{L_r'} & 0 & \frac{R_r'}{L_r'} & -pw\\ 0 & \frac{L_m R_r'}{L_r'} & pw & \frac{R_r'}{L_r'}\end{bmatrix}}_{[A]}\underbrace{\begin{bmatrix}\hat{i}_{s\alpha}\\ \hat{i}_{s\beta}\\ \hat{\psi}_{r\alpha}\\ \hat{\psi}_{r\beta}\end{bmatrix}}_{\hat{x}}+\underbrace{\begin{bmatrix}\frac{1}{\sigma L_s} & 0\\ 0 & \frac{1}{\sigma L_s}\\ 0 & 0\\ 0 & 0\end{bmatrix}}_{[B]}\underbrace{\begin{bmatrix}v_{s\alpha}\\ v_{s\beta}\end{bmatrix}}_{u}+\underbrace{\begin{bmatrix}L_{11} & L_{12}\\ L_{21} & L_{22}\\ L_{31} & L_{32}\\ L_{41} & L_{42}\end{bmatrix}}_{[L]}\underbrace{\begin{bmatrix}e_1\\ e_2\end{bmatrix}}_{[e]}$$

(3.14)

$$e=\begin{bmatrix}e_1\\ e_2\end{bmatrix}=y-\hat{y}=\begin{bmatrix}i_{s\alpha}-\hat{i}_{s\alpha}\\ i_{s\beta}-\hat{i}_{s\beta}\end{bmatrix} \qquad \textbf{(3.15)}$$

Simulation Results of Luenberger Observer is in Appendix B2. This deterministic approach requires a correct speed feedback. Installation of speed sensors is not feasible and increases the cost for all applications. In the next chapter, a stochastic approach Extended Kalman Filter (EKF) which also estimates different variables such as speed, load, rotor and stator resistances will be explained.

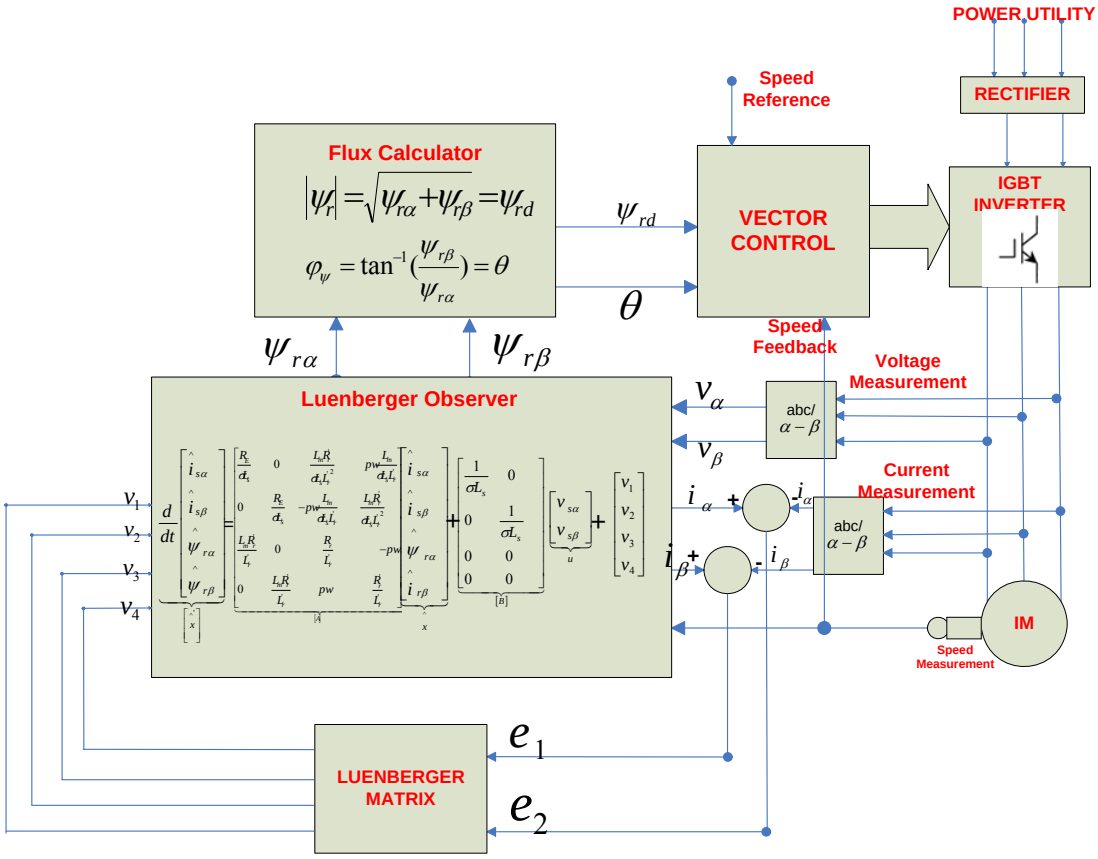

Figure 3.3 Direct Vector Control with Luenberger Observer

4. EXTENDED KALMAN FILTER BASED SCIM OBSERVER

Kalman Filter is one of the most well-known and often-used stochastic estimation methods that are used for control algorithms. It was first proposed in 1960 by R.E. Kalman (Kalman, 1960).

In high performance control of SCIM, estimation of parameters and states of SCIM is essential in order not to use additional flux and speed sensors. Because, it is sometimes impossible to use a speed sensor and sometimes sensors are not feasible to use in industrial applications. Besides, SCIM model which is also parameter varying requires also estimation of rotor and/or stator resistances in order to correctly estimate speed and flux in a wide speed range. Frequency and temperature variations effect stator and rotor resistances. Especially, estimation of the rotor and stator resistances is very critical in order to achieve sensorless high performance control at low speeds.

A kalman filter based observer can estimate not only the state variables of any system, but also can estimate system parameters of process with its recursive property. In this recursive property, it is sufficient to use priori state of the system without saving it in a memory after usage.

SCIM mathematical model which is nonlinear, parameter varying such as rotor and stator resistances, multivariable and having a higher order complex dynamics are applicable for an Extended Kalman Filter (EKF) based observer. EKF based observer which estimates state variables and parameters with stochastic approach can be suitably used in estimation of unknown parameters and states of SCIM. Because, SCIM is suitable for stochastic approach modeling because of noisy currents and voltages flowing through the VSI. Besides, sensor errors, modeling errors of nonlinear model of SCIM and other defects are defined in stochastic model. As a result, EKF based observer gives convenient estimation results for unknown parameters and states such as rotor flux, rotor speed, load, stator and rotor resistances.

4.1 Introduction to Kalman Filters

In order to apply kalman filter based algorithms, linearized system model should be identified in state space model. Process and measurement noises should also be added to system model because of the stochastic behavior of the filter. Besides, SCIM mathematical model should be discretized owing to digital implementation. Before implementing EKF based SCIM observer original Discrete Kalman Filter will be introduced. Discrete kalman filters are used in linear models.

System Equation for any process;

$$x_{k+1} = Ax_k + Bu_k + w_k \quad \textbf{(4.1)}$$

Measurement Equation for any process;

$$z_k = Hx_k + v_k \quad \textbf{(4.2)}$$

Random variables w and v represent process and measurement noise. It is assumed that they are in the form of white noise, Gaussian distributed and independent.

$$p(w) = N(0, Q) \quad \textbf{(4.3)}$$

$$p(v) = N(0, R) \quad \textbf{(4.4)}$$

Practically, Q and R might change with each time step of measurement. But, it is assumed that they are constant. Where;

A: System Matrix (Mathematical Model of System)

B: Input Matrix

H: Measurement Matrix

x: State Vector

z: Measurement Vector

u: Control Input Vector

Kalman filter estimates each step by using previous values obtaining feedbacks from noisy measurements. Therefore, algorithm steps can be divided into two parts: time update and measurement update equations (Welch, 2001). Time update equations are used for projection of current state by using error covariance matrix. Measurement update equations are used for getting the feedback from the system and kalman filter equations.

Discrete Kalman filter Algorithm Recursive Related Steps are;

(1) Propose the state vector

$$\hat{x}_k = A\hat{x}_{k-1} + Bu_k \quad \textbf{(4.5)}$$

(2) Propose the Error Covariance Matrix

$$P_k^- = AP_{k-1}A^T + Q \quad \textbf{(4.6)}$$

(3) Compute the Kalman Gain

$$K_k = P_k^- H^T (HP_k^- H^T + R)^{-1} \quad \textbf{(4.7)}$$

(4) Update Error Covariance matrixes

$$P_k = (I - K_k H)P_k^- \quad \textbf{(4.8)}$$

(5) Estimate system equation;

$$\hat{x}_k = \hat{x}_k^- + K_k(z_k - H\hat{x}_k^-)u_k \quad \textbf{(4.9)}$$

Where P^- priori estimate error covariance matrix and P is the posteriori error covariance matrix.

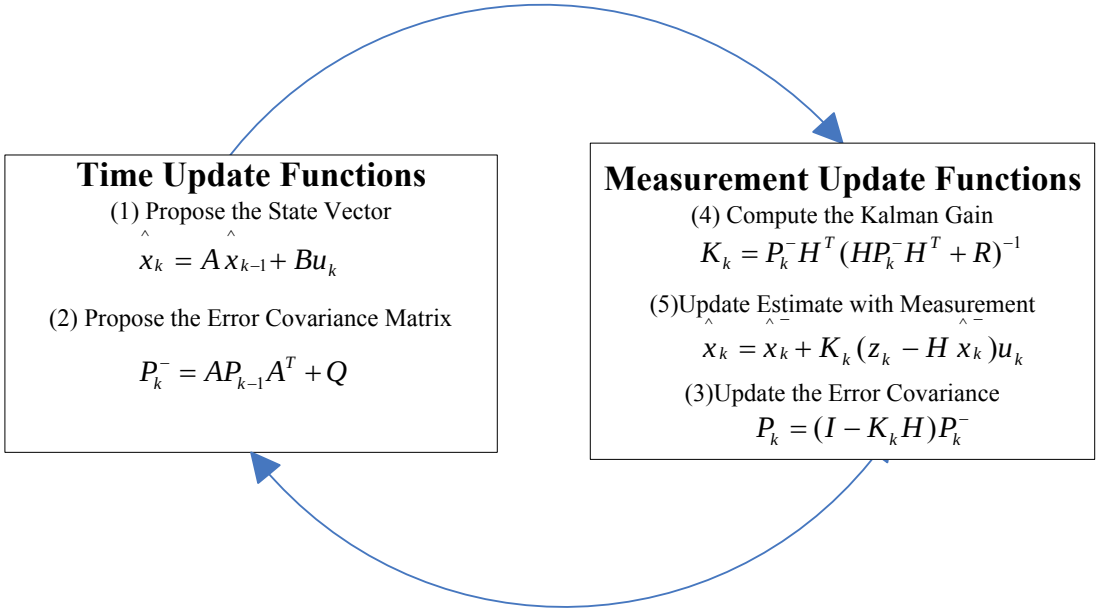

Figure 4.1 Time and Measurement Update Equations

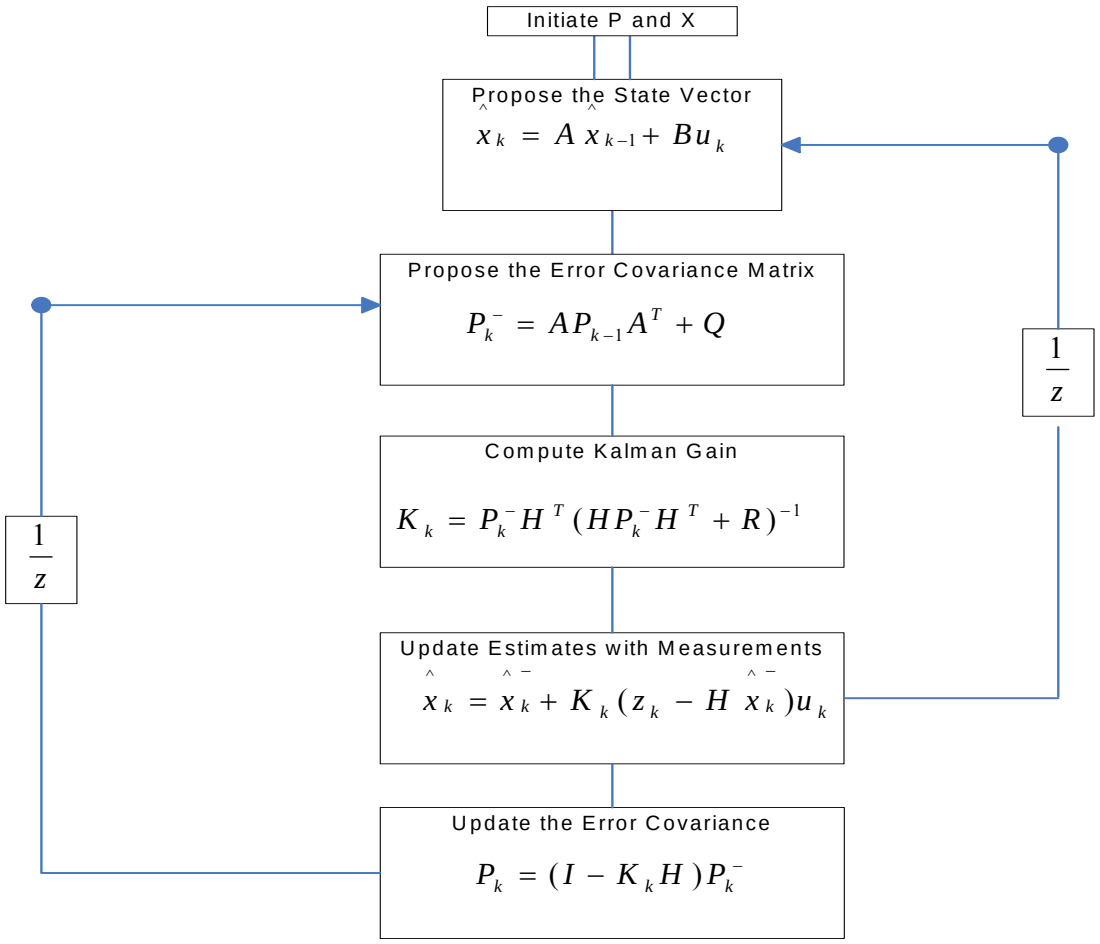

Figure 4.2 Discrete Kalman Filter Algorithm

4.2 Extended Kalman Filter (EKF)

As described in the previous section, kalman filters are used in linear models. EKF is used for nonlinear models by deriving the nonlinear system matrix. System equation for nonlinear system is;

$$x_{k+1|k} = \phi(k+1, k, x_{k|k+1}, u_k) + w_k \quad \textbf{(4.10)}$$

$$z_k = h_e(x_k, u_k) + v_k \quad \textbf{(4.11)}$$

Where ϕ and h_e are nonlinear functions of the system. In order to adapt these nonlinear equations to Kalman Filter algorithm equations should be linearized by derivation.

$$\phi_{k+1} = \left.\frac{d\phi(k, x_k, u_k)}{dx_k}\right|_{x_k = \hat{x}} \quad \textbf{(4.12)}$$

$$H_k = \left.\frac{dh(k, x_k)}{dx_k}\right|_{x_k = \hat{x}_k} \quad \textbf{(4.13)}$$

So linearized state space model is;

$$x_{k+1} = \phi(k, x_k, u_k) + w_k \quad \textbf{(4.14)}$$

$$y = h(k, x_k) + v_k \quad \textbf{(4.15)}$$

We divide the algorithm into two parts; time update and measurement update equations. So, recursive algorithm steps are;

(0) propose the initial conditions P_0 *and* x_0

(1) Propose the state vector

$$x_{k+1|k} = \phi(k+1, k, x_{k|k+1}, u_k) \quad \textbf{(4.16)}$$

(2) Propose the Error Covariance Matrix

$$P_{k+1|k} = \frac{d\phi}{dx}\Big|_{x=x_k|k} P_{k|k} \frac{d\phi}{dx}^T \Big|_{x=x_k k} + Q \tag{4.17}$$

(3) Compute the Kalman Gain

$$K_k = P_{k|k-1} \frac{dh}{dx}^T \Big|_{x=x|k-1} \left(\frac{dh}{dx}\Big|_{x=x_{k-1}} P_{k|k-1} \frac{dh}{dx}^T \Big|_{x=x|k-1} + R \right)^{-1} \tag{4.18}$$

(4) Update Error Covariance matrixes

$$P_{k|k} = P_{k|k-1} - K_k \frac{dh}{dx}\Big|_{x=x_{k|k-1}} P_{k|k-1} \tag{4.19}$$

(5) Estimate system equation;

$$x_{k|k} = x_{k|k-1} + K_k (y_k - h(x_{k|k-1}, k)) \tag{4.20}$$

Where

$$\phi(k+1, k, x_{k|k-1}, u_k) = A_k(x_{k|k}) x_{k|k} + B_k(x_{k|k}) u_k \tag{4.21}$$

These are the system vector and the output vector respectively, and they can be calculated.

$$x_{k+1} = f(k, x_k, u_k) + w_k = A(x_k) x_k + B u_k + w_k \tag{4.22}$$

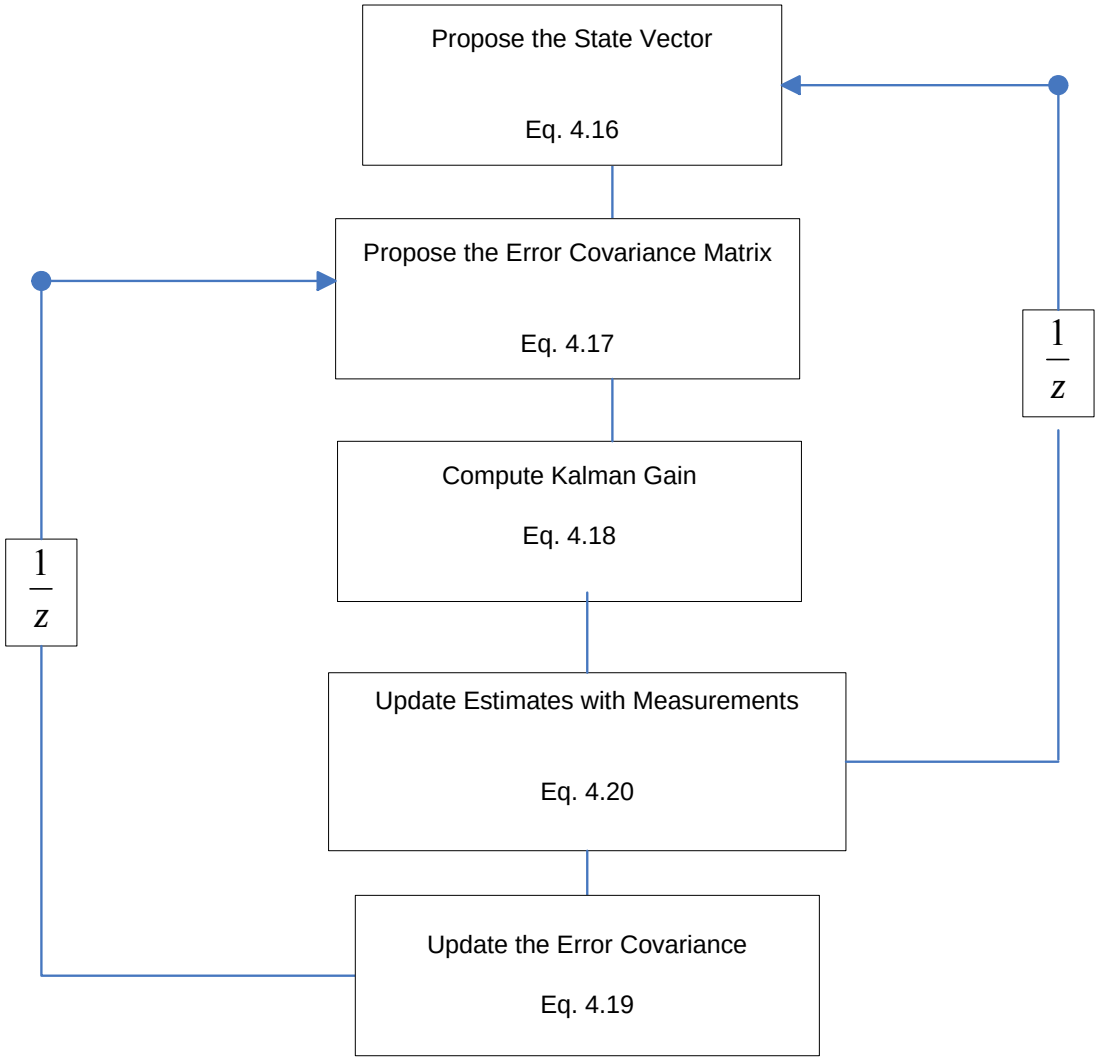

Figure 4.3 EKF Algorithm

4.3 Extended Kalman Filter Based SCIM Observer with Load Estimation

In order to apply EKF based SCIM observer, first nonlinear dynamic model of SCIM will be written. As stated in chapter 2 in detail, SCIM mathematical model is a fifth order nonlinear, parameter varying and multivariable. EKF based observers give convenient results, so load equation of SCIM is also added to system matrix. In the literature EKF based SCIM observer is usually fifth order and speed is defined as a parameter. There are also studies that use mechanical expressions to estimate the speed in order to increase speed estimation performance at steady state conditions. Besides, SCIM mathematical model will be expanded and load also be estimated with a 6th order system matrix.

Discretized SCIM model expanded with load expressions;

$$\begin{pmatrix} i_{s\alpha}(k+1) \\ i_{s\beta}(k+1) \\ \psi_{r\alpha}(k+1) \\ \psi_{r\beta}(k+1) \\ \omega_m(k+1) \\ T_L(k+1) \end{pmatrix} = \begin{pmatrix} 1-a_2-a_3 & 0 & a_4 & a_5 w_m & 0 & 0 \\ 0 & 1-a_2-a_3 & -a_5 w_m & a_4 & 0 & 0 \\ a7 & 0 & 1-a_6 & -a_8 w_m & 0 & 0 \\ 0 & a_7 & a_8 w_m & 1-a_6 & 0 & 0 \\ -a_{10}\psi_{r\beta} & a_{10}\psi_{r\alpha} & 0 & 0 & 1 & -a_9 \\ 0 & 0 & 0 & 0 & 0 & 1 \end{pmatrix}$$

$$\begin{pmatrix} i_{s\alpha}(k) \\ i_{s\beta}(k) \\ \psi_{r\alpha}(k) \\ \psi_{r\beta}(k) \\ \omega_m(k) \\ T_L(k) \end{pmatrix} + \begin{pmatrix} a_1 & 0 \\ 0 & a_1 \\ 0 & 0 \\ 0 & 0 \\ 0 & 0 \\ 0 & 0 \end{pmatrix} \begin{pmatrix} V_{s\alpha} \\ V_{s\beta} \end{pmatrix} + w_k \qquad \textbf{(4.23)}$$

$$a_1 = \frac{T}{L_s - \frac{{L_m}^2}{Lr}}\ , \qquad a_2 = R_s a_1\ , \quad a_3 = \frac{{L_m}^2 R_r a_1}{{L_r}^2}\ , \qquad a_4 = \frac{a_3}{L_m}$$

$$a_5 = \frac{L_m p a_1}{L_r}, \qquad a_6 = \frac{R_r T}{L_r} \qquad a_7 = L_m a_6, \qquad a_8 = pT\ ,$$

$$a_9 = \frac{T}{J} \qquad a_{10} = \frac{1.5 p a_9 L_m}{L_r}$$

$$\phi = \begin{pmatrix} 1-a_2-a_3 & 0 & a_4 & a_5 w_m & 0 & 0 \\ 0 & 1-a_2-a_3 & -a_5 w_m & a_4 & 0 & 0 \\ a7 & 0 & 1-a_6 & -a_8 w_m & 0 & 0 \\ 0 & a_7 & a_8 w_m & 1-a_6 & 0 & 0 \\ -a_{10}\psi_{r\beta} & a_{10}\psi_{r\alpha} & 0 & 0 & 1 & -a_9 \\ 0 & 0 & 0 & 0 & 0 & 1 \end{pmatrix} \qquad \textbf{(4.24)}$$

$$\frac{d\phi}{dx} = \begin{pmatrix} 1-a_2-a_3 & 0 & a_4 & a_5 w_m & a_5\psi_{r\beta} & 0 \\ 0 & 1-a_2-a_3 & -a_5 w_m & a_4 & -a_5\psi_{r\alpha} & 0 \\ a7 & 0 & 1-a_6 & -a_8 w_m & -a_8\psi_{r\beta} & 0 \\ 0 & a_7 & a_8 w_m & 1-a_6 & a_8\psi_{r\alpha} & 0 \\ -a_{10}\psi_{r\beta} & a_{10}\psi_{r\alpha} & a_{10} i_{s\beta} & -a_{10} i_{s\alpha} & 1 & -a_9 \\ 0 & 0 & 0 & 0 & 0 & 1 \end{pmatrix} \qquad \textbf{(4.25)}$$

EKF algorithm proposed in (Barut,2003) is given below.

(0) propose the initial conditions P_0 *and* x_0

(1) Propose the state vector

$$\hat{x}_k^- = f(k, \hat{x}_{k-1}, u_k) \tag{4.26}$$

(2) Propose the Error Covariance Matrix

$$P_k^- = \frac{d\phi}{dx} P_{k-1} \frac{d\phi}{dx}^T + Q \tag{4.27}$$

(3) Update Error Covariance matrixes

$$P_k = P_k^- - P_k^- H^T \left[H P_k^- H^T + R \right]^{-1} H P_k^- \tag{4.28}$$

(4) Compute the Kalman Gain

$$K_k = P_k H^T R^{-1} \tag{4.29}$$

(5) Estimate system equation;

$$\hat{x}_k = \hat{x}_k^- + K_k (y_k - h(x_{k|k-1}, k) \tag{4.30}$$

EKF Algorithm with load estimation proposed in (Barut, 2003) is simulated in Matlab/Simulink. Simulations Results are in Appendix C1.

4.4 EKF with Rotor Resistance Estimation

As explained in the beginning of this chapter estimation of rotor and stator resistances is very important to achieve high performance control in a wide speed range. A seventh order EKF based observer is achieved to estimate rotor resistance as well as estimating speed and load torque.

Discretized SCIM model expanded with load and rotor resistance expressions;

$$\begin{pmatrix} i_{s\alpha}(k+1) \\ i_{s\beta}(k+1) \\ \psi_{r\alpha}(k+1) \\ \psi_{r\beta}(k+1) \\ \omega_m(k+1) \\ T_L(k+1) \\ R_r(k+1) \end{pmatrix} = \begin{pmatrix} 1-a_2R_r(k)-a_4 & 0 & a_3R_r(k) & a_5w_m & 0\ 0 & 0 \\ 0 & 1-a_2R_r(k)-a_4 & -a_5w_m & a_3R_r(k) & 0\ 0 & 0 \\ a_7R_r(k) & 0 & 1-a_6R_r(k) & -a_8w_m & 0\ 0 & 0 \\ 0 & a_7R_r(k) & a_8w_m & 1-a_6R_r(k) & 0\ 0 & 0 \\ -a_9\psi_{r\beta} & a_9\psi_{r\alpha} & 0 & 0 & 1\ -a_{10} & 0 \\ 0 & 0 & 0 & 0 & 0\ 1 & 0 \\ 0 & 0 & 0 & 0 & 0\ 0 & 1 \end{pmatrix}$$

$$\begin{pmatrix} i_{s\alpha}(k) \\ i_{s\beta}(k) \\ \psi_{r\alpha}(k) \\ \psi_{r\beta}(k) \\ \omega_m(k) \\ T_L(k) \\ R_r(k) \end{pmatrix} + \begin{pmatrix} a_1 & 0 \\ 0 & a_1 \\ 0 & 0 \\ 0 & 0 \\ 0 & 0 \\ 0 & 0 \\ 0 & 0 \end{pmatrix} \begin{pmatrix} V_{s\alpha} \\ V_{s\beta} \end{pmatrix} + w_k \qquad \textbf{(4.31)}$$

$$a_1 = \frac{T_s}{L_s - L_m{}^2 / L_r} \qquad a_2 = \frac{L_m{}^2 a_1}{L_r{}^2} \qquad a_3 = \frac{a_2}{L_m} \qquad a_4 = R_s a_1 \qquad a_5 = \frac{L_m p a_1}{L_r}$$

$$a_6 = \frac{T_s}{L_r} \qquad a_7 = L_m a_6 \qquad a_8 = pT_s \qquad a_9 = \frac{1.5 p a_7}{J} \qquad a_{10} = \frac{T_s}{J_L}$$

$$\phi = \begin{pmatrix} 1-a_2R_r(k)-a_4 & 0 & a_3R_r(k) & a_5w_m(k) & 0\ 0 & 0 \\ 0 & 1-a_2R_r(k)-a_4 & -a_5w_m(k) & a_3R_r(k) & 0\ 0 & 0 \\ a_7R_r(k) & 0 & 1-a_6R_r(k) & -a_8w_m(k) & 0\ 0 & 0 \\ 0 & a_7R_r(k) & a_8w_m(k) & 1-a_6R_r(k) & 0\ 0 & 0 \\ -a_9\psi_{r\beta}(k) & a_9\psi_{r\alpha}(k) & 0 & 0 & 1\ -a_{10} & 0 \\ 0 & 0 & 0 & 0 & 0\ 1 & 0 \\ 0 & 0 & 0 & 0 & 0\ 0 & 1 \end{pmatrix} \qquad \textbf{(4.32)}$$

$$\frac{d\phi}{dx} = \begin{pmatrix} 1-a_2R_r(k)-a_4 & 0 & a_3R_r(k) & a_5w_m(k) & a_5\psi_{r\beta}(k) & 0 & -a_2i_{s\alpha}(k)+a_3\psi_{r\alpha}(k) \\ 0 & 1-a_2R_r(k)-a_4 & -a_5w_m(k) & a_3R_r(k) & -a_5\psi_{r\alpha}(k) & 0 & -a_2i_{s\beta}(k)+a_3\psi_{r\beta}(k) \\ a_7R_r(k) & 0 & 1-a_6R_r(k) & -a_8w_m(k) & -a_8\psi_{r\beta}(k) & 0 & a_7i_{s\alpha}(k)-a_6\psi_{r\alpha}(k) \\ 0 & a_7R_r(k) & a_8w_m(k) & 1-a_6R_r(k) & a_8\psi_{r\alpha}(k) & 0 & a_7i_{s\beta}(k)-a_6\psi_{r\beta}(k) \\ -a_9\psi_{r\beta}(k) & a_9\psi_{r\alpha}(k) & a_9i_{s\beta}(k) & -a_9i_{s\alpha}(k) & 1 & -a_{10} & 0 \\ 0 & 0 & 0 & 0 & 0 & 1 & 0 \\ 0 & 0 & 0 & 0 & 0 & 0 & 1 \end{pmatrix}$$

(4.32)

Simulation Results are in Appendix C2

4.5 EKF with Stator Resistance Estimation

Stator resistance variations because of temperature also affect high performance sensorless control of SCIM. Besides, accurate estimation of stator resistance is vital to achieve Direct Torque Control which is stator flux oriented vector control. So, Stator resistance is also estimated with EKF algorithm as well as estimating load torque and speed by using seventh order SCIM model.

Discretized SCIM model expanded with load and Stator resistance expressions;

$$\begin{pmatrix} i_{s\alpha}(k+1) \\ i_{s\beta}(k+1) \\ \psi_{r\alpha}(k+1) \\ \psi_{r\beta}(k+1) \\ \omega_m(k+1) \\ T_L(k+1) \\ R_s(k+1) \end{pmatrix} = \begin{pmatrix} 1-a_2R_r-a_1R_s(k) & 0 & a_3R_r & a_5w_m(k) & 0 & 0 & 0 \\ 0 & 1-a_2R_r-a_1R_s(k) & -a_5w_m(k) & a_3 & 0 & 0 & 0 \\ a_7R_r & 0 & 1-a_6R_r & -a_8w_m(k) & 0 & 0 & 0 \\ 0 & a_7R_r & a_8w_m(k) & 1-a_6R_r(k) & 0 & 0 & 0 \\ -a_9\psi_{r\beta}(k) & a_9\psi_{r\alpha}(k) & 0 & 0 & 1 & -a_{10} & 0 \\ 0 & 0 & 0 & 0 & 0 & 1 & 0 \\ 0 & 0 & 0 & 0 & 0 & 0 & 1 \end{pmatrix}$$

$$\begin{pmatrix} i_{s\alpha}(k) \\ i_{s\beta}(k) \\ \psi_{r\alpha}(k) \\ \psi_{r\beta}(k) \\ \omega_m(k) \\ T_L(k) \\ R_s(k) \end{pmatrix} + \begin{pmatrix} a_1 & 0 \\ 0 & a_1 \\ 0 & 0 \\ 0 & 0 \\ 0 & 0 \\ 0 & 0 \\ 0 & 0 \end{pmatrix} \begin{pmatrix} V_{s\alpha} \\ V_{s\beta} \end{pmatrix} + w_k \qquad \textbf{(4.33)}$$

$$\phi = \begin{pmatrix} 1-a_2R_r-a_1R_s(k) & 0 & a_3R_r & a_5w_m(k) & 0 & 0 & 0 \\ 0 & 1-a_2R_r-a_1R_s(k) & -a_5w_m(k) & a_3 & 0 & 0 & 0 \\ a_7R_r & 0 & 1-a_6R_r & -a_8w_m(k) & 0 & 0 & 0 \\ 0 & a_7R_r & a_8w_m(k) & 1-a_6R_r & 0 & 0 & 0 \\ -a_9\psi_{r\beta}(k) & a_9\psi_{r\alpha}(k) & 0 & 0 & 1 & -a_{10} & 0 \\ 0 & 0 & 0 & 0 & 0 & 1 & 0 \\ 0 & 0 & 0 & 0 & 0 & 0 & 1 \end{pmatrix} \qquad \textbf{(4.34)}$$

$$\frac{d\phi}{dx}=\begin{pmatrix} 1-a_2R_r-a_1R_s(k) & 0 & a_3R_r & a_5w_m & a_5\psi_{r\beta} & 0 & -a_1i_{s\alpha}(k) \\ 0 & 1-a_2R_r-a_1R_s(k) & -a_5w_m(k) & a_3R_r(k) & -a_5\psi_{r\alpha} & 0 & -a_1i_{s\beta}(k) \\ a_7R_r & 0 & 1-a_6R_r & -a_8w_m & -a_8\psi_{r\beta} & 0 & 0 \\ 0 & a_7R_r & a_8w_m(k) & 1-a_6R_r & a_8\psi_{r\alpha} & 0 & 0 \\ -a_9\psi_{r\beta}(k) & a_9\psi_{r\alpha}(k) & a_9i_{s\beta}(k) & -a_9i_{s\alpha}(k) & 1 & -a_{10} & 0 \\ 0 & 0 & 0 & 0 & 0 & 1 & 0 \\ 0 & 0 & 0 & 0 & 0 & 0 & 0 \end{pmatrix} \quad \textbf{(4.35)}$$

Simulation Results are in Appendix C3

4.6 Simultaneous Stator and Rotor Resistance Estimation with EKF

There are only few studies that simultaneously estimate stator and rotor resistances. Braided EKF algorithm in (Barut, 2008) is achieved in order to estimate stator and rotor resistances simultaneously. Two EKF algorithms which are in the same configuration except for the seventh state executes in an appropriate order. One algorithm is estimating stator resistance (EKF_S), while the other is estimating rotor resistance (EKF_R). Estimated rotor and stator resistance values are passed into the other EKF algorithm in the next step. The major constraint in this algorithm is the increased computational complexity. So, study in (Barut, 2008) starts and stops each EKF algorithm at each time step (100 μs).

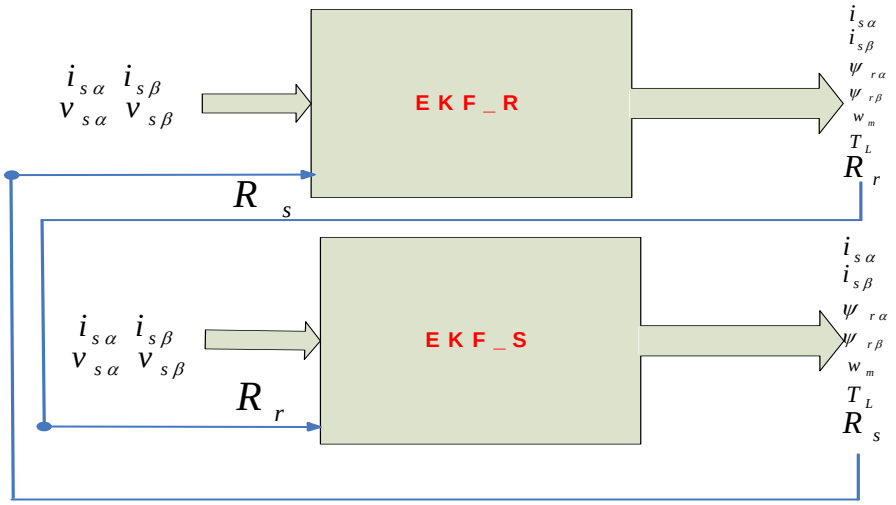

Figure 4.4 Braided EKF Algorithm

In this study, 8th order EKF based SCIM estimator which is simultaneously estimating rotor and stator resistances as well as flux, speed and load torque is also tried.

Discretized SCIM model expanded with simultaneous stator and rotor resistance expressions;

$$\begin{pmatrix} i_{s\alpha}(k+1) \\ i_{s\beta}(k+1) \\ \psi_{r\alpha}(k+1) \\ \psi_{r\beta}(k+1) \\ \omega_m(k+1) \\ T_L(k+1) \\ R_r(k+1) \\ R_s(k+1) \end{pmatrix} = \begin{pmatrix} 1-a_2R_r(k)-a_1R_s(k) & 0 & a_3R_r(k) & a_5w_m & 0 \\ 0 & 1-a_2R_r(k)-a_1R_s(k) & -a_5w_m & a_3R_r(k) & 0 \\ a_7R_r(k) & 0 & 1-a_6R_r(k) & -a_8w_m & 0 \\ 0 & a_7R_r(k) & a_8w_m & 1-a_6R_r(k) & 0 \\ -a_9\psi_{r\beta} & a_9\psi_{r\alpha} & 0 & 0 & 1 \\ 0 & 0 & 0 & 0 & 0 \\ 0 & 0 & 0 & 0 & 0 \\ 0 & 0 & 0 & 0 & 0 \end{pmatrix}$$

$$\begin{pmatrix} 0 & 0 & 0 \\ 0 & 0 & 0 \\ 0 & 0 & 0 \\ 0 & 0 & 0 \\ -a_{10} & 0 & 0 \\ 1 & 0 & 0 \\ 0 & 1 & 0 \\ 0 & 0 & 1 \end{pmatrix} \begin{pmatrix} i_{s\alpha}(k) \\ i_{s\beta}(k) \\ \psi_{r\alpha}(k) \\ \psi_{r\beta}(k) \\ \omega_m(k) \\ T_L(k) \\ R_r(k) \\ R_s(k) \end{pmatrix} + \begin{pmatrix} a_1 & 0 \\ 0 & a_1 \\ 0 & 0 \\ 0 & 0 \\ 0 & 0 \\ 0 & 0 \\ 0 & 0 \\ 0 & 0 \end{pmatrix} \begin{pmatrix} V_{s\alpha} \\ V_{s\beta} \end{pmatrix} + w_k \qquad \textbf{(4.36)}$$

$$\phi = \begin{pmatrix} 1-a_2R_r(k)-a_1R_s(k) & 0 & a_3R_r(k) & a_5w_m & 0 & 0 & 0 & 0 \\ 0 & 1-a_2R_r(k)-a_1R_s(k) & -a_5w_m & a_3R_r(k) & 0 & 0 & 0 & 0 \\ a_7R_r(k) & 0 & 1-a_6R_r(k) & -a_8w_m & 0 & 0 & 0 & 0 \\ 0 & a_7R_r(k) & a_8w_m & 1-a_6R_r(k) & 0 & 0 & 0 & 0 \\ -a_9\psi_{r\beta} & a_9\psi_{r\alpha} & 0 & 0 & 1 & -a_{10} & 0 & 0 \\ 0 & 0 & 0 & 0 & 0 & 1 & 0 & 0 \\ 0 & 0 & 0 & 0 & 0 & 0 & 1 & 0 \\ 0 & 0 & 0 & 0 & 0 & 0 & 0 & 1 \end{pmatrix}$$

(4.37)

$$\frac{d\phi}{dx} = \begin{pmatrix} 1-a_2R_r(k)-a_1R_s(k) & 0 & a_3R_r(k) & a_5w_m(k) & a_5\psi_{r\beta}(k) & 0 \\ 0 & 1-a_2R_r(k)-a_1R_s(k) & -a_5w_m(k) & a_3R_r(k) & -a_5\psi_{r\alpha}(k) & 0 \\ a_7R_r(k) & 0 & 1-a_6R_r(k) & -a_8w_m(k) & -a_8\psi_{r\beta}(k) & 0 \\ 0 & a_7R_r(k) & a_8w_m(k) & 1-a_6R_r(k) & a_8\psi_{r\alpha}(k) & 0 \\ -a_9\psi_{r\beta}(k) & a_9\psi_{r\alpha}(k) & a_9i_{s\beta}(k) & -a_9i_{s\alpha}(k) & 1 & -a_{10} \\ 0 & 0 & 0 & 0 & 0 & 1 \\ 0 & 0 & 0 & 0 & 0 & 0 \\ 0 & 0 & 0 & 0 & 0 & 0 \end{pmatrix}$$

$$\begin{pmatrix} -a_2i_{s\alpha}(k)+a_3\psi_{r\alpha}(k) & -a_1i_{s\alpha}(k) \\ -a_2i_{s\beta}(k)+a_3\psi_{r\beta}(k) & -a_1i_{s\beta}(k) \\ a_7i_{s\alpha}(k)-a_6\psi_{r\alpha}(k) & 0 \\ a_7i_{s\beta}(k)-a_6\psi_{r\beta}(k) & 0 \\ 0 & 0 \\ 0 & 0 \\ 1 & 0 \\ 0 & 1 \end{pmatrix} \quad \textbf{(4.32)}$$

Algorithm is simulated by simultaneously changing stator and rotor resistances as well as different loading conditions. Simulation results are in Appendix ??

4.7 EKF in Direct Vector Control

EKF based observer can also be used with the direct vector control algorithm. EKF based observer with direct vector control block diagram is in the Figure 4.5. Simulation Results are in Appendix D2.

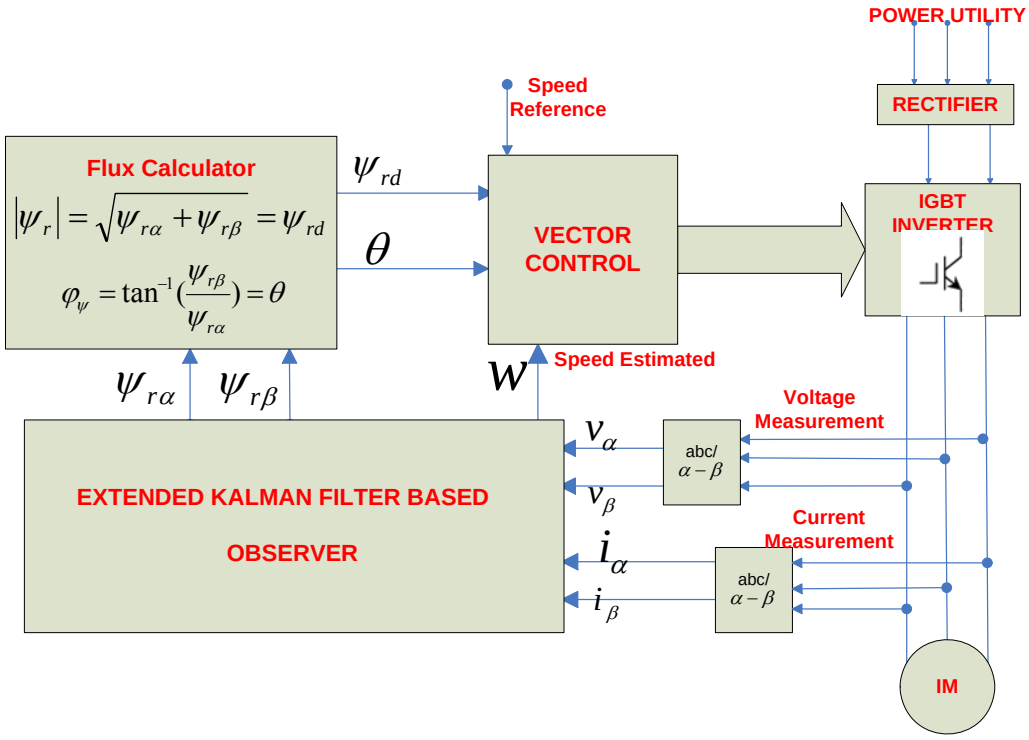

Figure 4.5 EKF with Direct Vector Control.

4.8 Conclusion

EKF algorithm can be analyzed as follows;

Stability: For linear and dynamic systems stability of Kalman Filters were proved by Kalman. Extended Kalman Filter (EKF) stability is not certain. But, EKF for speed and load estimation (or determination) of Induction Machines have impressive results.

Success: Success of EKF not only depends on the measurement data, but also depends on the correct choice of the covariance matrices. Squirrel Cage Induction machines which are an example of benchmark control because of its nonlinearity and variable parameter behavior such as rotor resistance have impressive results on EKF algorithms for parameter or state estimation.

Implementation: The best known disadvantage of EKF is the computational complexity. It requires high performance processors to implement. Nowadays, innovations on VLSI technology make digital implementation of EKF algorithms available with Digital Signal Processors (DSP)

EKF based observer is introduced in detail and simulated. Simulation Results are in Appendix C. Main constraint of the EKF based SCIM observer is the determination of Q and R constants. Q and R should be chosen correctly in order to get correct results. Besides, these matrices are taken as constants, optimal values of Q and R change in the various speed and load regions in reality. In spite of the constraint of the determination of Q and R matrixes, EKF based observer gives convenient results in the transient and steady state conditions as shown in the Appendix C.

5. ELECTRICAL DRIVE CIRCUITS USED IN SCIM CONTROL

High performance control of SCIM requires changing frequency and voltage applied to the motor in order to control speed and/or torque required. There are various types of frequency and/or voltage converters. The type of the converter depends on the application and the cost. When a high performance control and energy-efficient SCIM drive are required, cost of the circuit increases. If the load requires high dynamic performance such as mills, cranes etc., high performance converter which is processing in a few microseconds and additional regenerative breaking circuit is obliged in order not to damage any equipment because of the high voltages occurring during deceleration or breaking of the motor. High performance control also depends on the performance and quality of the converter as well as the control type and the accuracy of the estimation of electrical and mechanical uncertainties discussed in Chapter 3 and 4. Therefore, understanding the electrical drive circuits used in high performance control of SCIM is essential in order to find the optimal solution for the load requirements. A simple block diagram of the power converter is in the figure 5.1. Cycloconverters and inverter circuits are commonly used in SCIM control by changing the frequency and voltage. With the developed semiconductor technologies voltage source inverters have become more popular last few decades (Bose, 2002).

5.1 Cycloconverters

A Cycloconverter is a power converter that changes amplitude and frequency of input voltage. There are different types of cycloconverter circuits. 3 phases to 3 phase type with 36 thyristors was commonly used in SCIM control. Historically, cycloconverters are the first used converters in AC motor control. A typical three phase bridge cycloconverter with 36 thyristors is in the figure. Each phase group of cycloconverter has a 120 degree phase shift in order to apply a balanced sine wave to the motor. Cycloconverters can be used for high power AC motor applications which does not require wide speed and torque range including zero speed and over speed region such as pumps and fans. Because, cycloconverters operation region is not

wide as inverters as well as its dynamic performance is very poor due to the harmonics generated by the circuit structure.

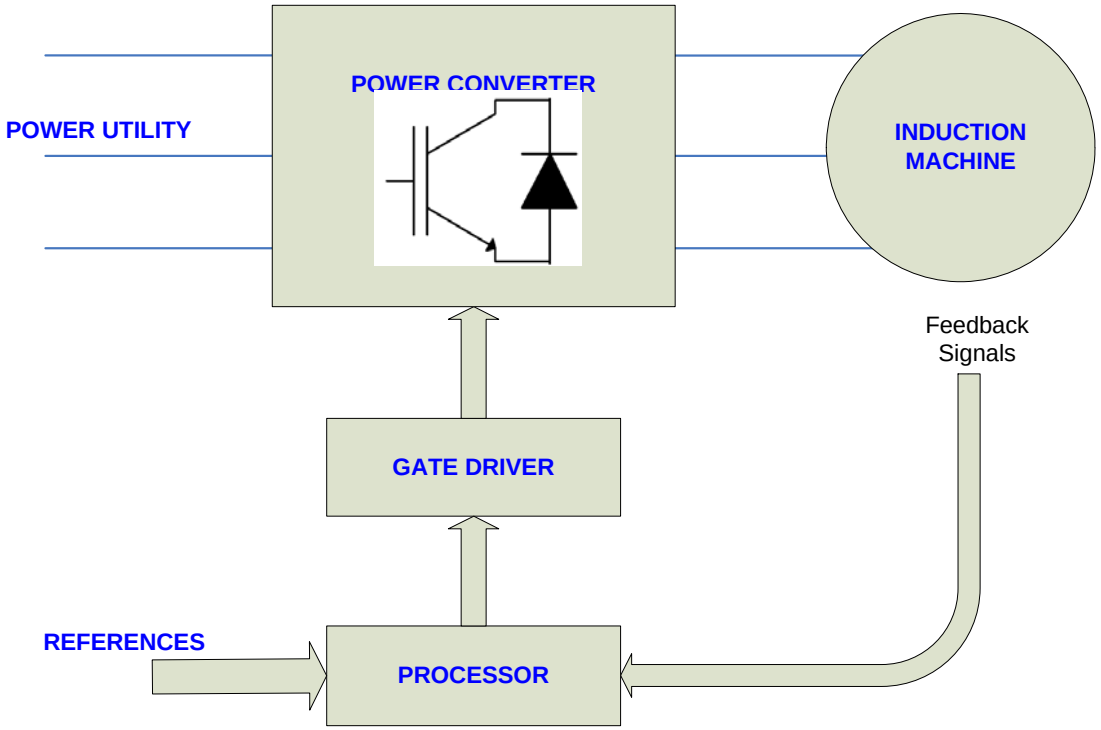

Figure 5.1 Block diagram of the drive system

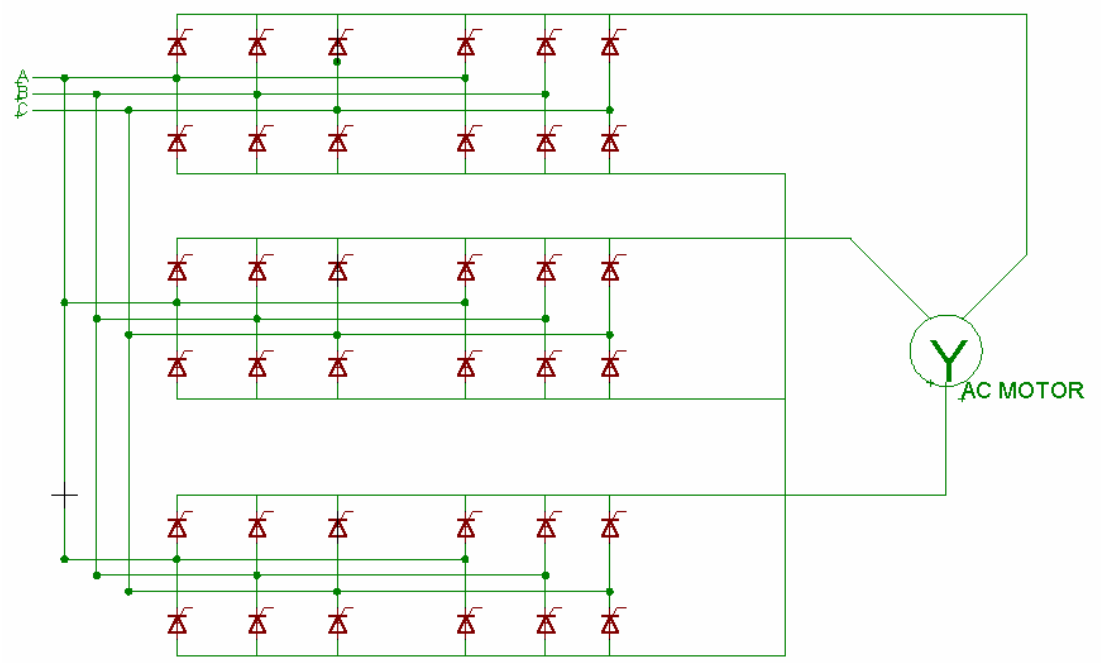

Figure 5.2 A Typical Cycloconverter Circuit

Cycloconverters have some disadvantages compared to the inverters; (Bose, 2002)

- Complex harmonics are generated which needs to be eliminated.
- Line power factor is very poor.
- Motors operated with cycloconververters can not be easily used above line frequency.
- Large inductors that needs to be connected to the motor side increases cost.
- Circulating currents causes additional loads to the thyristors which increases losses.

Because of the disadvantages written above inverter circuits are taking over cycloconverter circuits in the industry.

5.2 Inverters

Inverter circuits receive DC voltage and convert it to determined frequency and voltage level. Inverters consist of two switches for each leg. Turning on and off these switches applies current to the load. Two main types of the inverters are used in SCIM control. Current Source inverters can be used in high power AC motor applications, while two-level voltage source inverters are used in low power applications and three-level inverters in high power AC motor applications.

5.2.1 Current Source Inverters

This type of inverters should not be confused with commonly used current controlled voltage source inverters. A current source inverter is a variable current source with an inductor connected in series controlling the DC voltage with the current feedback loop. Thyristors are generally preferred because of the symmetric voltage blocking property. Asymetric power switches such as IGBTs, MOSFETs and IGCTs require additional series connected diodes as shown in the Figure 5.3

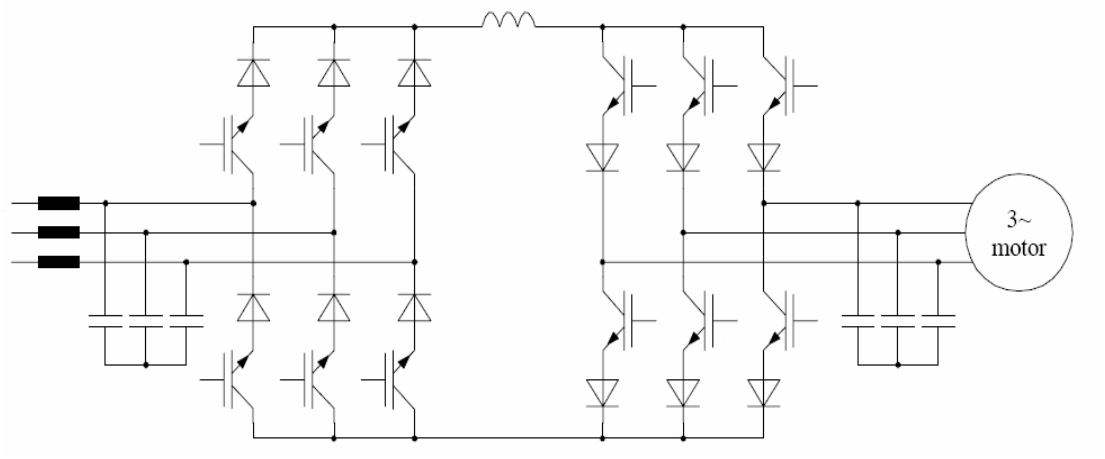

Figure 5.3 A Current Source Inverter with IGBTs

Six step thyristor rectifier and inverter configuration shown in the figure 5.4 can be used at high power AC motor applications. Generated DC variable voltage by 6 pulse thyristor rectifier supplies the series connected inductor.

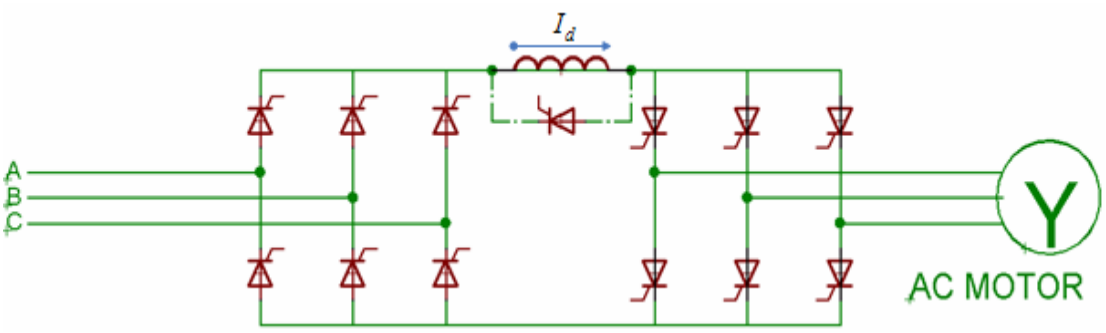

Figure 5.4 A Current Source Inverter with Tyristors

Current component of the motor is adjusted by current (I_d) flowing through the inductor. This current is used in current loop as shown in the figure 5.5. Changing the angle α changes the DC link voltage as well as the current in the load. Ideally, inductor in the DC link should be as large as possible. However, because of the size and cost effects, optimal value of the inductor must be chosen. At steady state conditions, rectifier DC voltage is equal to inverter DC voltage. Therefore, voltage in the inverter is not boosted and current flowing to the load remains constant. CSI output requires additional capacitors in the output due to instantenous voltage spikes occurring in the motor side because of the commutation effect. (Vas, 1990)

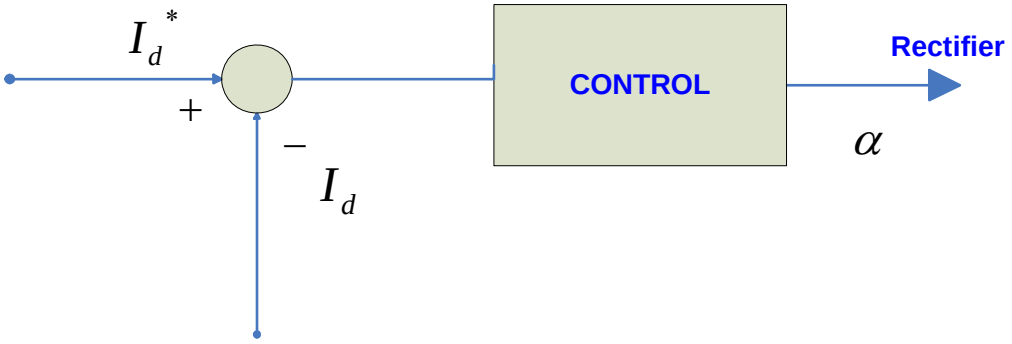

Figure 5.5 Current Source Inverter Current Control Loop

Both CSI types explained above operate with the same basic principle. CSIs have important disadvantages;

- Dynamic performance of CSI is poor compared to the Voltage Source Inverters(VSI)
- CSI can not be operated at no load, while VSI can be operated at no load.
- CSI has to be in closed loop current control, whereas VSI operates open loop
- CSI consists of one rectifier and one inverter. But, multimotor and multi-inverter applications can be used in VSI.

5.2.2 Voltage Source Inverters

Voltage Source Inverters (VSI) are the most preferred inverters in SCIM control due to its high dynamic performance and efficiency. Asymetric power blocking switches such as IGBTs, MOSFETs, GTOs and IGCTs are favorable to use for inverter circuits. IGBTs are preferred at low voltage applications, while IGCTs are the new generation power switches for the medium voltage applications. A rectifier and capacitors supply DC voltage to the inverter in the front end. Generally, this front end can be a passive diode bridge as well as an active front rectifier with an IGBT in order to be energy efficient in four quadrant operation. At low power applications two-level configuration is adequate while three-level inverters are preferred at high power and medium voltage applications.

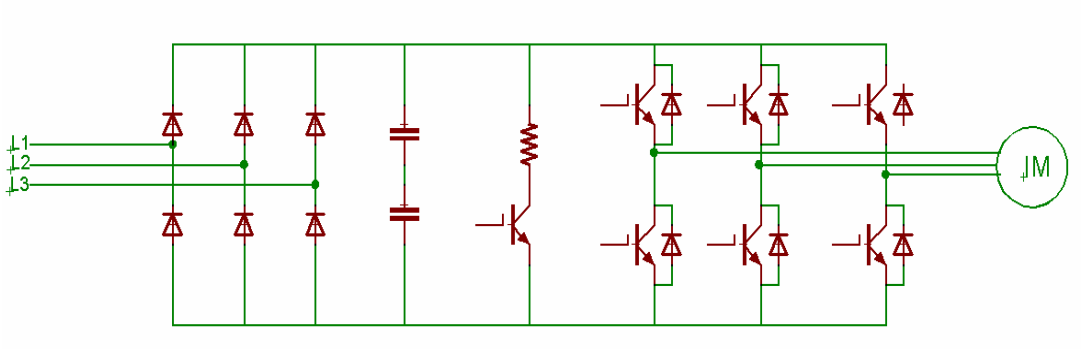

Figure 5.6 A Voltage Source Inverter with diode bridge rectifier

Two level VSI supplied by a diode rectifier requires dynamic braking resistor, and this resistor turns on when regenerative energy coming from inverter side and feeding the DC bus. So, DC bus voltage can be reduced to appropriate level. Addition of freewheeling diodes connected to each IGBTs help to switch off the IGBT by conducting the current during turn off.

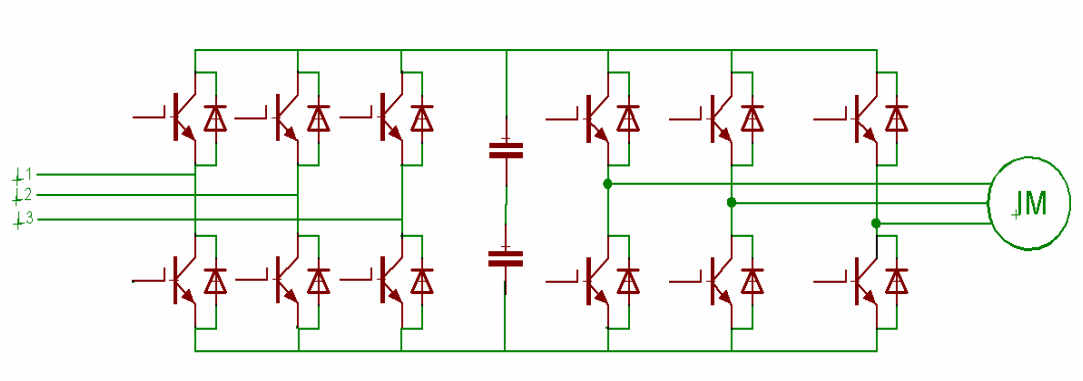

Figure 5.7 A Voltage Source Inverter with IGBT bridge rectifier

In order to be energy-efficient, rectifier circuit can be chosen as active switching devices, and during regeneration mode, IGBT rectifier can operate as an inverter and feeds the utility at certain voltage and frequency level as shown in the figure 5.7

5.3 PWM Methods for VSI

Classical PWM technique for a VSI is sine-triangle PWM method. There are also some other methods in the literature such as Selected Harmonic Elimination, Random PWM, Hysterisis Current Control PWM etc. Although there are numerous PWM techniques in the literature, Space Vector Modulation PWM (SVPWM) is an advanced and the best technique among other PWM techniques. First, conventional

sine-triangle PWM method will briefly be presented. Second, SVPWM will be described in detail.

5.3.1 Sine-Triangle PWM Method

This conventional method basically consists of comparison of fundamental frequency sine wave and triangular control signal. When the triangle signal intersects the fundamental sine wave, switching device turns on. As seen on the figure, the higher the switching frequency, the better the sine wave occurs and reduces the harmonics in the current and voltage. So, torque pulsations due to harmonics in the inverter are reduced.

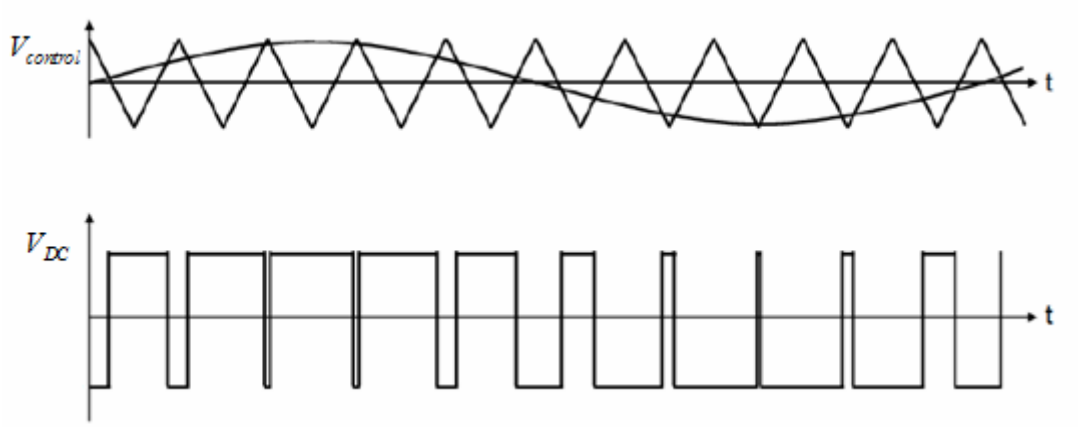

Figure 5.8 A Sine Triangle PWM Method

5.3.2 Space Vector Modulation PWM Method

Space Vector Modulation (SVPWM) is an advanced and complex method that requires a high level processor in order to calculate switching times. This method is a $\alpha - \beta$ transformation based method that at every sampling time (switching frequency) switching times of the power switch is updated. This method has become very popular in recent years due to its high dynamic performance and its only requirement of $V_\alpha \, and \, V_\beta$ references coming from the cascaded controller. These controller can be either a scalar or a vector controller that is discussed in chapter 3. Besides, it is the best of the PWM method among other PWM methods because of the lower harmonics compared to other PWM methods.

5.3.2.1 SVPWM Principle

There are 8(2^3) possible switching states for two level PWM inverters two of which are (S0 and S7) redundant to produce zero output voltage. These 8 possible switching states can be represented in figure 5.9.

These switching states can be related to the line-to-line voltages and phase voltages as follows;

$$\begin{bmatrix} V_{ab} \\ V_{bc} \\ V_{ca} \end{bmatrix} = V_{DC} \begin{bmatrix} 1 & -1 & 0 \\ 0 & 1 & -1 \\ -1 & 0 & 1 \end{bmatrix} \begin{bmatrix} a \\ b \\ c \end{bmatrix} \quad \textbf{(5.1)}$$

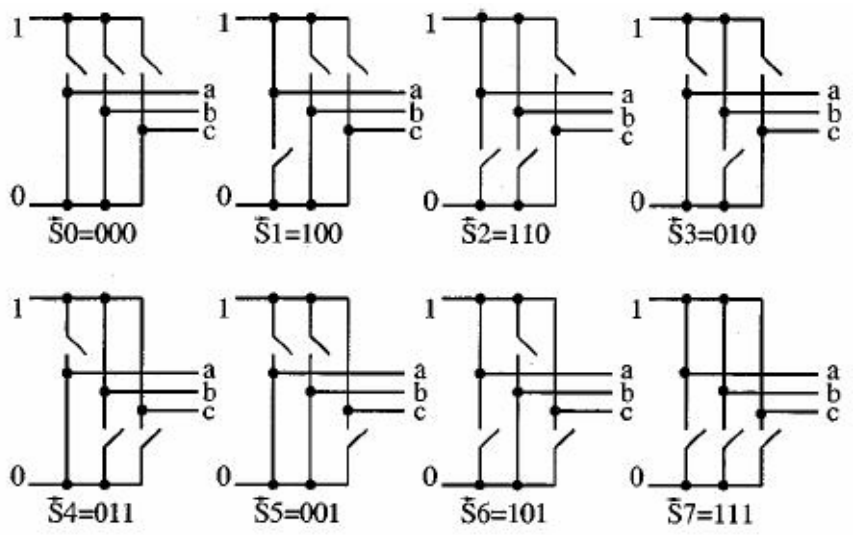

Figure 5.9 8 Possible Switching States

$$\begin{bmatrix} V_{an} \\ V_{bn} \\ V_{cn} \end{bmatrix} = \frac{V_{DC}}{3} \begin{bmatrix} 2 & -1 & -1 \\ -1 & 2 & -1 \\ -1 & -1 & 2 \end{bmatrix} \begin{bmatrix} a \\ b \\ c \end{bmatrix} \quad \textbf{(5.2)}$$

$$V_{ab} = V_a - V_b$$

$$V_{bc} = V_b - V_c \quad \textbf{(5.3)}$$

$$V_{ca} = V_c - V_a$$

$$V_{an} = \frac{(V_{ab} - V_{ca})}{3}$$

$$V_{bn} = \frac{(V_{bc} - V_{ab})}{3} \qquad \textbf{(5.4)}$$

$$V_{cn} = \frac{(V_{ca} - V_{bc})}{3}$$

According to equations (1) and (2) phase voltages and output line to line voltages in terms of DC link can be given as Table 5.1;

Table 5.1 SVPWM Switching Table (Voltages multiplied by V_{DC})

	Switching Vectors			**Line to Neutral Voltage**			**Line to Line Voltage**		
Voltage Vectors	**a**	**b**	**c**	V_{an}	V_{bn}	V_{cn}	V_{ab}	V_{bc}	V_{ca}
V_0	0	0	0	0	0	0	0	0	0
V_1	1	0	0	2/3	-1/3	-1/3	1	0	-1
V_2	1	1	0	1/3	1/3	-2/3	0	1	-1
V_3	0	1	0	-1/3	2/3	-1/3	-1	1	0
V_4	0	1	1	-2/3	1/3	1/3	-1	0	1
V_5	0	0	1	-1/3	-1/3	2/3	0	-1	1
V_6	1	0	1	1/3	-2/3	1/3	1	-1	0
V_7	1	1	1	0	0	0	0	0	0

The aim of SVPWM technique is to calculate the reference voltage vector (V_{ref}) using these 8 switching combinations.

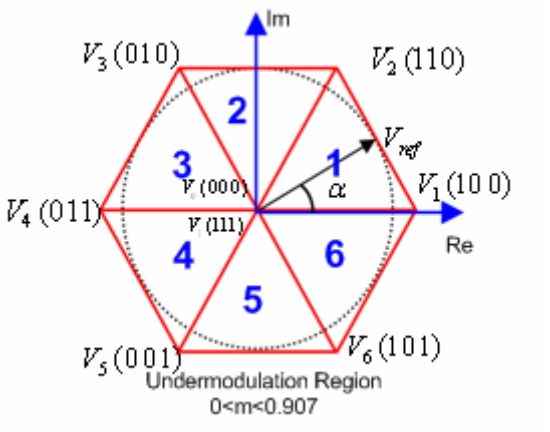

Figure 5.10 SVPWM Switching Sectors

V_{ref} shown in the figure 5.10 rotates in the circular orbit at angular velocity w. The objective of this method is to follow the reference voltage value which rotates in this circular orbit with the harmony of the switching states of the IGBTs. Sectors determine the switching states of the IGBTs and α, the angle value between real (α) and imaginary (β) axis determines the switching times. Determination of switching vectors can be implemented with 3 steps.

1. Determine the $V_\alpha, V_\beta, V_{ref}$ and angle (α)

$$\begin{bmatrix} V_\alpha \\ V_\beta \end{bmatrix} = \frac{2}{3}\begin{bmatrix} 1 & -\frac{1}{2} & -\frac{1}{2} \\ 0 & \frac{\sqrt{3}}{2} & -\frac{\sqrt{3}}{2} \end{bmatrix}\begin{bmatrix} V_{an} \\ V_{bn} \\ V_{cn} \end{bmatrix} \quad \textbf{(5.5)}$$

$$|V_{ref}| = \sqrt{V_\alpha{}^2 + V_\beta{}^2} \quad \textbf{(5.6)}$$

$$\alpha = \tan^{-1}(\frac{V_\beta}{V_\alpha}) = wt = 2\pi ft \quad \textbf{(5.7)}$$

f=fundamental frequency

***2.* Determination of T_1, T_2 and T_0**

Switching time duration at Sector 1;

$$T_z|V_{ref}|\begin{bmatrix} \cos(\alpha) \\ \sin(\alpha) \end{bmatrix} = T_1\frac{2}{3}V_{DC}\begin{bmatrix} 1 \\ 0 \end{bmatrix} + T_2\frac{2}{3}V_{DC}\begin{bmatrix} \cos(\pi/3) \\ \sin(\pi/3) \end{bmatrix} \quad \textbf{(5.8)}$$

Where, $0 \le \alpha \le 60$

$$T_1 = T_z m \frac{\sin(\pi/3 - \alpha)}{\sin(\pi/3)} \quad \textbf{(5.9)}$$

$$T_2 = T_z m \frac{\sin(\alpha)}{\sin(\pi/3)} \quad \textbf{(5.10)}$$

$$T_0 = T_Z - (T_1 + T_2)$$

Where, $T_z = \frac{1}{f_z}$ and

$$m = \frac{|V_{ref}|}{\frac{2}{3}V_{DC}} \text{ (Modulation index)} \quad \textbf{(5.11)}$$

Switching time duration at any sector;

$$T_1 = \frac{\sqrt{3}T_Z|V_{ref}|}{V_{DC}}\left(\sin\left(\frac{\pi}{3} - \alpha + \frac{n-1}{3}\pi\right)\right) \quad \textbf{(5.12)}$$

$$T_2 = \frac{\sqrt{3}T_Z|V_{ref}|}{V_{DC}}\left(\sin\left(\alpha - \frac{n-1}{3}\pi\right)\right) \quad \textbf{(5.13)}$$

$$T_0 = T_z - T_1 - T_2 \quad \textbf{(5.14)}$$

Where n=1 through 6 means that Sector 1 to 6

***3.* Determination of Switching Time of Each Switch**

Table 4.2 is presented to determine switching time calculations at each sector. PWM switching patterns are produced according to figure 5.11 at each sector.

5.3.2.2 Undermodulation or Linear Region

The equations given above are valid for the linear region of the inverter. Linear region or the undermodulation region means the region which is inside the hexagon. This linear region ends in the upper limit of the hexagon. If the modulation index is formulated as;

$$m = \frac{|V_{ref}|}{\frac{2}{3}V_{DC}} \tag{5.11}$$

Table 5.2: Switching Time Calculation At Each Sector

Sector	Upper Switches	Lower Switches
1	$S_1 = T_1 + T_2 + T_0/2$ $S_3 = T_2 + T_0/2$ $S_5 = T_0/2$	$S_4 = T_0/2$ $S_6 = T_1 + T_0/2$ $S_2 = T_1 + T_2 + T_0/2$
2	$S_1 = T_1 + T_0/2$ $S_3 = T_1 + T_2 + T_0/2$ $S_5 = T_0/2$	$S_4 = T_2 + T_0/2$ $S_6 = T_0/2$ $S_2 = T_1 + T_2 + T_0/2$
3	$S_1 = T_0/2$ $S_3 = T_1 + T_2 + T_0/2$ $S_5 = T_2 + T_0/2$	$S_4 = T_1 + T_2 + T_0/2$ $S_6 = T_0/2$ $S_2 = T_1 + T_0/2$
4	$S_1 = T_0/2$ $S_3 = T_1 + T_0/2$ $S_5 = T_1 + T_2 + T_0/2$	$S_4 = T_1 + T_2 + T_0/2$ $S_6 = T_2 + T_0/2$ $S_2 = T_0/2$
5	$S_1 = T_2 + T_0/2$ $S_3 = T_0/2$ $S_5 = T_1 + T_2 + T_0/2$	$S_4 = T_1 + T_0/2$ $S_6 = T_1 + T_2 + T_0/2$ $S_2 = T_0/2$
6	$S_1 = T_1 + T_2 + T_0/2$ $S_3 = T_0/2$ $S_5 = T_1 + T_0/2$	$S_4 = T_0/2$ $S_6 = T_1 + T_2 + T_0/2$ $S_2 = T_2 + T_0/2$

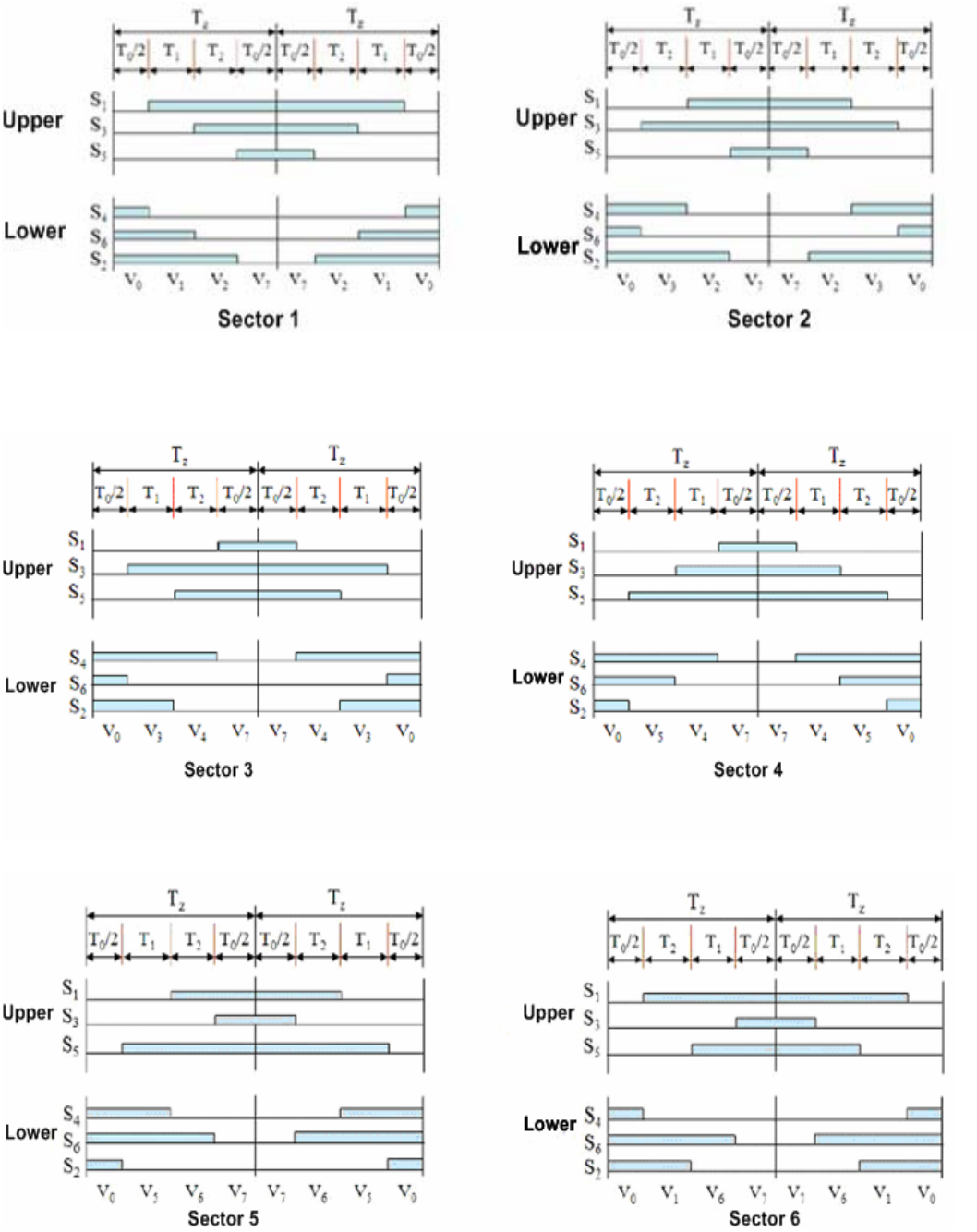

Figure 5.11 PWM Switching Patterns at Each Sector

Maximum value of modulation index is approximately 0.907 which means that 90.7 percent of DC bus available in linear region for PWM generation, while only 78 percent in conventional sine-triangular PWM techniques.

5.3.2.3 Overmodulation Region

Zero voltage time increases when the reference voltage increases. Overmodulation region starts when the modulation index exceeds 0.907. This means that reference voltage exceeds the hexagon in the figure. Different overmodulation algorithms are detailed in [9,16]. This developed algorithm divides the overmodulation region into two zones.

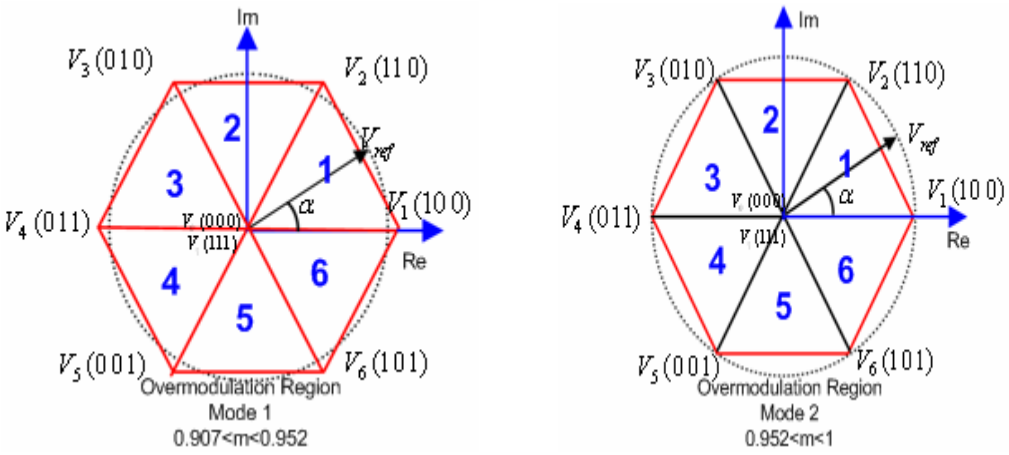

Figure 5.12 Overmodulation Region for SVPWM

Different equations to determine the switching time at overmodulation regions zone 1 zone 2 are required. More accurate PWM voltages need to be generated when overmodulation is required in order not operate as six pulse inverter operation. So, more than 90% of DC voltage is used and linear inverter operation is realized.

5.4 Three-Level Voltage Source Inverters

Three-level voltage source inverters are used in high power applications in order to generate better sine wave and fewer harmonic. There are 27(3^3) switching states three of which are redundant to produce zero voltage and 12 of which are redundant for the ability to produce half voltages. Three-level inverter circuit which is in Figure 5.13 consists of a neutral point in the middle of the DC circuit where the DC voltage level is $\frac{V_{DC}}{2}$. So, if the S2 is ON, half of the DC voltage is applied to the load. If S1 and S2 and ON at the same time, the whole DC voltage is applied to the load.

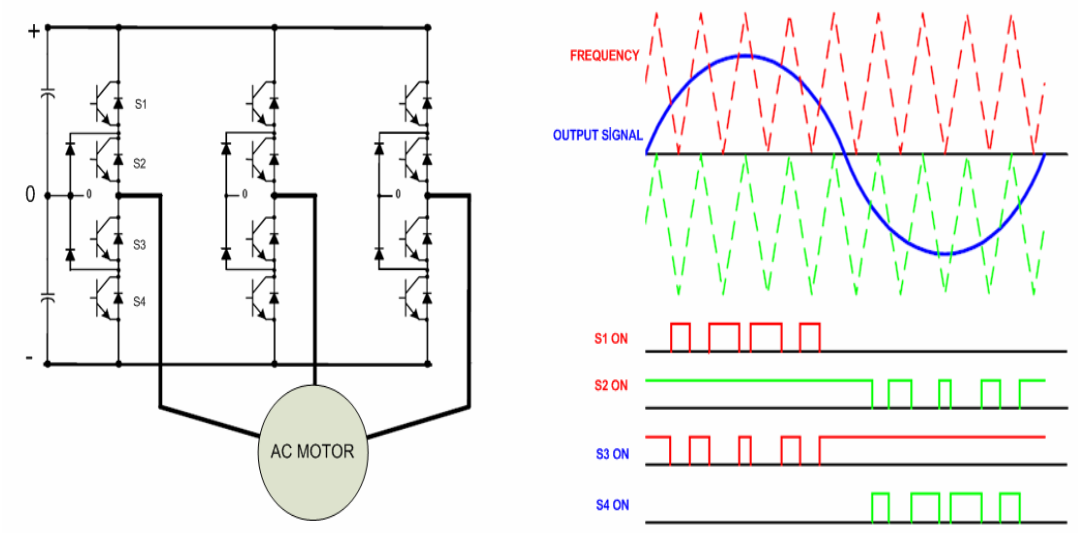

Figure 5.13 Three Level Inverter and Switching Sequence

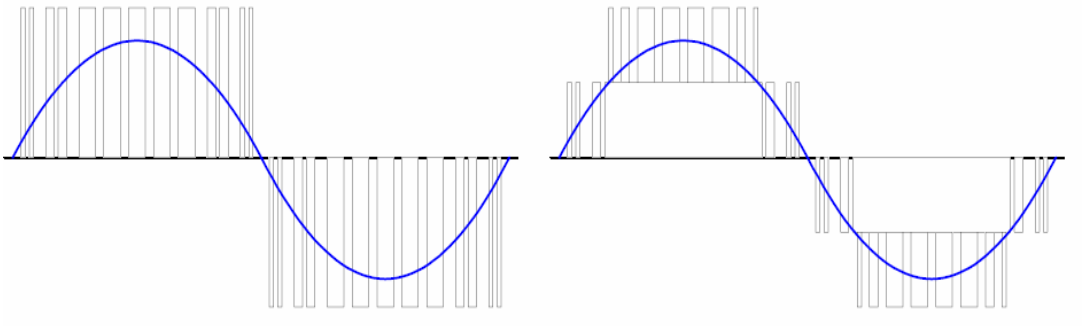

Figure 5.14 Two-Level and Three Level Voltage Waveforms

5.5 Summary

Simulation of SVPWM method is in Appendix E. VSIs are the best solution for the SCIM high performance control applications. In spite its computational complexity, SVM is the most popular method because of lower harmonics and higher modulation indexes compared to the other methods. In the next chapter, design criteria of the IGBT gate driver circuits will be explained in detail.

6. EXPERIMENTAL TEST BED FOR SCIM CONTROL

1. Introduction of Power Module

As explained in Chapter 5 in detail, two-level VSIs are the most common power electronic circuit in SCIM control. Because of the simplicity of its control circuits, lower switching losses compared to the other switching devices and also availability to work at higher frequencies, IGBTs are commonly used in inverters which are used in motor control applications. IGBT gate drive circuit is not so complex compared to other power electronic devices gate drivers. In spite of simplicity of gate drive circuits, some important notices should be taken into consideration in order to protect IGBTs. A two level voltage source inverter IGBT power module supplied by ABB is used in the experiments. This voltage source inverter consists of input inductor, a bridge diode, capacitor units and VSI as shown in the figure 6.1. Unfortunately, drives used in the industry are close to control their semiconductors. They are designed for customer purposes. An IGBT gate drive circuit has to be designed in order to control each semiconductor. In this chapter, experimental test bed requirements will be explained in detail.

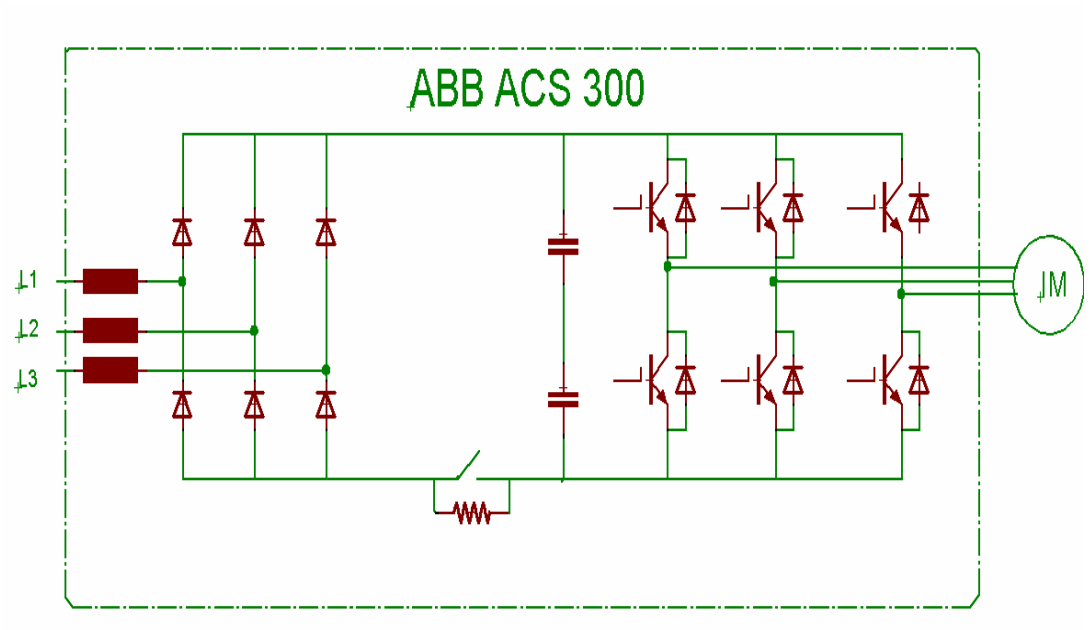

Figure 6.1 ABB IGBT Power Module

6.2 IGBT Control Requirements

IGBT internally consists of physically a combination of two thyristors and one MOSFET as shown in the figure 6.1. Basically, simple +15V between gate and emitter are adequate to turn on an IGBT. However, some details should be taken into consideration in order to operate more efficient and protect IGBT.

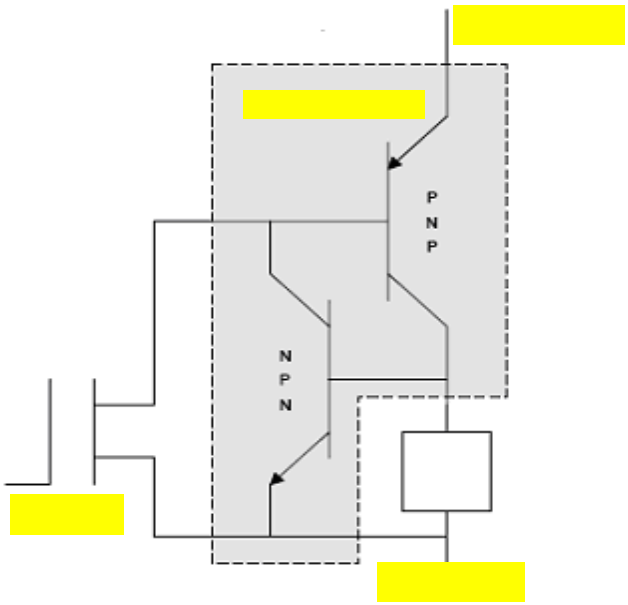

Figure 6.2 IGBT Internal Structure

On State Requirements: Required optimal gate on state voltage of an IGBT is +15V (V_{GE}). The higher the V_{GE} , the shorter the switching time occurs and this reduces switching losses. Value of V_{GE} affirmatively effects the collector current limit in U series IGBTs. Level of this value is so important that lower V_{GE} voltage applied might cause failures in switching of an IGBT.

Off State Requirements: Required gate off state voltage of an IGBT is -5V to -15V (V_{GE}). Turn off characteristic of an IGBT is heavily dependent on this value. The higher the $-V_{GE}$ value the shorter the switching time occurs. If $-V_{GE}$ value is selected too small, dv/dt currents might occur, these currents become higher if the load is a nonlinear load such as an AC motor or any inductance. Consequently, setting the -

V_{GE} value to minimum -5V is so important. Practically, selection of -V_{GE} value to -15V will be more reliable in order to switch off IGBT.

Gate Resistance Requirements: Switching characteristic of turn on and off an IGBT is directly dependent on the variation in gate resistance. If R_G is selected at higher value, longer switching time and greater switching loss occur as well as causing unwanted dv/dt currents. Optimal R_G value is essential for performance and efficiency of switching device.

Drive Current: Because of the MOS gate structure of IGBT, gate current flow is essential to charge and discharge an IGBT. These charging dynamic characteristics are used to calculate the average drive voltage and power so as to select the appropriate gate drive power components such as regulators and transformers.

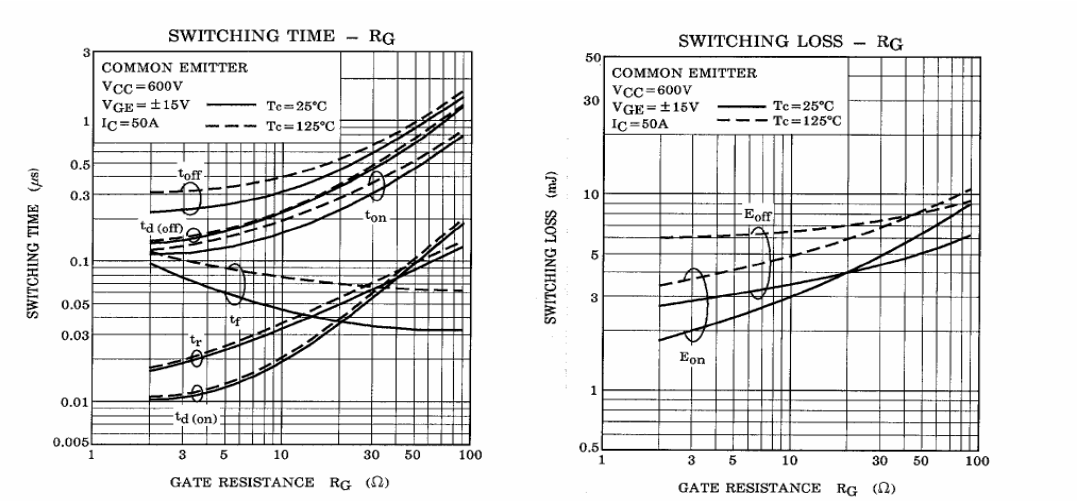

Figure 6.3 An example of IGBT Gate Resistance and Switching Loss

The drive gate peak current can be calculated with the equation below.

$$I_{GP} = \frac{V_{GE} + |-V_{GE}|}{R_G + R_{\text{int}}} \qquad \textbf{(6.1)}$$

$+V_{GE}$: Positive gate voltage -

V_{GE} : Negative gate voltage

R_G : Gate Resistance

R_{int} : Internal Resistance of IGBT

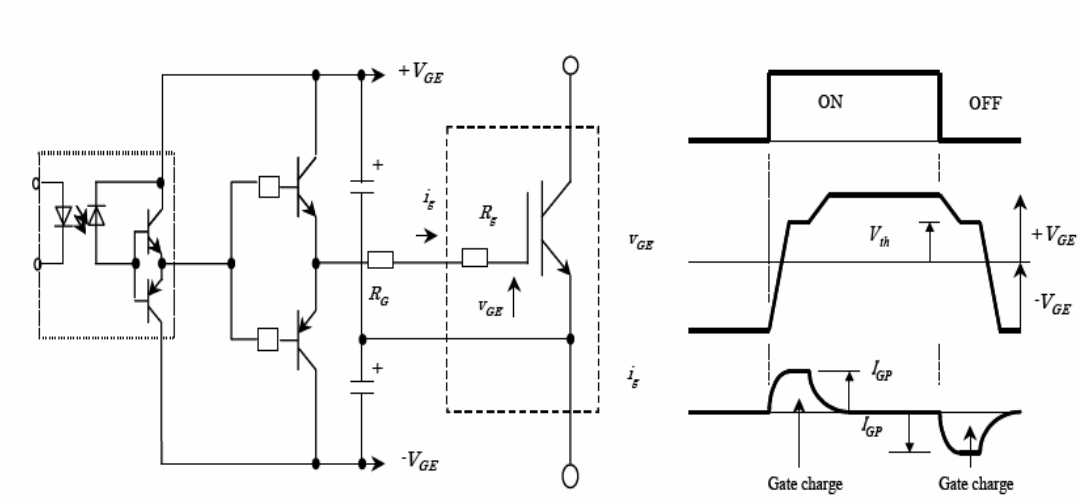

Figure 6.4 Ideal Gate Drive Circuit and gate charge and discharge currents

The average value of the drive current I_G is calculated with the equation below.

$$I_G = -I_G = f_c x(Q_g + C_{ies} x|-V_{GE}|) \qquad \textbf{(6.2)}$$

f_c: Switching frequency

Q_g : Gate charge from 0V to $+V_{GE}$

C_{ies} : IGBT input capacitance

Q_g value is highly dependent on the gate resistance. So, optimal gate resistance selection is an important issue for the gate drive power supply design as well as the switching loss and the switching time of the IGBT.

Dead Time: In order to prevent short circuits between upper and lower IGBTs in inverters, it is essential to set dead time in an appropriate value. IGBT turn off time lasts longer than IGBT turn on time. There should be a short delay that when IGBT turn off signal is sent to IGBT, turn on signal to other IGBT should be delayed in an appropriate level in order to prevent leg short circuits. During this dead time lower and upper IGBTs are in off state preventing the DC link from any short circuit. If gate resistance is increased, switching time lasts longer. Therefore, it is essential to increase dead time.

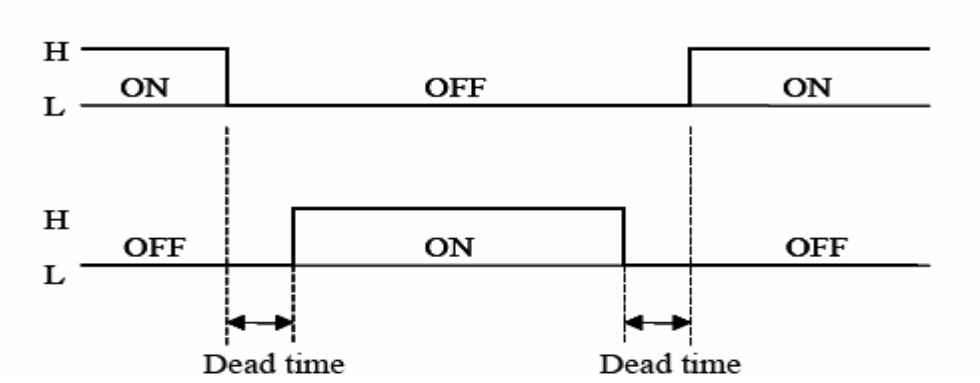

Figure 6.5 Dead Time of IGBTs in One Leg

It is essential to protect IGBT against overvoltages like all MOS gate components. If the voltage exceeds 20V between gate and emitter, IGBT might be destroyed. In order to protect IGBTs from overvoltages two zener diodes have to be connected like in figure 6.4. It is also necessary to connect a large value resistance between gate and emitter to protect IGBTs from overcurrents.

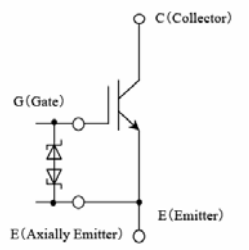

Figure 6.6 Overvoltage Protection

IGBT Short Circuit Protection: If any short circuit occurs in the IGBT, this short circuit must be stopped immediately. In order to detect short circuits in IGBTs V_{CE} saturation voltage is measured. In short circuit conditions saturation voltages exceed appropriate level. As soon as this value exceeds the specified value (usually 7V) all the IGBTs in the inverter circuit must be stopped immediately. V_{CE} increases in direct proportional to the collector current because of the internal resistance of IGBT and inversely proportional to the V_{GE} value. As seen in figure 6.5 7V value is the saturation voltage in the I_C-V_{CE} curve. This curve means that if current goes to short circuit value V_{CE} reaches about 7V. IGBT gate drive circuit should be able to detect saturation voltage and stop all the PWM signals generated by the controller. This

operation has to be as fast as possible due to the risk of IGBT failure in a short time. Any fuse installation to the circuit is not adequate to protect. Protection should detect the short circuit and stop all the references in a few microseconds.

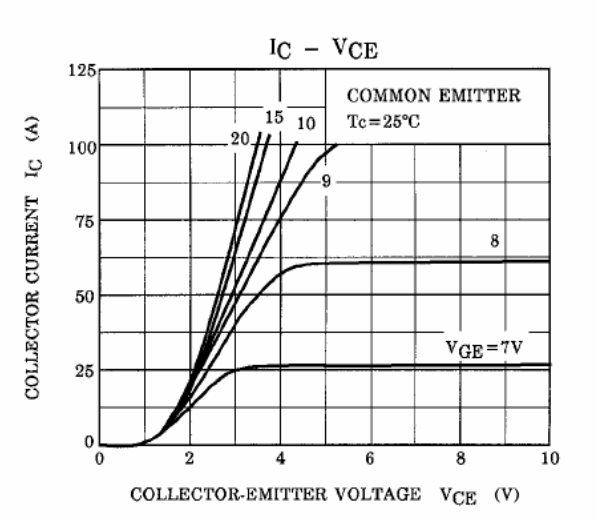

Figure 6.7 A Typical I_C-V_{CE} Curve

6.3 An Intelligent IGBT Gate Drive- HCPL-316

An intelligent gate drive circuit is implemented with the help of the gate drive circuit design considerations written above. There are various types of integrated circuits that do the V_{CE} saturation voltage detection in the market. HCPL-316 integrated circuit is preferred due to its simplicity and optically isolated fault output. Representation of gate drive circuit with VSI is shown in Figure 6.7. This circuit not only produces optically isolated PWM signals generated by the controller, but also sends a fault output to the controller [1]. Besides, any critical voltage deviations or loss of V_{GE} value also causes a fault. This intelligent gate driver optocoupler does not operate without an IGBT or with broken IGBT indicating the fault signal to the controller.

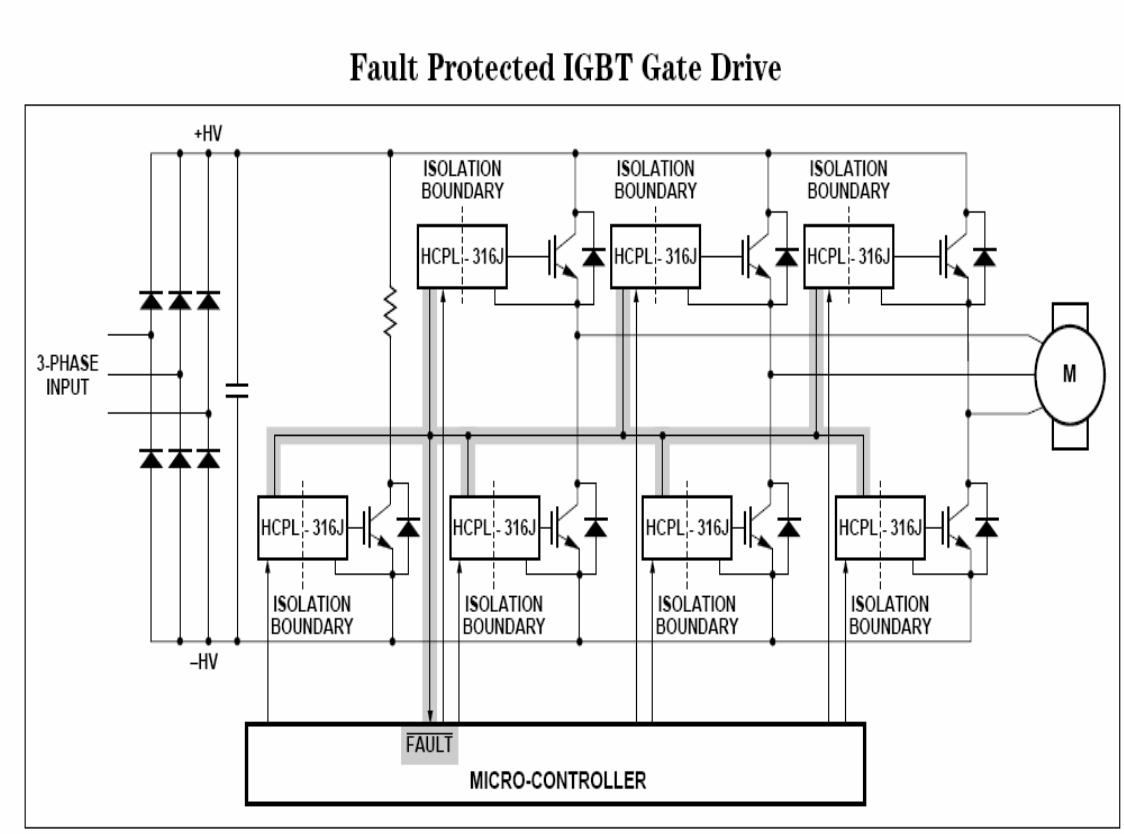

Figure 6.8 HCPL-316 Gate Driver and VSI representation

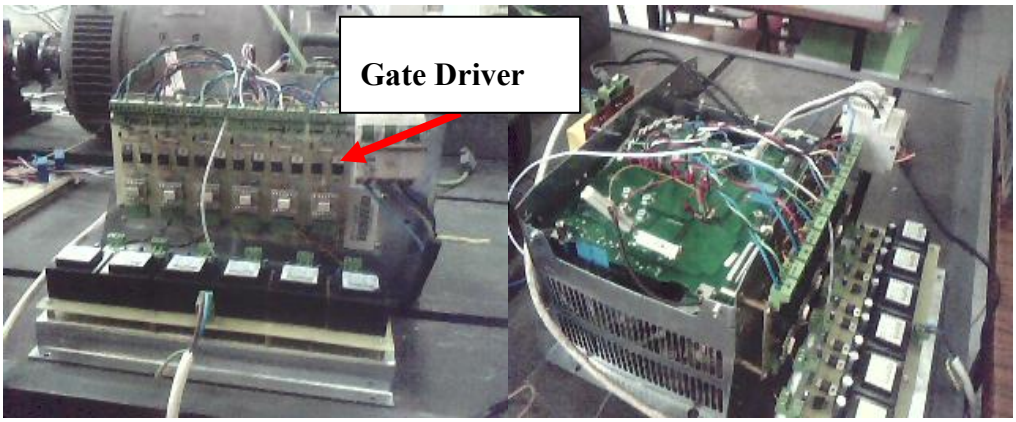

Figure 6.9 Picture of Power Module and HCPL-316 Gate Driver

6.3 Experimental Setup

Experimental circuit consists of ABB ACS 300, HCPL-316 Gate Driver and DS1104 controller board. There are also voltage and current sensors installed in the motor

circuit. Speed Encoder and Torque Sensor will measure the speed and torque respectively to compare the correctness of the estimation algorithm.

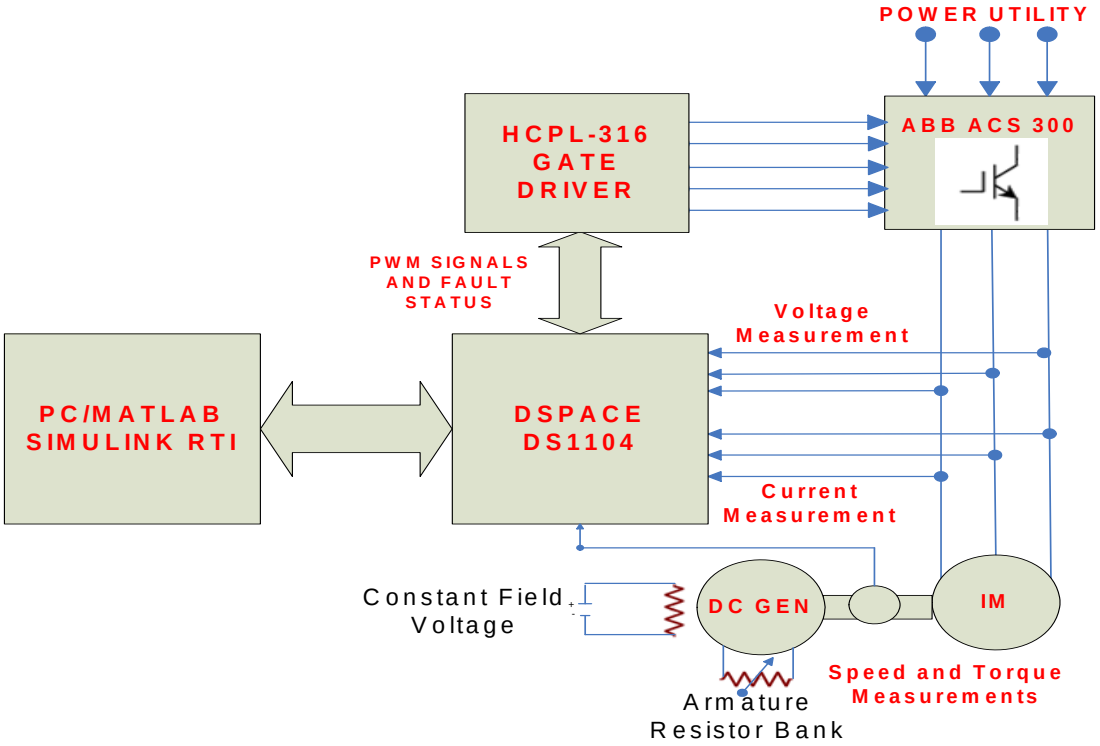

Figure 6.10 Experimental Setup Representation

A DC generator is used to load induction machine. Resistor banks are applied to the armature circuit of DC generator and SCIM is loaded. SCIM data and DC generator plate data are in table 6.1 and 6.2 respectively.

Table 6.1 SCIM Data

Rs	**Rr**	**Lm**	**Lr**	**Ls**	**n**
2,283	2,133	0.22	0.231	0.231	1430
ohm	*ohm*	*mH*	*mH*	*mH*	*rpm*
V	**J**	**p**	**P**	**B**	
380	0.05	2	3	0.001	
volt	$kg.m^2$		*KW*	Nm/(rad/s)	

Table 6.2 DC Generator Data

Ra	**La**	**Ia**	**Nm**	**TL**	**V**
1	10	17	1500	24	110
ohm	*mH*	*Amper*	*Rpm*	*Nm*	*Volt*
J	**P**	**P**	**B**		
0.0825	2	3.9	0.002		
$kg.m^2$		*KW*	Nm/(rad/s)		

Controller: Dspace DS1104 controller board is used for digital implementation. Simulink simulations are directly downloaded to DS1104 and results are observed through the Dspace Controldesk Software.

Speed Measurement: Heidenhain ERN120 series 1024 counts per revolution incremental encoder is used for the speed measurement.

Torque Measurement: Dr. Staiger Mohilo 0160 DM series 50 Nm torque transducer is used for the torque measurement.

Current Measurement: LEM LA55P current transducers with 1:2000 turns ration are used for current measurements

Voltage Measurement: LEM LV100-250 voltage transducers with 250V/50mA turns ratio are used for voltage measurements.

On the other hand A Control techniques open loop V/f drive is also used to achive EKF algorithms in the experiments. EKF algorithms used in SCIM control are tested

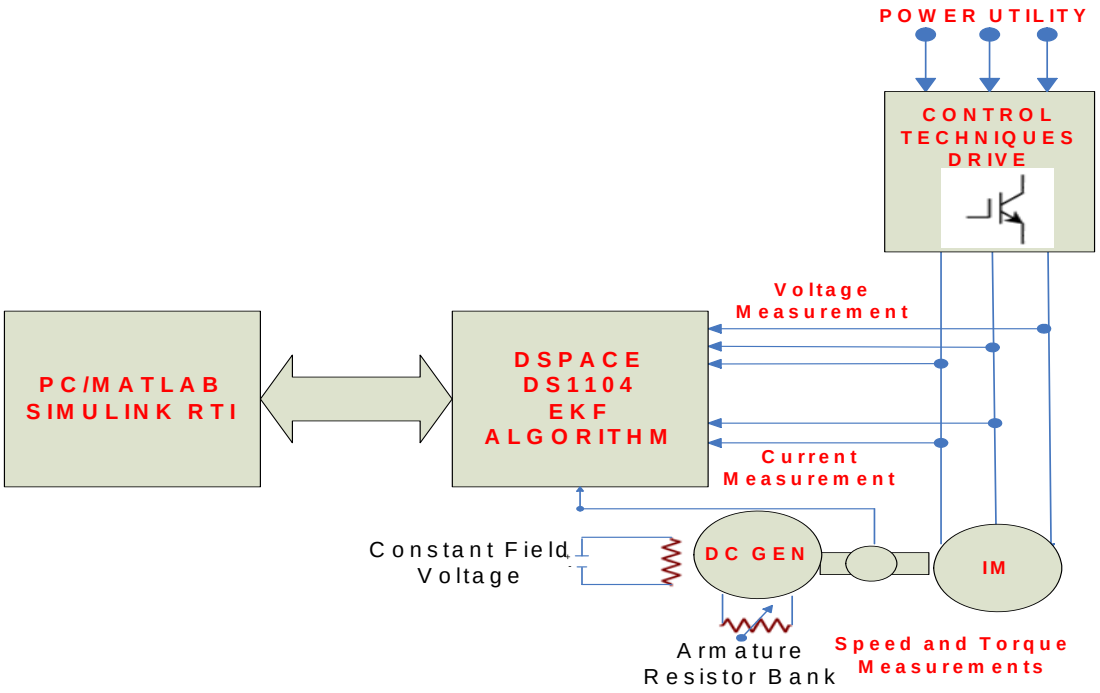

Figure 6.11 Another Experimental Setup Representation

7. SIMULATION AND EXPERIMENTAL RESULTS

In this study, high performance control of SCIM will be realized with simulation and experimental results. In order to perform this study, first step is a real SCIM model to implement. $\alpha - \beta$ Model of SCIM first realized in Matlab/Simulink to achieve a reliable dynamic model. In the following sections same SCIM $\alpha - \beta$ motor model will be tried to be controlled. Motor Data:

Rs=2.283 ohm Rr=2.133 ohm
Lm=0.22 ohm Ls=0.231 ohm
Lr=0.231 ohm P=2
n=1430 rpm (149.7 rad/s)
V=380V P=3KW
J=0.05 B=0.001

Nonlinear SCIM $\alpha - \beta$ model is realized in Matlab/Simulink. This nonlinear model will be used in direct vector control algorithms and observers. Simulation is started at nominal frequency and voltage. Nominal Torque of the motor is applied at 2^{nd} seconds. Simulation results of the Machine model are in Appendix A.

7.1 Simulation Results for Direct Vector Control

Direct Vector Control Algorithm is tested for 5 seconds. Simulation includes the whole speed range of the machine. Besides, Direct Vector Control with Luenberger Observer is simulated. Simulation Results are in Appendix B.

7.2 Simulation Results of 6^{th} order EKF.

6^{th} order EKF algorithm which estimates rotor fluxes, speed and load are simulated via Matlab/Simulink with Ts=1e-4 sample time for 5 seconds. At t=2.5 load is increased from 5Nm to 20Nm. Motor parameters are;

Po=diag1x[1 1 1 1 1 1 1 1]

Q=diag10^{-8} x[1 1 0 0 1 1]

R=diag 10^{-6} x[1 0;0 1;];

Algorithm also estimates the viscous friction constant.

$T_L = Bw + T_e \quad T_L = 20.15$ from figure C1.2

20.15=B*151.79 rad/s+20

B=0.001 which is used in the SCIM model.

Simulation Results are in Appendix C1

7.3 Simulation Results for 7th order EKF (Rotor Resistance)

EKF based observer which estimates rotor resistance as well as load torque, speed and flux is simulated for 8 seconds at 100 microseconds. Model rotor resistances are changed at different times and algorithm follows these changes very quickly that is shown in figure C2.1. EKF parameters;

Po=diag1x[1 1 1 1 1 1 1 1]

Q=diag10^{-8} x[1 1 0 0 1 1 0.1 0.1]

R=diag 10^{-6} x[1 0;0 1;];

Simulation Results are in Appendix C2

7.4 Simulation Results for 7th order EKF (Stator Resistance)

EKF based observer which estimates stator resistance as well as load torque, speed and flux is simulated for 8 seconds at 100 microseconds. Model rotor resistances are changed at different times and algorithm follows these changes very quickly that is shown in figure C3.1

Po=diag1x[1 1 1 1 1 1 1]

Q=diag10^{-8} x[1 1 0 0 1 1 0.1]

R=diag 10^{-6} x[1 0;0 1;];

Simulation Results are in Appendix C3

7.5 Simulation Results for 8th order EKF (Stator and Rotor Resistance)

EKF based observer which simultaneously estimates stator and rotor resistances as well as load torque, speed and flux is simulated for 8 seconds at 100 microseconds.

Algorithm is tested by simultaneously changing rotor and/or stator resistances and different loading conditions.

Po=diag1x[1 1 1 1 1 1 1 1]

Q=diag10^{-8} x[1 1 0 0 1 1 0.1 0.1]

R=diag 10^{-6} x[1 0;0 1;];

Simulation results are in Appendix C4

7.6 Simulation Results for Direct Vector Control with EKF

EKF outputs can be used in direct vector algorithms. Simulation results of direct vector control method using EKF based observer are in Appendix C5

7.7 Simulation Results For Space Vector PWM

SVPWM Voltage signals operating in undermodulation region is generated. These generated voltages are applied to the motor. SCIM motor which is simulated with the ideal sinusoidal signals in Chapter 2 is operated in open loop V/Hz control without slip and IR compensation. Switching frequency is selected at 3 kilo hertz and DC link voltage is 538V.

Simulation results are in Appendix D.

7.8 Experimental Results

7^{th} and 8^{th} order EKF algorithms are tested in different speed and loading conditions. Variations in the rotor and stator resistances in speed reversals are shown different loading conditions in wide speed range are shown.

In the experimental Setup;

- Dspace DS1104 controller board is used for digital implementation. Simulink simulations are directly downloaded to DS1104 and results are observed through the Dspace Controldesk Software.

- Heidenhain ERN120 series 1024 counts per revolution incremental encoder is used for the speed measurement.

- Dr. Staiger Mohilo 0160 DM series 50 Nm torque transducer is used for the torque measurement.
- LEM LA55P current transducers with 1:2000 turns ration are used for current measurements
- LEM LV100-250 voltage transducers with 250V/50mA turns ratio are used for voltage measurements.

Experimental Results are in Appendix E.

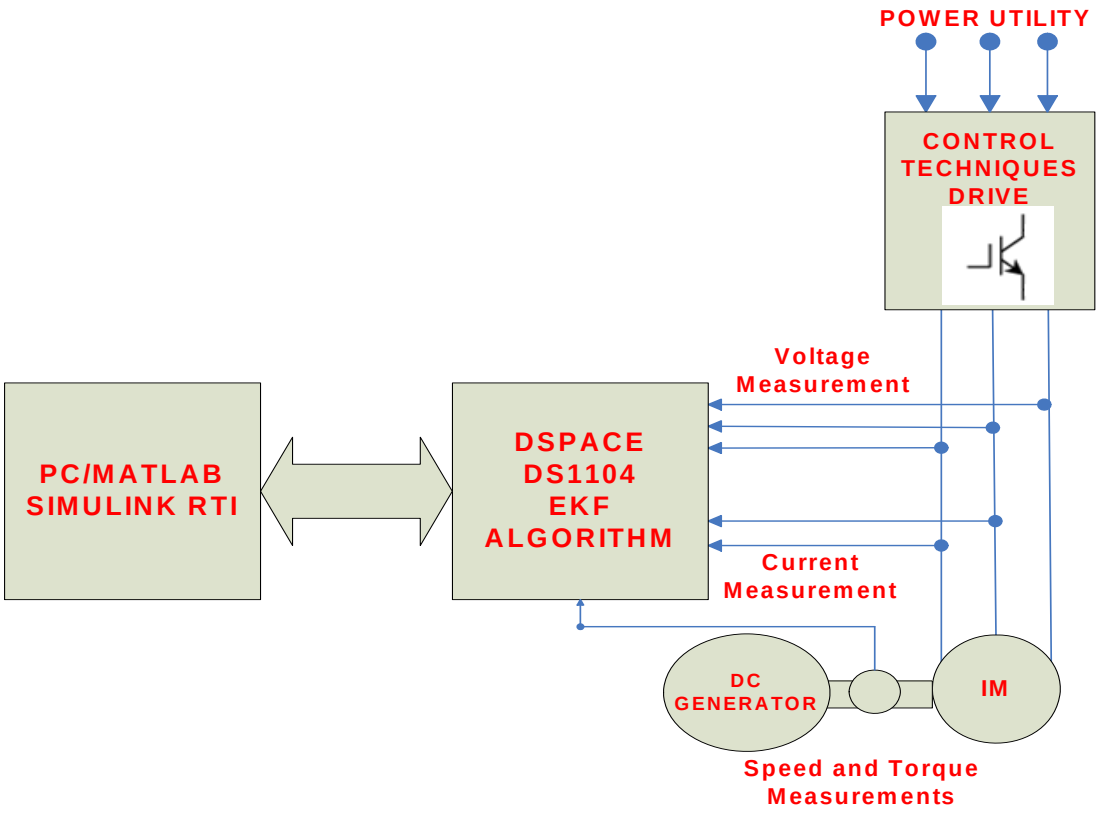

Figure 7.1 Experimental Setup to achieve EKF Algorithms

8. CONCLUSION

In this study, speed sensorless direct vector control algorithm is implemented. The main problem of high performance sensorless control of SCIM is parameter variations. The main constraint of sensorless high performance SCIM control is rotor and stator resistance variations because of frequency and temperature effects due to different speed and loading conditions. Stator and rotor resistances need to be simultaneously estimated especially at low speeds.

In this study EKF based observer to achieve high performance speed sensorless control of SCIM are designed. 7^{th} order EKFs which estimates rotor or stator resistances are simulated and experimented. More accurate speed estimation requires simultaneous estimation of rotor and stator resistances especially at low speeds. Therefore a novel 8^{th} order EKF based estimator that simultaneously estimate rotor and stator resistances is designed and implemented. Results are expanded with the experimental results. In simulations, simultaneous estimation of rotor and stator resistances effect each other, but it is not an instability. In the experiments of simultaneous estimation good rotor resistance estimation results are taken while stator resistance estimation is very poor. Inductance values of the machines are also need to be known accurately in order to achieve stator resistance estimation. As a result, eight order EKF fails simultaneous accurate estimation of stator and rotor resistances. Braided EKF in (Barut, 2008) give accurate estimation while eighth order EKF fails.

Main constraint of EKF algorithms is the determination of the Q matrices. Q matrices are taken constant in this study. But, different speed and loading conditions requires different optimal Q matrices. So, new algorithms need to be innovated to achieve this problem.

Another constraint of EKF algorithm is the computational complexity. However, this will not be a problem with new innovations in the processor technologies. Undisputedly, faster and cheaper processors will be in the market in the future.

In conclusion, EKF based estimator which has impressive results for the electrical and mechanical uncertainties of SCIM due to its stochastic behavior can be used in high performance SCIM control in the industry with the new innovations of determination of Q matrices.

REFERENCES

Agilent Technologies, 1999**,** HCPL-316 Datasheet

Akin, B., Orguner, U, and Ersak, A., 2003. State estimation of induction motor using unscented kalman filter*, Procedings of the IEEE Conference on Control Applications (CCA 2003), 1, 915-919.*

Akin, E., Ertan H.B. and Uctug, M.Y., 1994. A method for stator Resistance measurement suitable for vector control, *Procedings of the 20th IEEE International Conference on Control and Instrumentation (IECON'94), 3, 2122-2126.*

Al-Tayie, J.K. and Acarnley, P.P., 1997. Estimation of speed, stator temparature and rotor temparature in cage induction motor using the extended kalman filter algorithm, *IEE Proceedings on Electric Power Applicaitons, 27 (6), 1119-1127.*

Atkinson, D.J., Acarnley, P.P., 1997, Estimation of speed, stator temparature and rotor temparature in cage induction motor drive using the extended kalman filter algorithm, *IEE Proceedings on Electric Power Applications, s144(5), 301-309.*

Barut, M., 2005, Sincap kafesli asenkron motorların algılayıcısız yüksek başarımlı kontrolüne yönelik genişletilmiş kalman filtresi tasarım ve uygulaması", *Doktara Tezi, ITU Fen Bilimleri Enstütüsü*

Barut, M., Bogosyan, O.S, Gökaşan M., 2005. An EKF based estimator for speed sensorless vector control of induction motors, *Electric Power Components & Systems, formerly Electric Machines and Power Systems, Taylor-Francis, 33(7), 727-744.*

Barut, M., Bogosyan, O.S, Gökaşan M., 2008. Experimental Evaluation of Braided EKF for Sensorless Control of Induction Motors, *IEEE Transactions on Industrial Electronics, Volume 55 No.2, 620-632.*

Bose, B. K., 1997. High performance control estimation in AC Drives, *Proceedings of the 23rd International Conference on Control and Instrumentation (IEOCON'97), 2, 377-385.*

Bose, B. K., 2002. Modern Power Electronics and AC Drives, *Prentice Hall PTR, New Jersey.*

Bose, B. K., 2006. Power Electronics and Motor Drives: Advances and Trends, *Elsevier/Academic Press.*

Dspace, 2002, DS1104 R&D Controller Board RTI Reference. *Dspace, Datasheet.*

Dspace, 2002, DS1104 R&D Controller Board RTLib Reference. *Dspace, Datasheet.*

Fuji Electric, 2004, Fuji IGBT Modules Application Manual.

Gökaşan, M., 1989, Sincap kafesli asenkron makinalarda modern kontrol yöntemlerinin uygulanması, Doktora Tezi, İTÜ Fen Bilimleri Enstitüsü.

Holmes, G., Lipo T., 2003, Pulse width modulation for power converters: principles and practice, John Wiley.

Holtz, J., 1994, Pulse width modulation for electric power conversion, IEEE Trans. Ind. Appl., vol. 26, pp. 63-72.

Holtz, J., 2002, Sensorless control of induction motor drives, proceedings of IEEE, 90(8), 1359-1394.

Holtz, J., 2006. Sensorless control of Induction Machines- With or Without Signal Injection?, *IEEE Transactions on Industrial Electronics, Volume 53 No.1, 7-30.*

Kalman, R.E., 1960, A new approach to linear filtering and prediction problems, *Transactions of the ASME- Journel of Basic Engineering 82(D), 33-45.*

Krause, P.C., Wasynczuk, O. And Sudhoff, S.D., 2002, Analysis of Electrical Machinery and Drive Systems, *IEEE Press, New Jersey.*

Leonard, W., 2001, Control of Electrical Drives**,** *Berlin; New York: Springer,*

Lorenz, R.D., Lipo, T.A. and Novotny, D.W., 1994, Motion control with induction motors, *Proceedings of the IEEE, 82(8), 1215-1240*

Luenberger, D.G., 1971, An introduction to observers, *IEEE Transactions on Automatic Control 16(6), 596-602.*

Mohan, N., 1995, Power Electronics: Converters, Applications, and Design, *New York: John Wiley and Sons.*

Mohan N., 2000, Electric Drives, an Integrative Approach, *Mnpere Minneapolis*

Ong, C.M., 1998, Dynamic Simulation of Electric Machinery using Matlab/Simulink, *Prentice Hall, New Jersey.*

Rashid, M.H., 2001, Power Electronics Handbook, *Academic Pres.*

Sarıoğlu, M.K., Gökaşan, M., Bogosyan, O.S., 2003. Asenkron Makinalar ve Kontrolü, Birsen Yayınevi, Istanbul.

Shi, K.L., Chan T.F., Wong, Y.K., Ho, S.L., 2000. Speed estimation of induction motor drive using extended kalman filter, IEEE Transactions on Industrial Electronics, Vol. 49, No. 1, pp.124-133, February 2002.

Takahashi, I. and Noguchi, T., 1986, A New quick-response and high efficiency control strategy of an induction motor*, IEEE Transactions on Industry Applications, 22(5), 820-827*

Texas Instruments, 1997, Sensorless Control with Kalman Filter on TMS320 Fixed-Point DSP, *Application Note: bpra057*.

Vas, P., 1990, Vector Control of AC Machines, *Clarendon Press, Oxford.*

Vas, P., 1998, Sensorless Vector and Direct Torque Control of AC Machines, *Oxford University Pres, Oxford.*

Welch, G., Bishop G., 2001, An Introduction to Kalman Filter, *University of North Carolina at Chapel Hill Department of Computer Science Chapel Hill ACM Inc.*

APPENDIX A

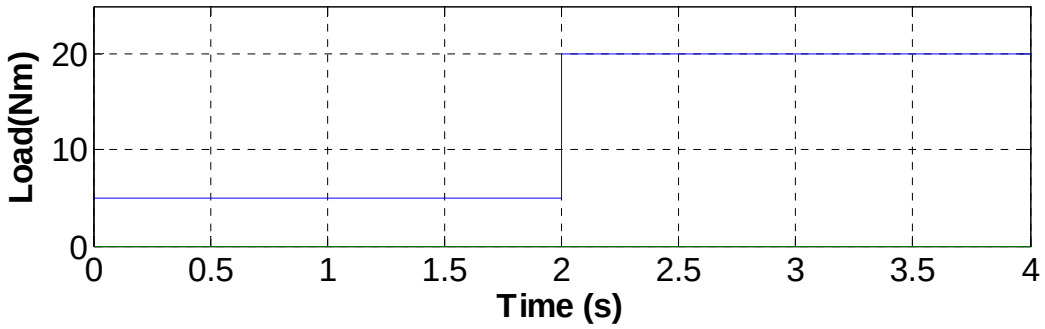

Figure A1 Motor Model Simulations (Load)

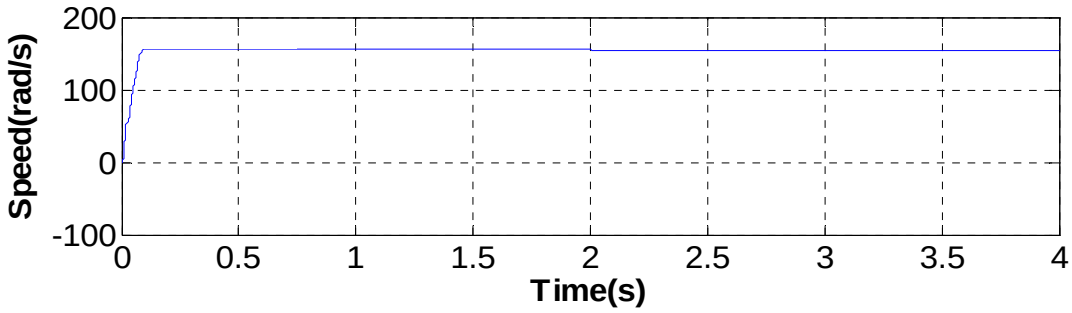

Figure A2 Motor Model Simulations (Speed)

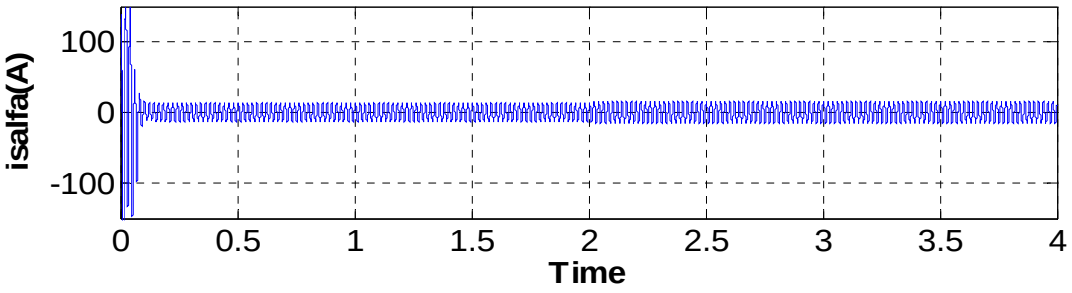

Figure A3 Motor Model Simulations (Current)

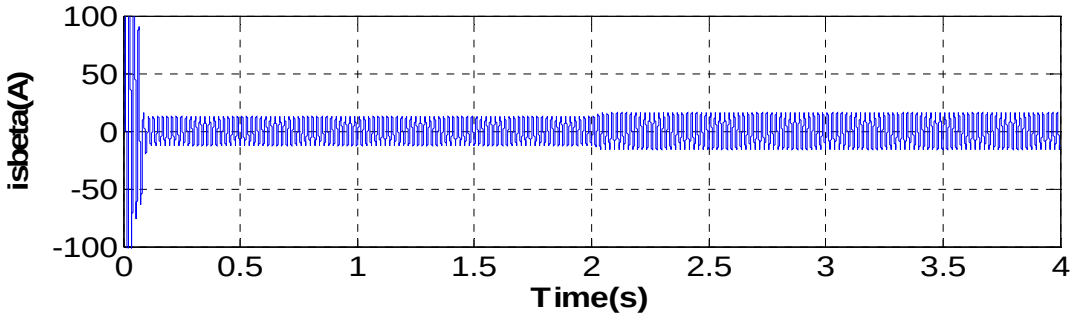

Figure A4 Motor Model Simulations (Current)

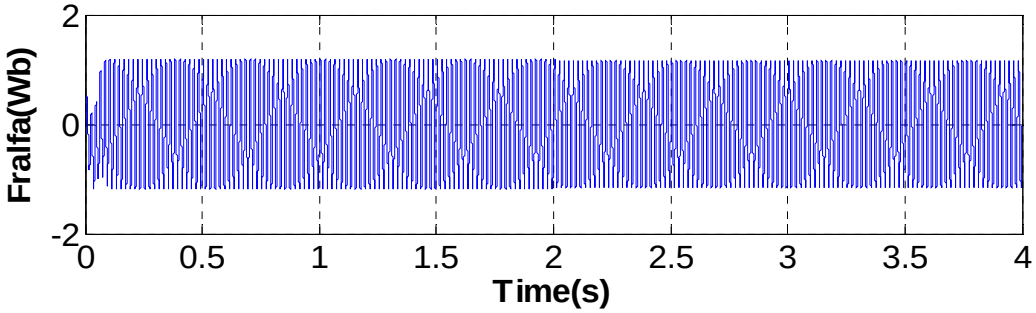

Figure A4 Motor Model Simulations (Flux)

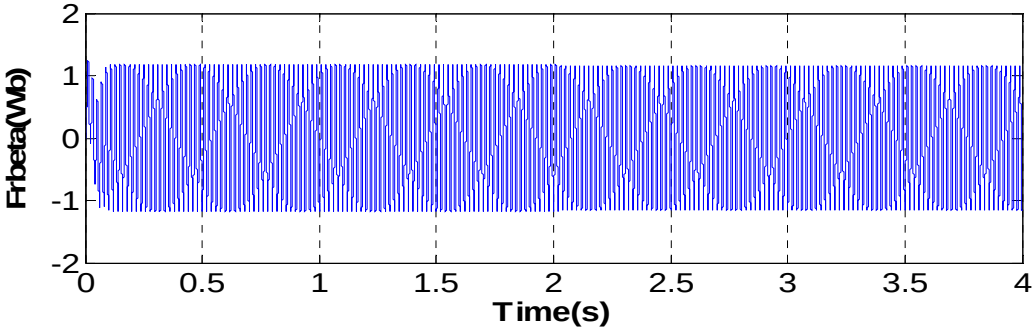

Figure A2 Motor Model Simulations

APPENDIX B

Direct Vector Control is Simulated for 5 seconds.

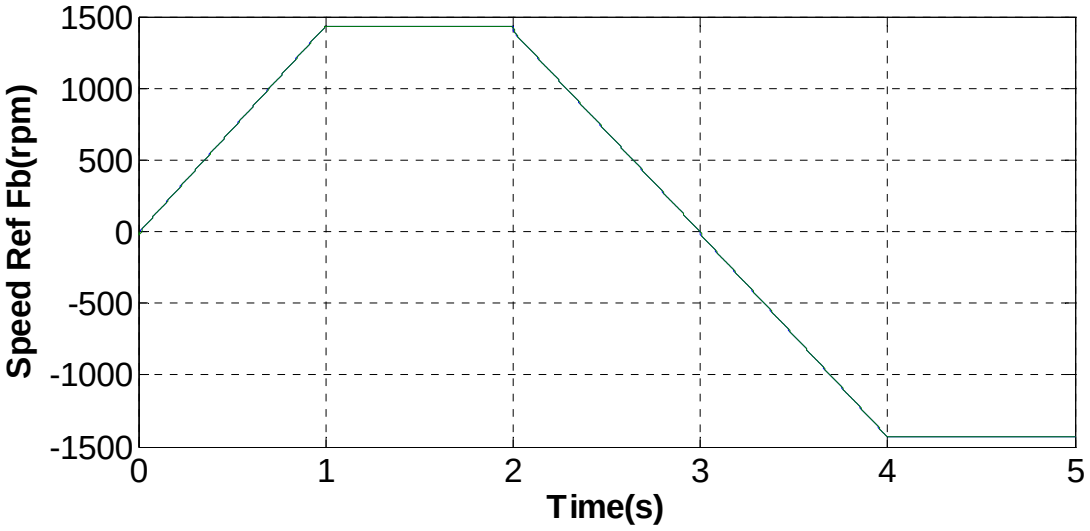

Figure B1 Motor Speed Reference and Speed Feedback

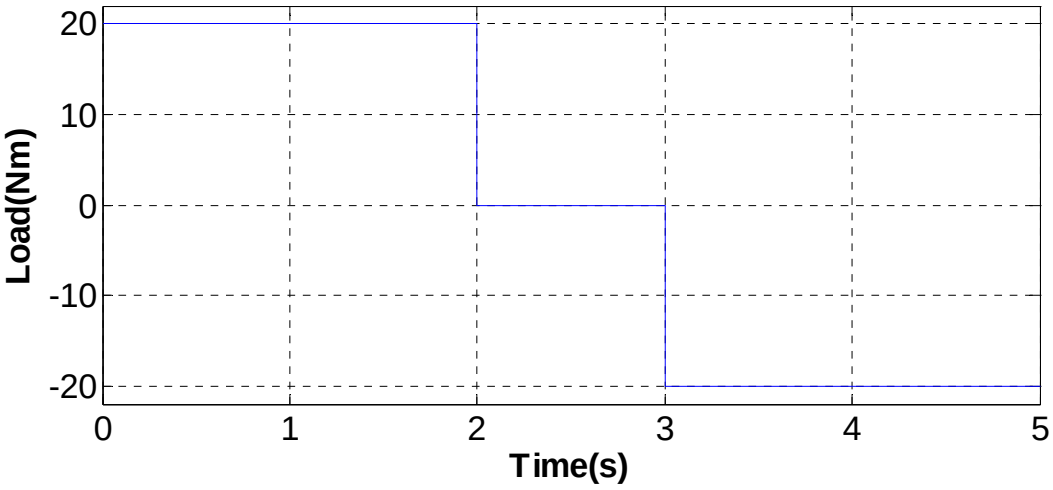

Figure B2 Motor Load Applied

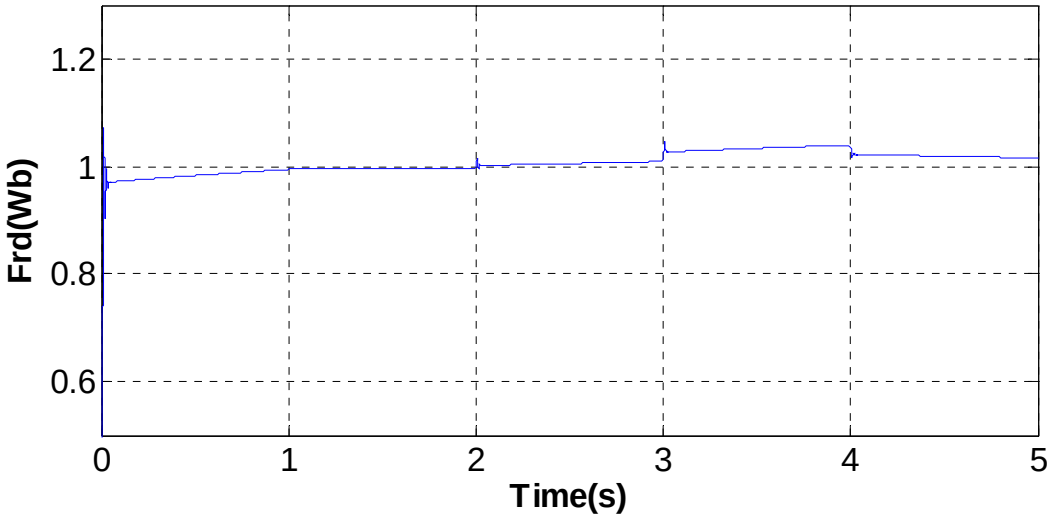

Figure B3 ψ_{rd} rotor flux

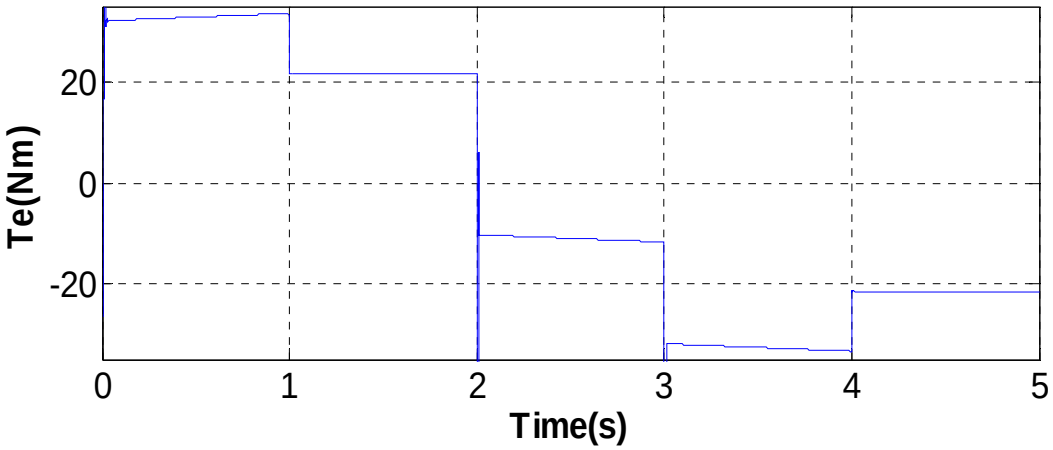

Figure B4 Electromagnetic Torque

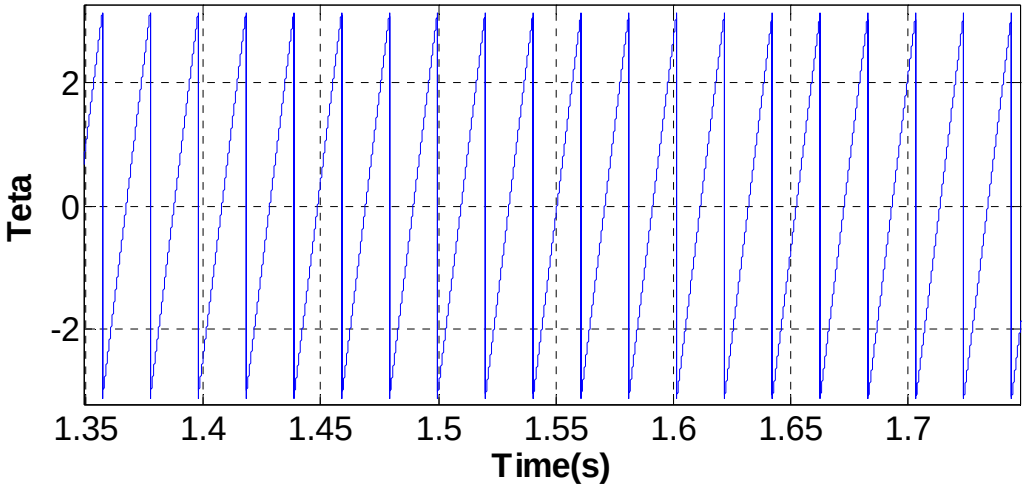

Figure B5 Rotor Teta

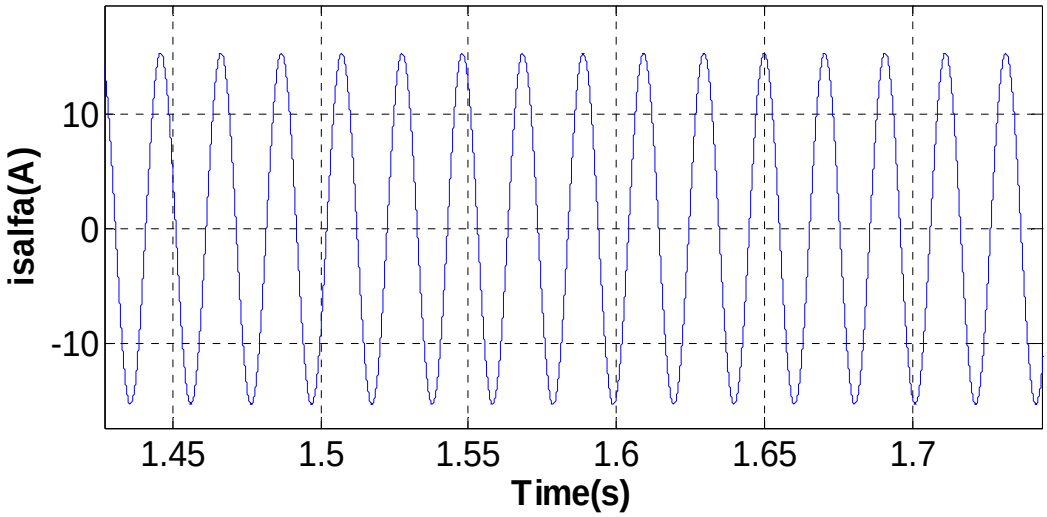

Figure B6 Alfa Component Stator Current

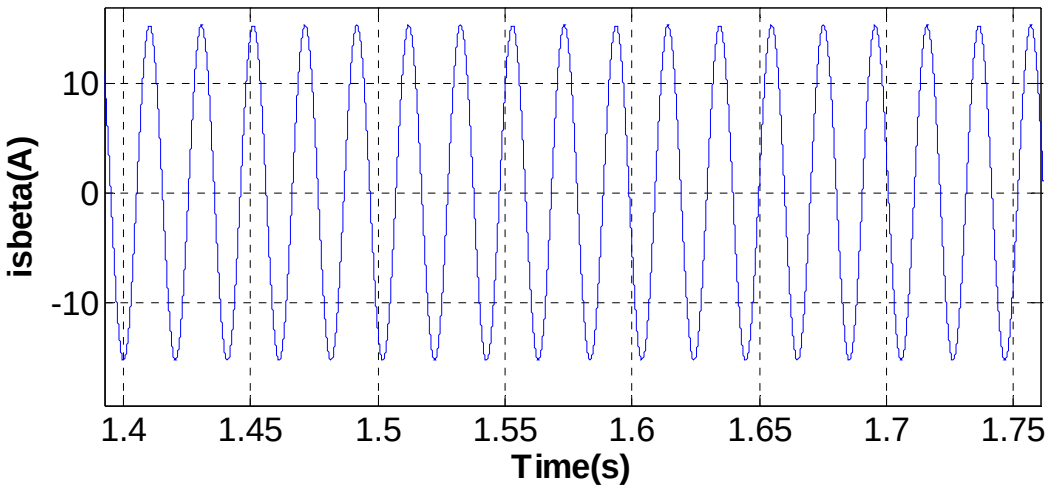

Figure B7 Beta Component Stator Current

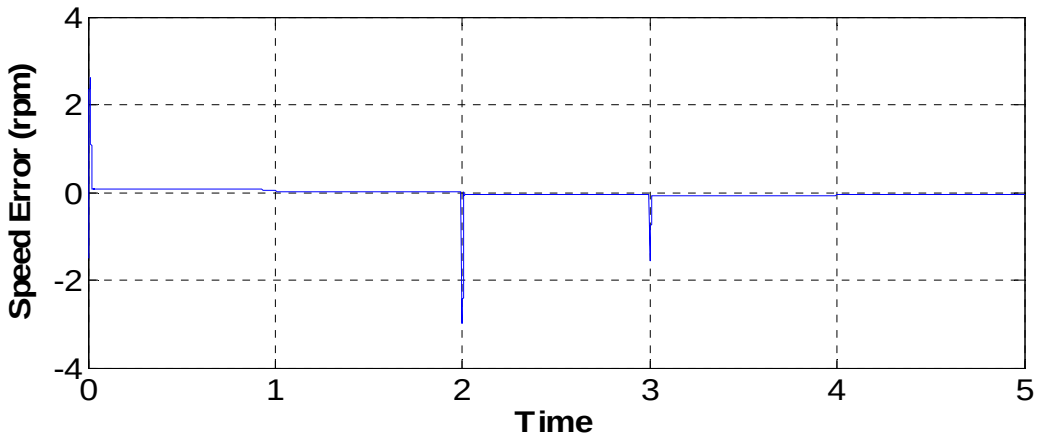

Figure B8 Speed Error

Simulation results of Direct Vector Control with Luenberger Observer

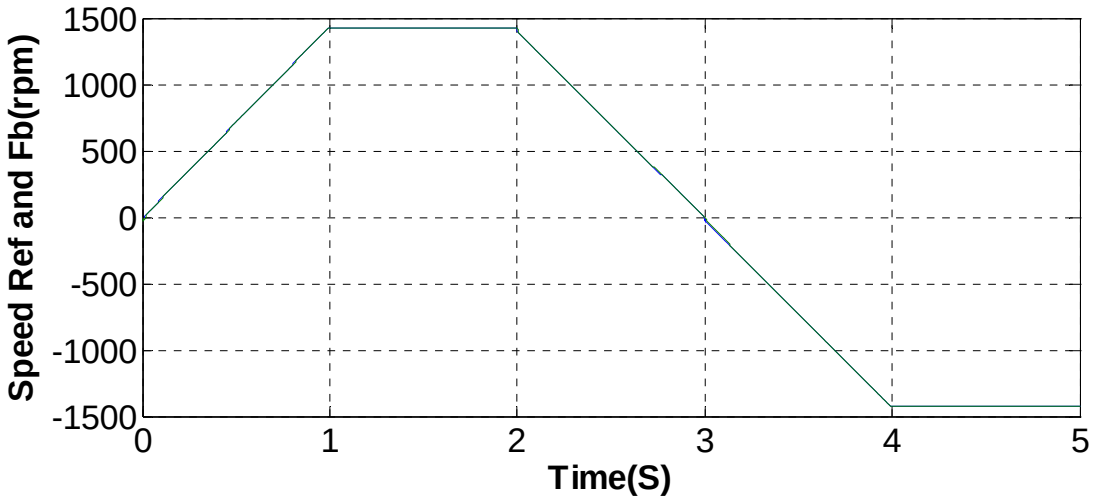

Figure B9 Motor Speed Reference and Speed Feedback

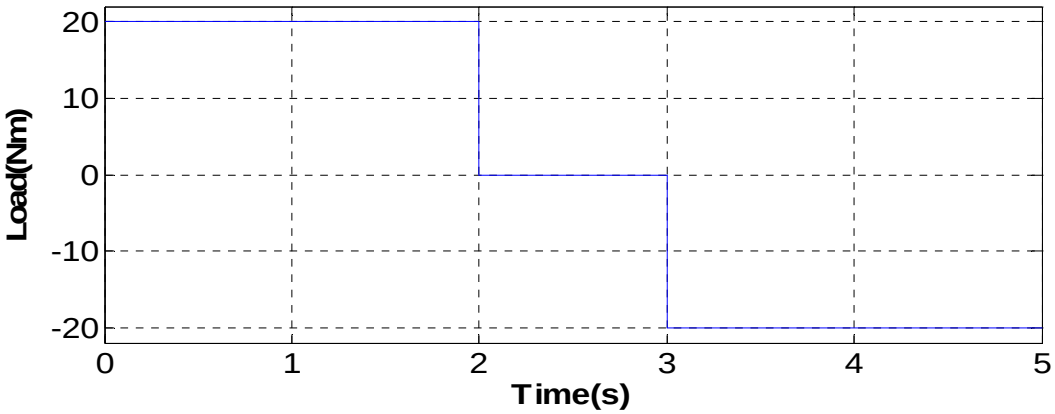

Figure B10 Motor Load Applied

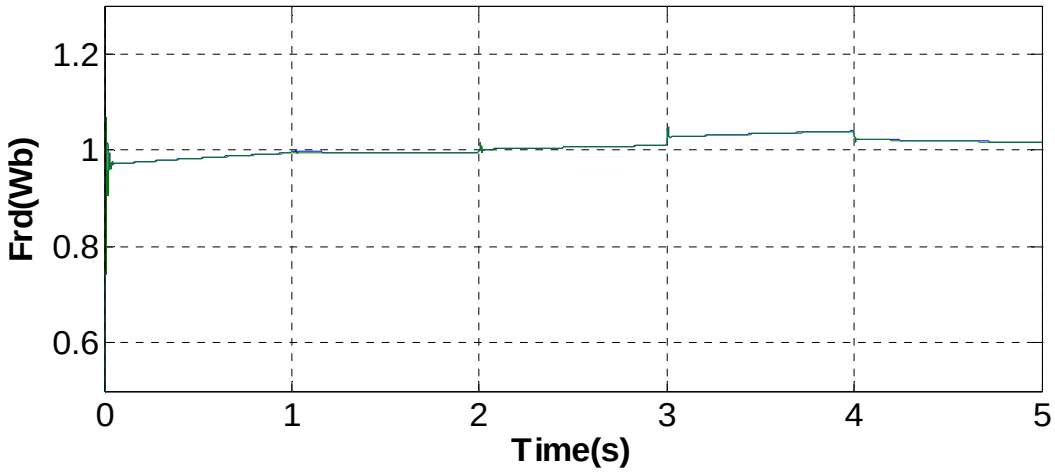

Figure B11 ψ_{rd} rotor flux

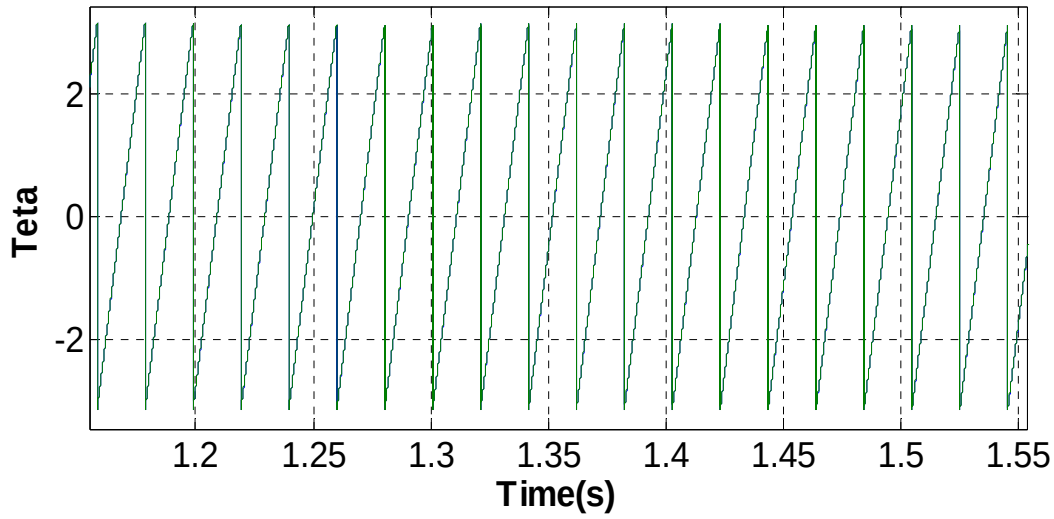

Figure B12 Teta

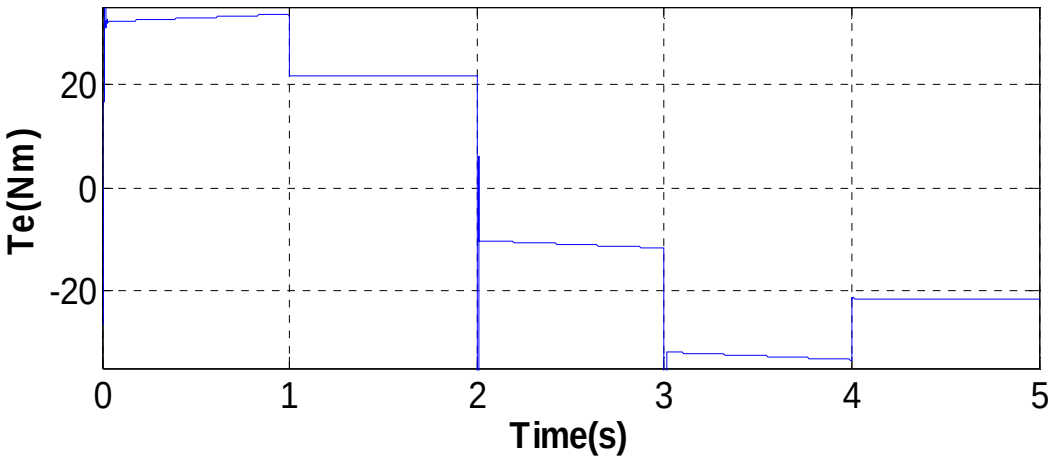

Figure B13 Electromagnetic Torque

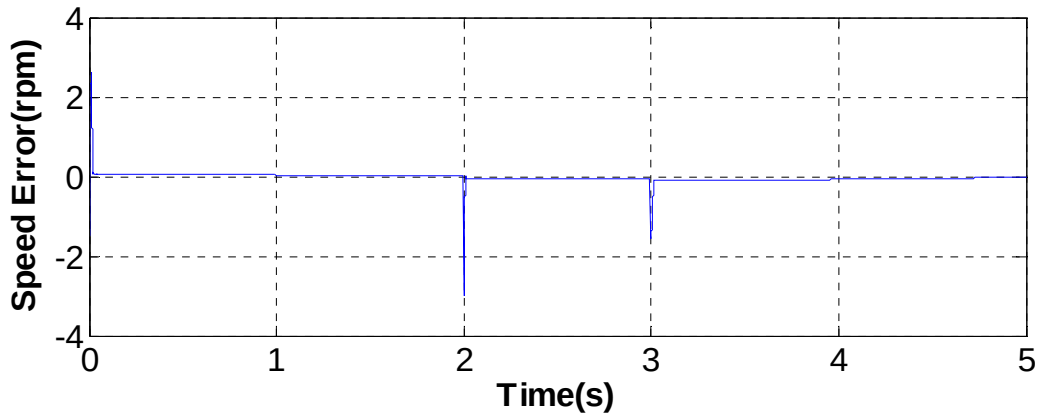

Figure B14 Speed Error

APPENDIX C1

EKF with Load Torque

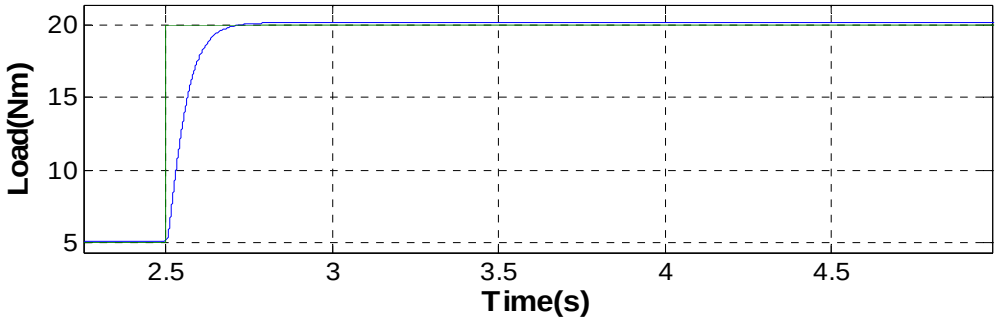

Figure C1.1 Estimated and Applied Torque

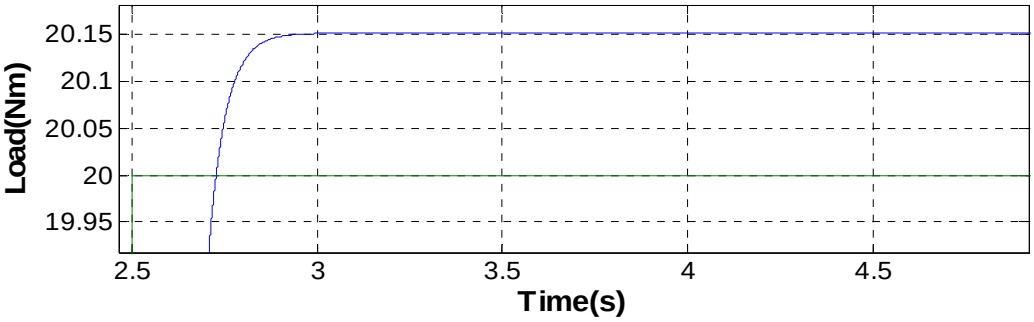

Figure C1.2 Estimated and Applied Torque

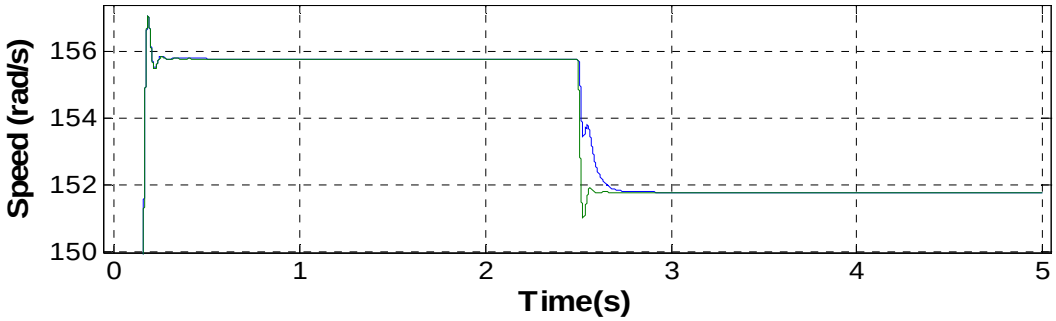

Figure C1.3 Estimated and Measured Speed

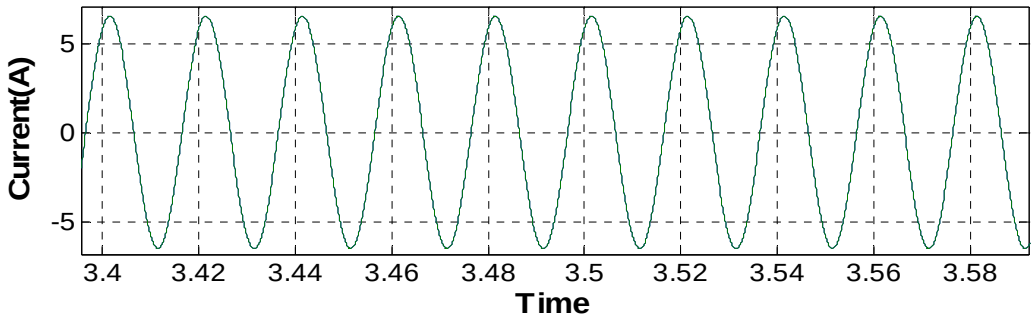

Figure C1.4 Estimated and Measured Current

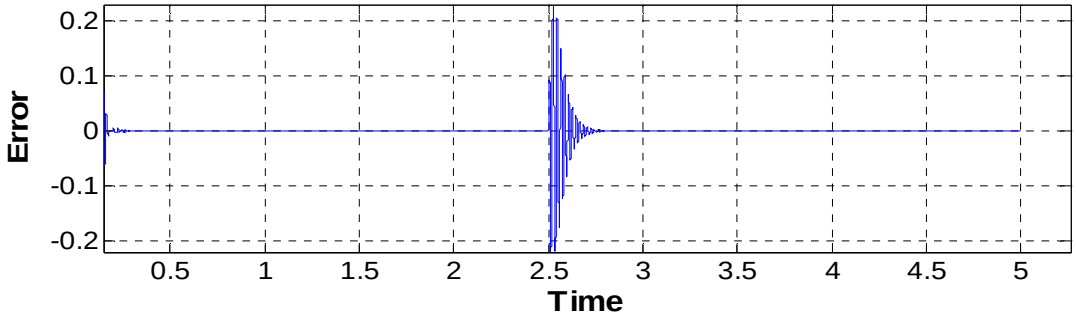

Figure C1.5 Error

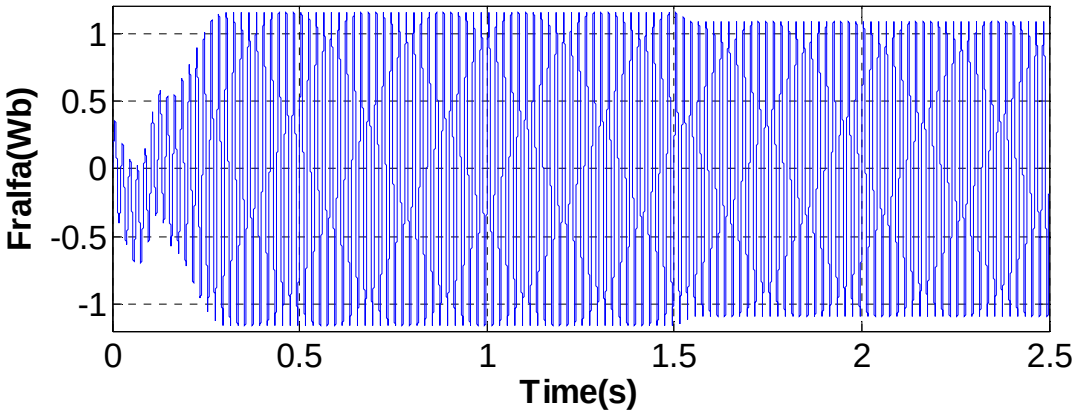

Figure C1.6 Estimated Rotor Flux

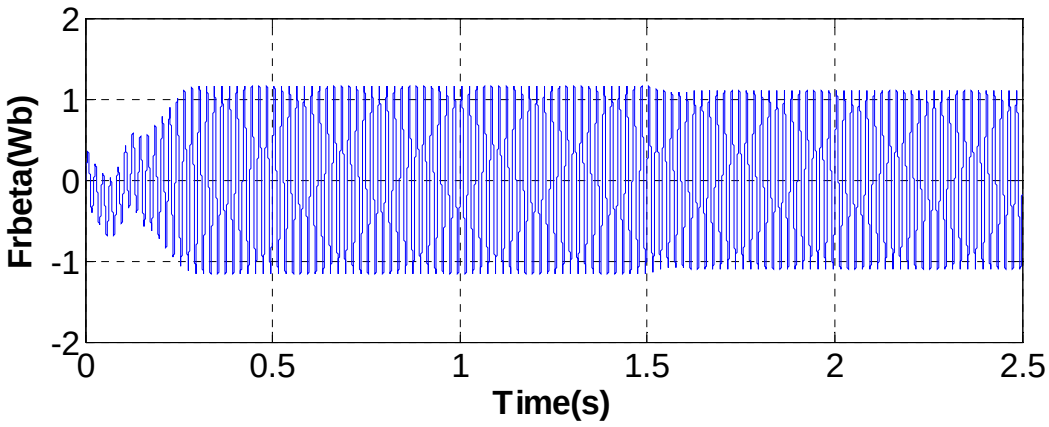

Figure C1.7 Estimated Rotor Flux

APPENDIX C2

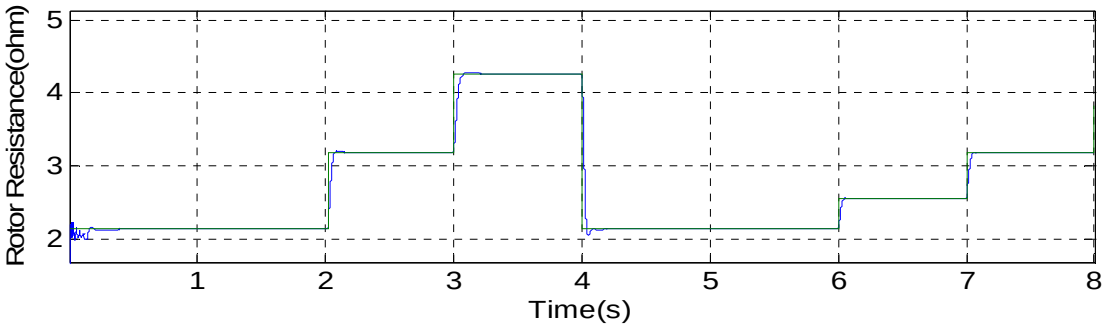

Figure C2.1 Estimated and Model Rotor Resistances

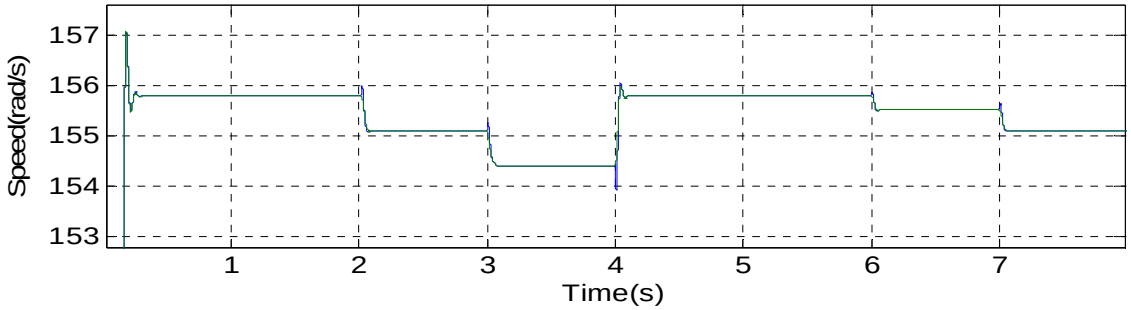

Figure C2.2 Estimated and Measured Speed

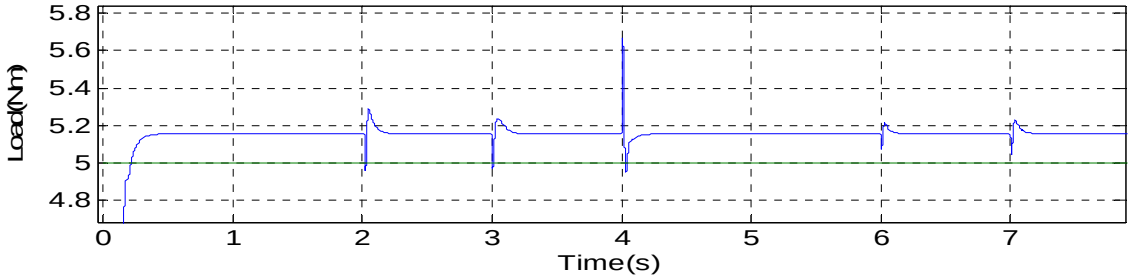

Figure C2.3 Estimated and Applied Torque

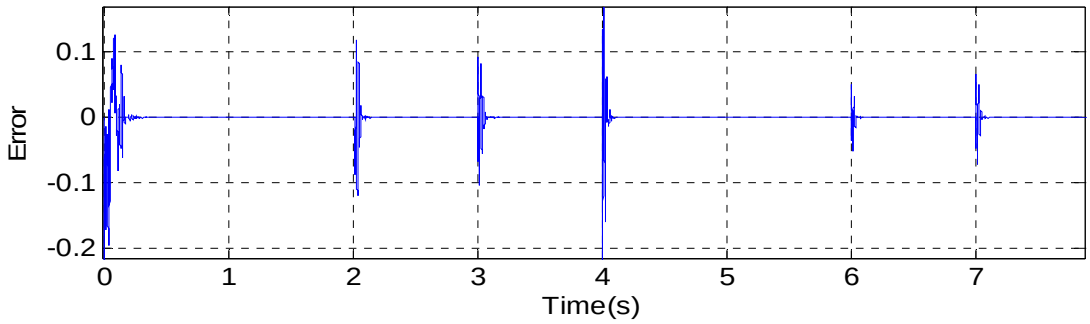

Figure C2.4 Error

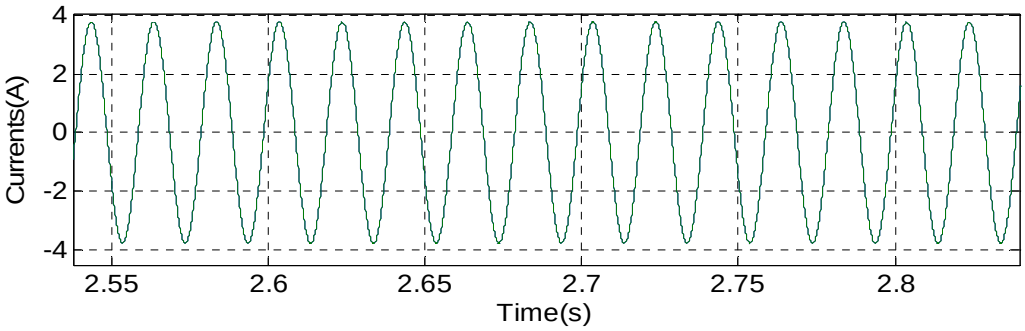

Figure C2.5 Currents

APPENDIX C3

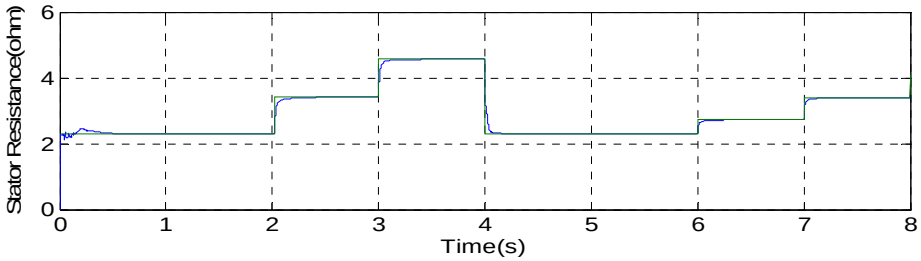

Figure C3.1 Estimated and Model Rotor Resistances

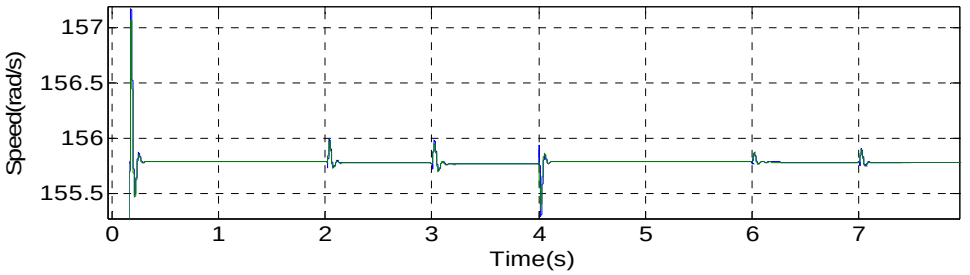

Figure C3.2 Estimated and Model Speed

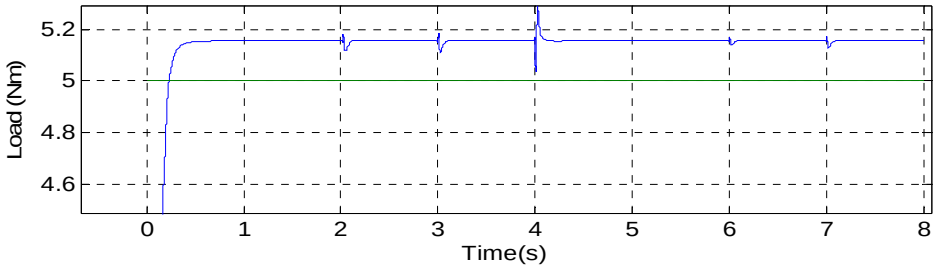

Figure C3.3 Estimated and Applied Load

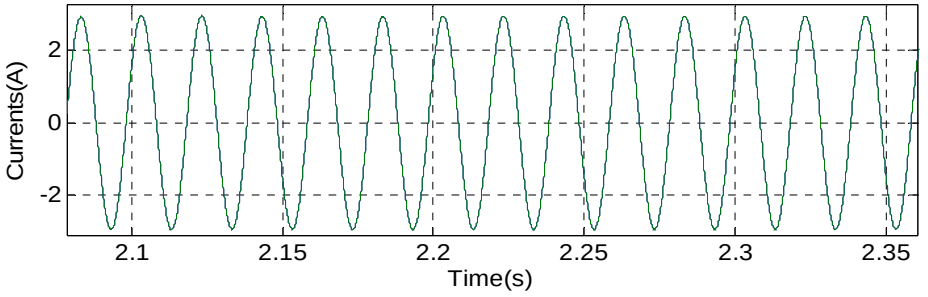

Figure C3.4 Estimated and Model Currents

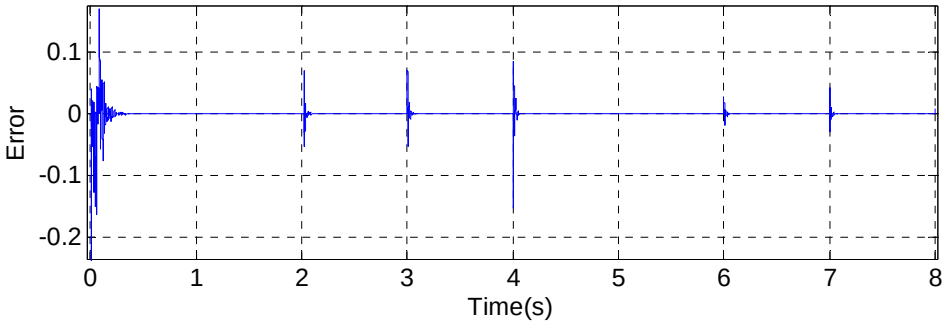

Figure C3.5 Error

APPENDIX C4

8th Order EKF (Simultaneous Rotor and Stator Resistance Estimation)

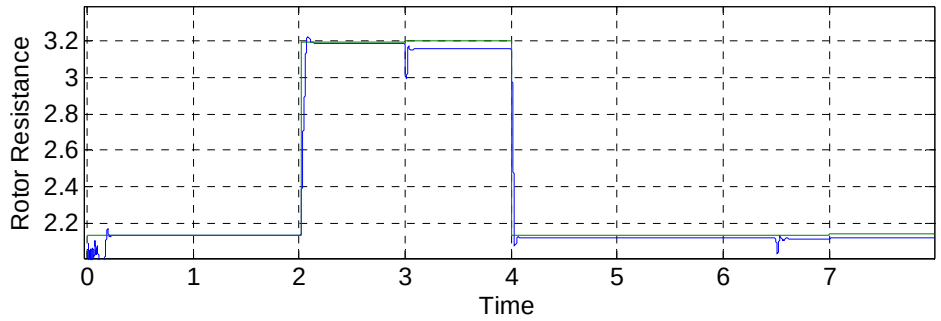

Figure C4.1 Estimated and Model Rotor Resistance

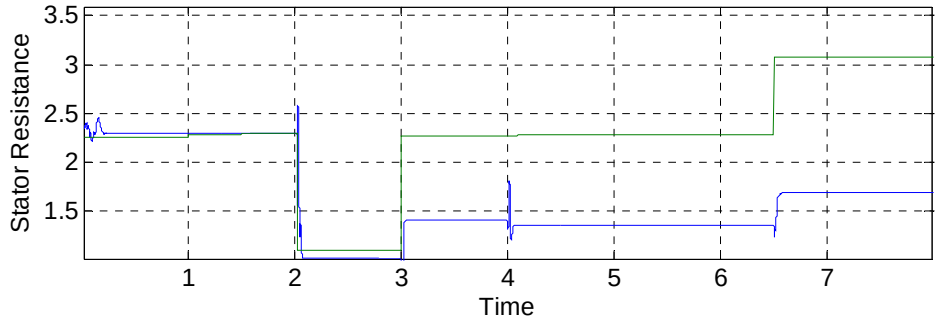

Figure C4.2 Estimated and Model Stator Resistance

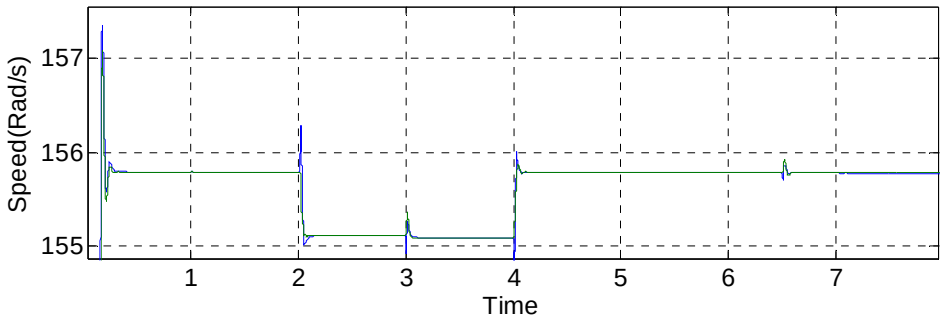

Figure C4.3 Estimated and Model Speed

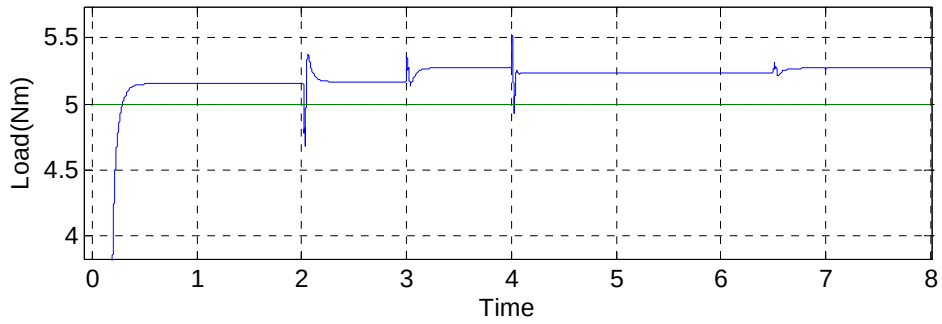

Figure C4.4 Estimated and Applied Load

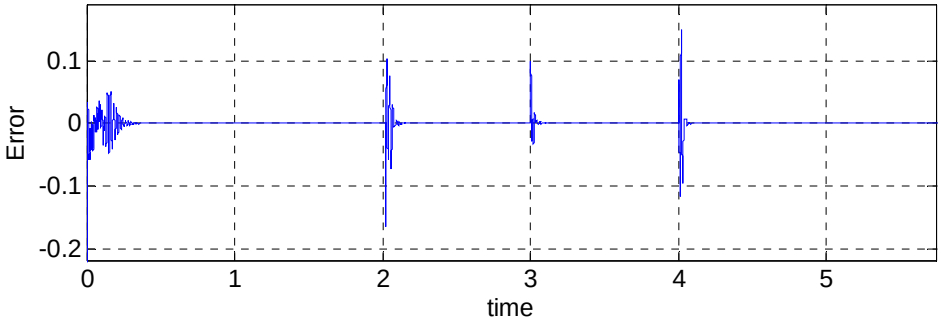

Figure C4.5 Error

APPENDIX C5

EKF with Direct Vector Control

EKF algorithm is applied to the Direct Vector Control Method in 5 seconds.

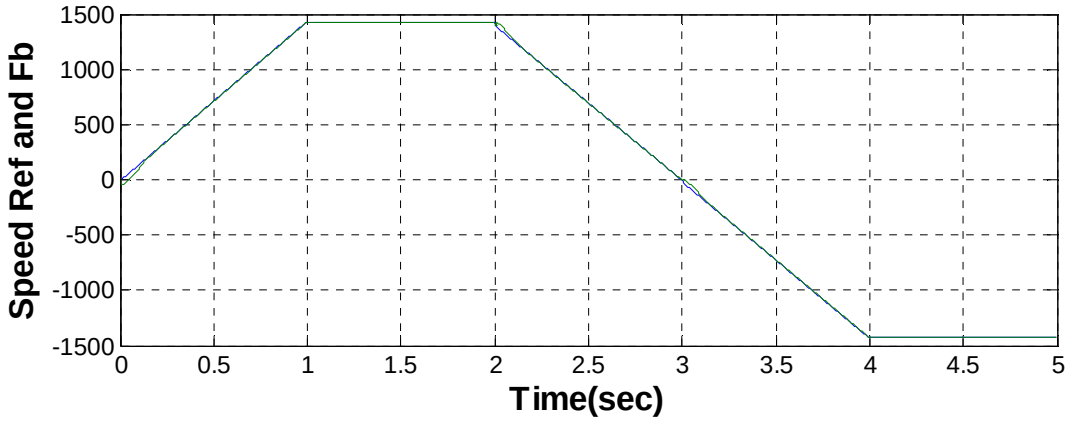

Figure C5.1 Estimated and Measured Speed

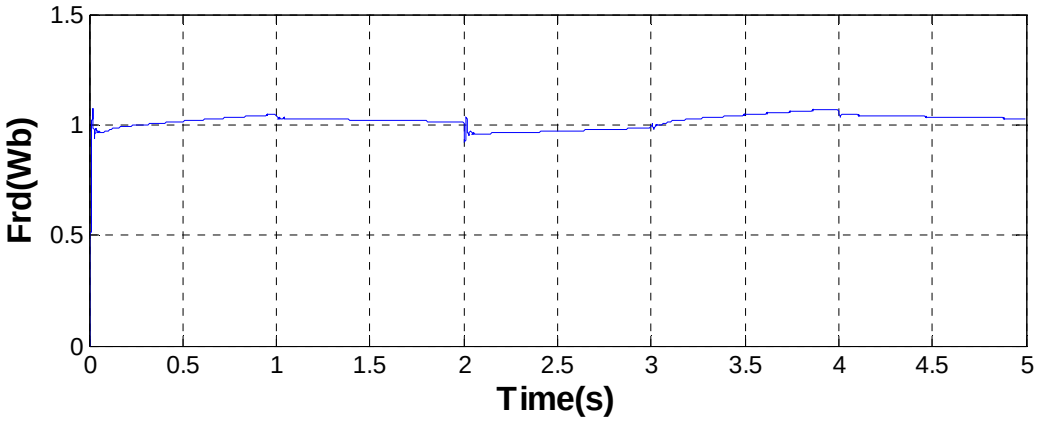

Figure C5.2 Estimated Flux ψ_{rd}

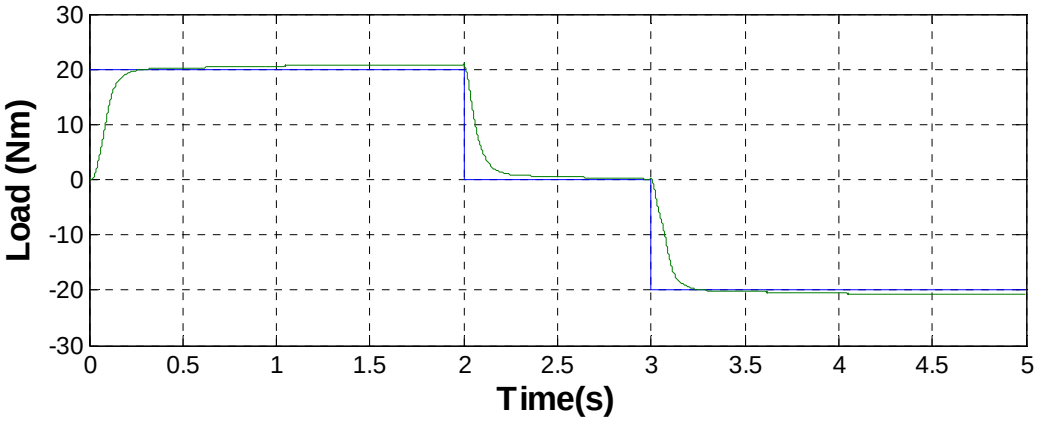

Figure C5.3 Estimated and Applied Load

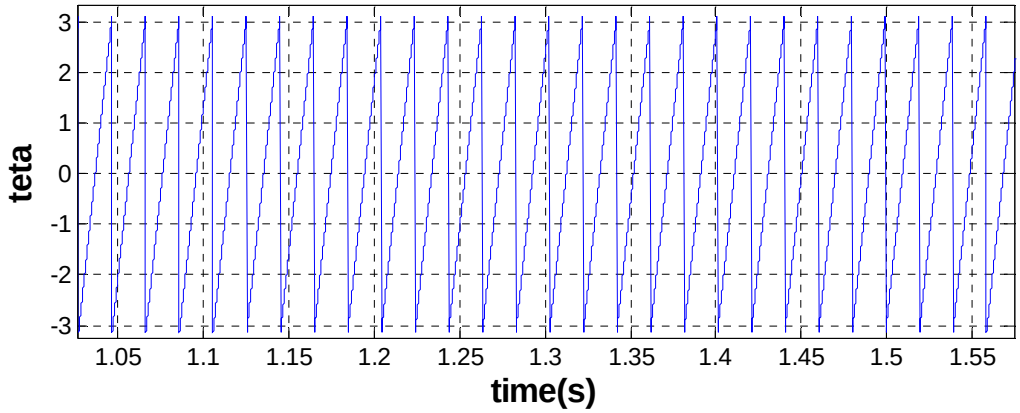

Figure C5.4 Teta

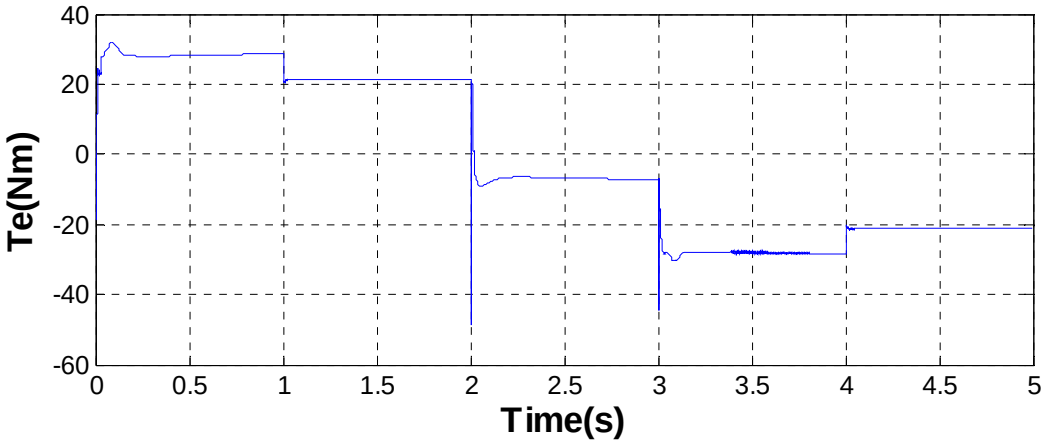

Figure C5.6 Electromagnetic Torque

APPENDIX D

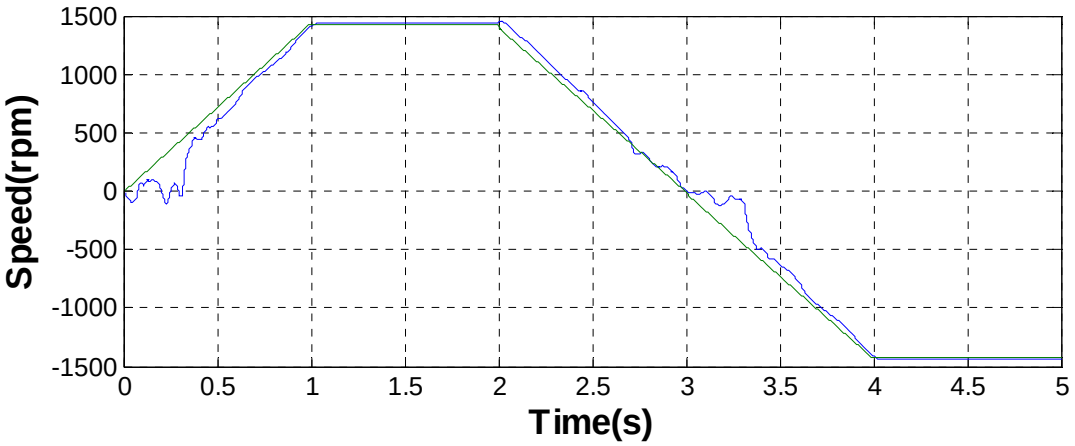

Figure D1 Speed Reference and Speed Feedback

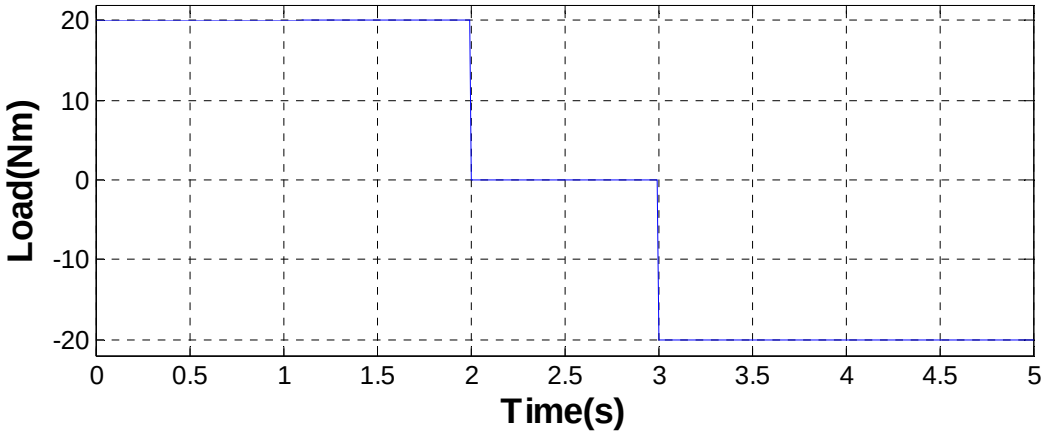

Figure D2 Load Appied

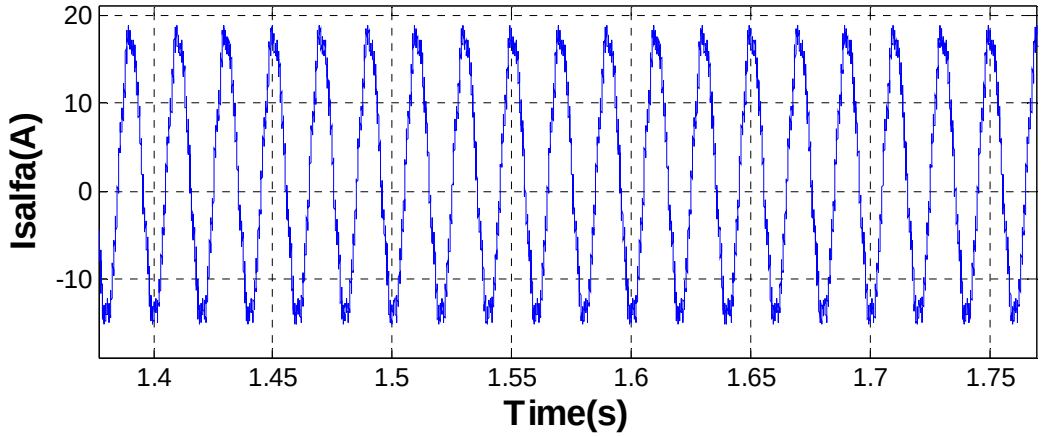

Figure D3 Motor Current at any Steady State

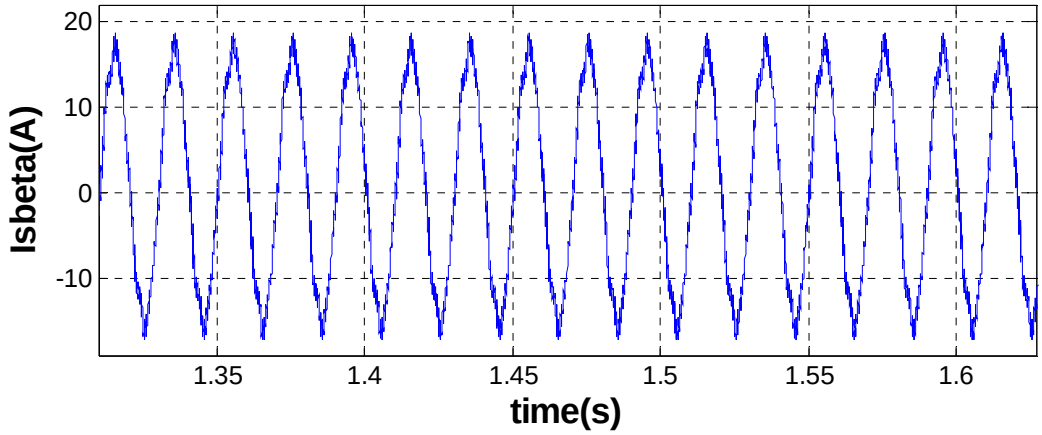

Figure D4 Motor Current at any Steady State

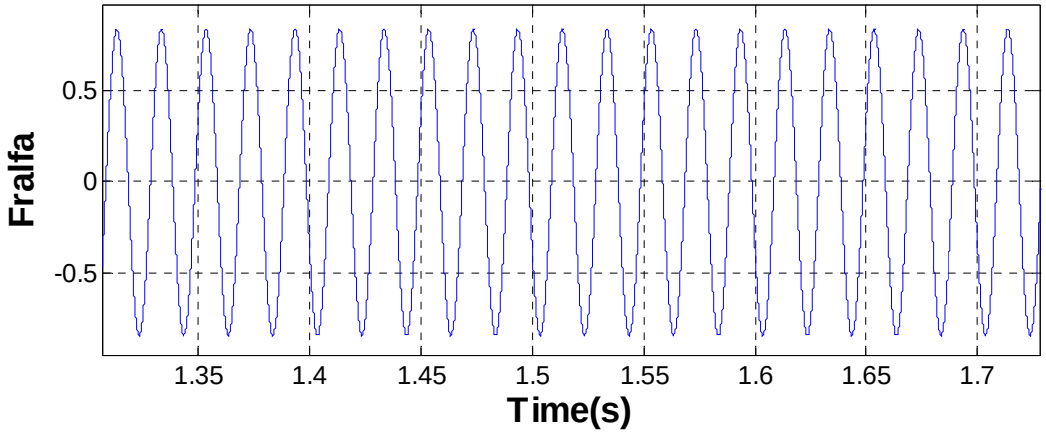

Figure D5 Rotor Flux

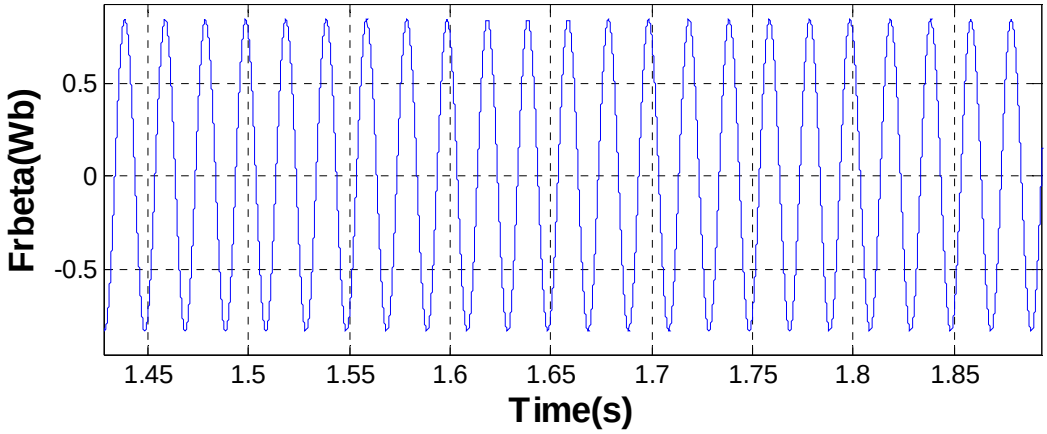

Figure D6 Rotor Flux

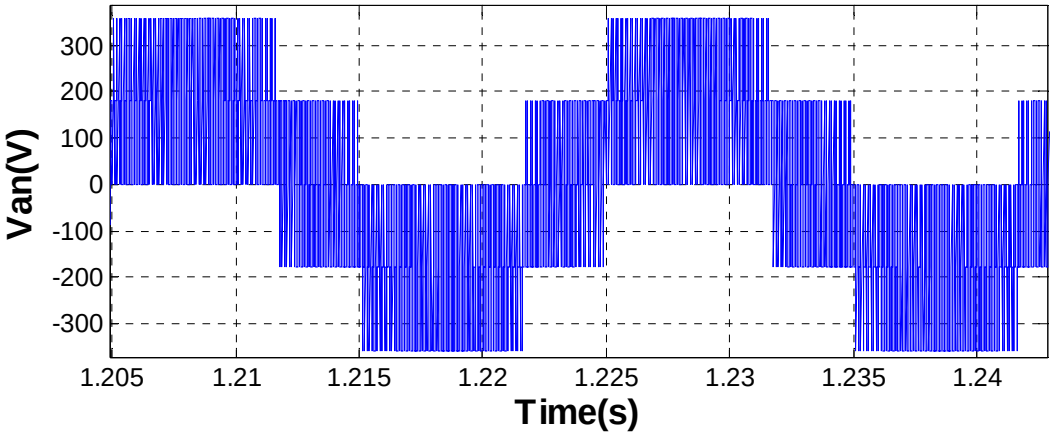

Figure D7 Motor Line to Neutral Voltage

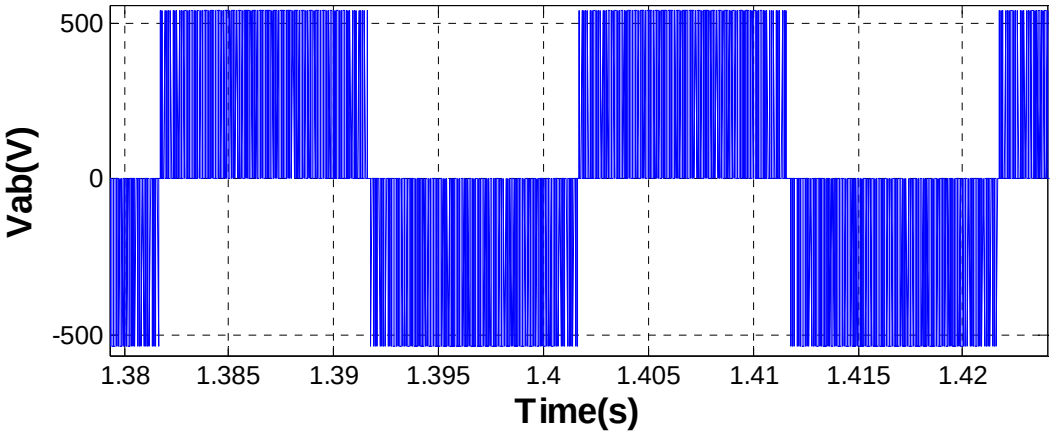

Figure D8 Motor Line to Line Voltage

APPENDIX E

Experimental Results

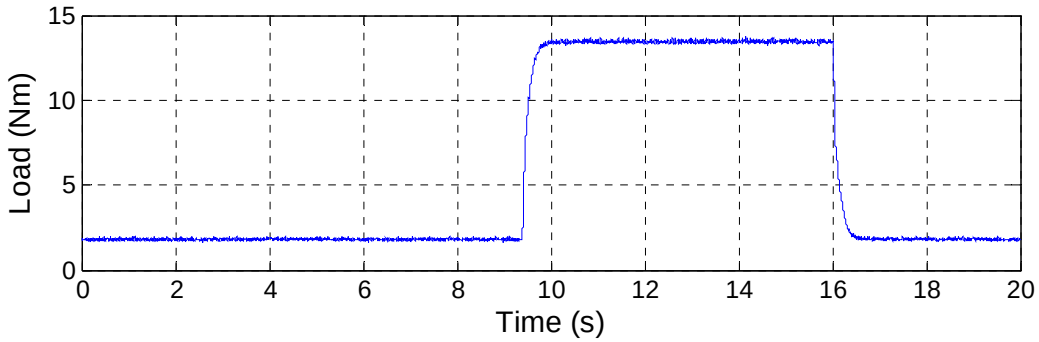

Figure E1 Estimated Load Applied to the motor

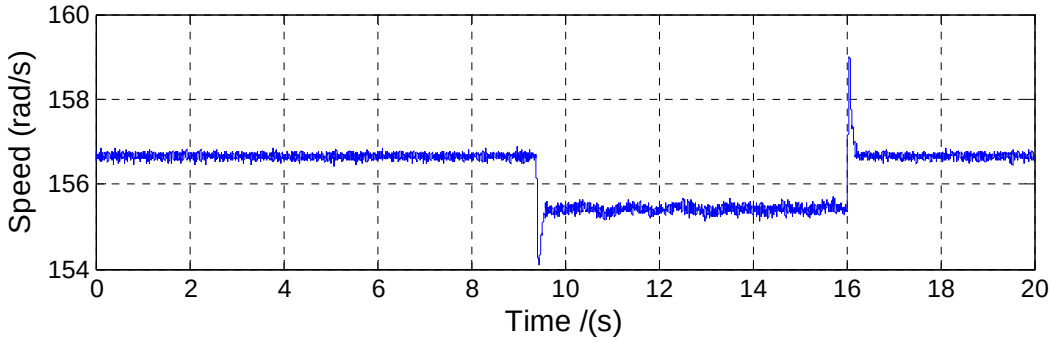

Figure E2 Estimated Speed

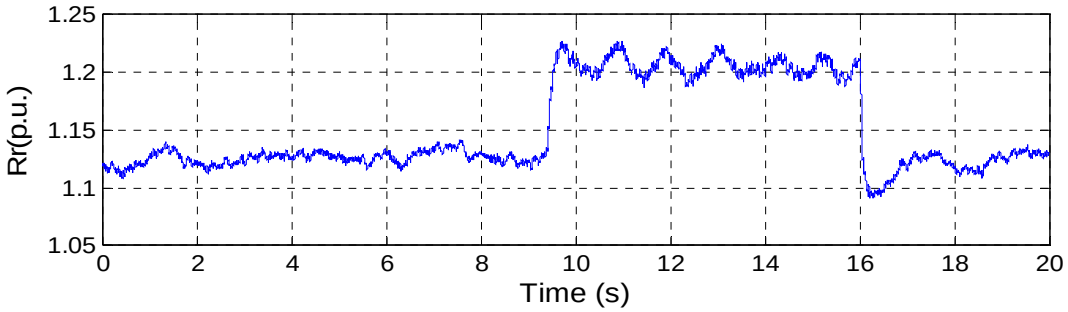

Figure E3 Estimated Rotor Resistance

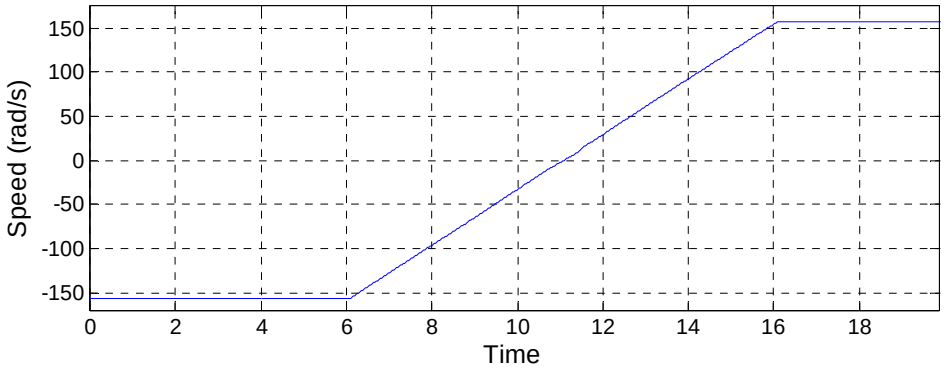

Figure E4 Speed Reversal

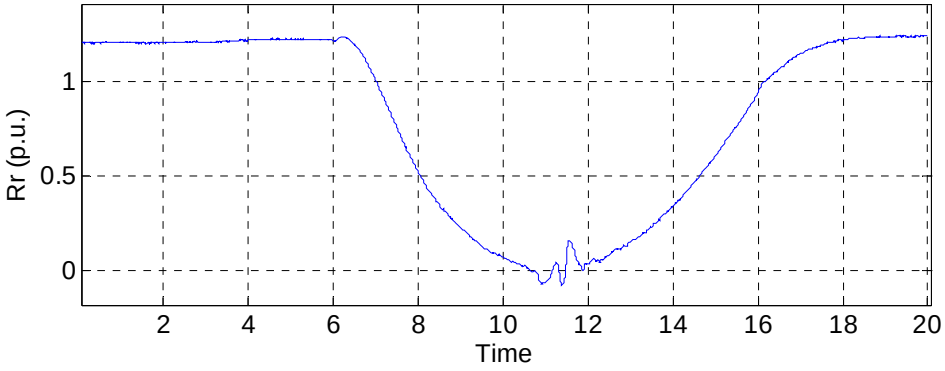

Figure E5 Estimated Rotor Resistance Variations with Speed Reversal

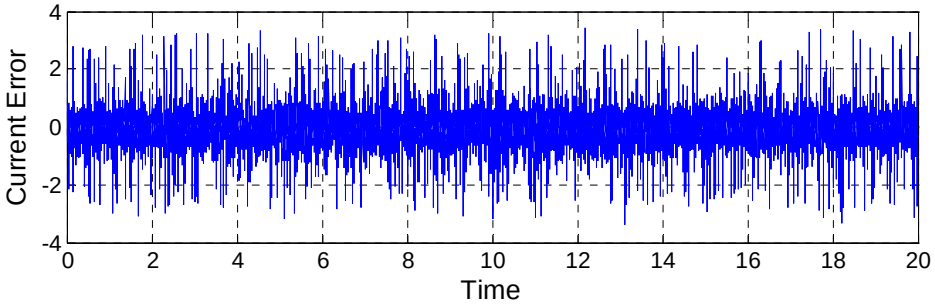

Figure E6 Current Error

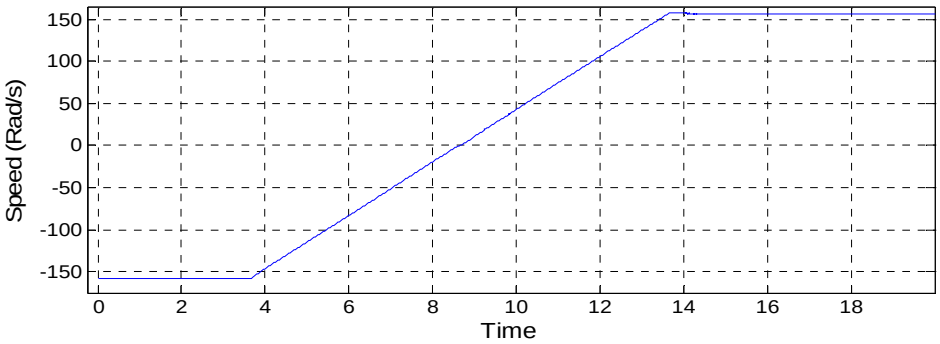

Figure E7 Speed Reversal of 8th Order EKF

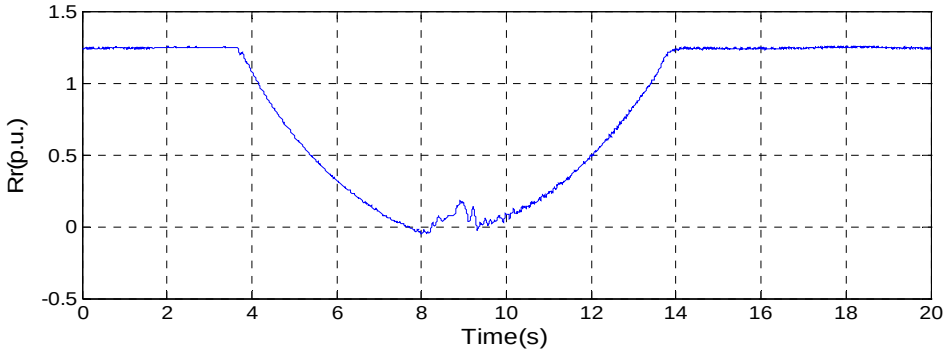

Figure E9 Rotor Resistance Variation of 8th Order EKF

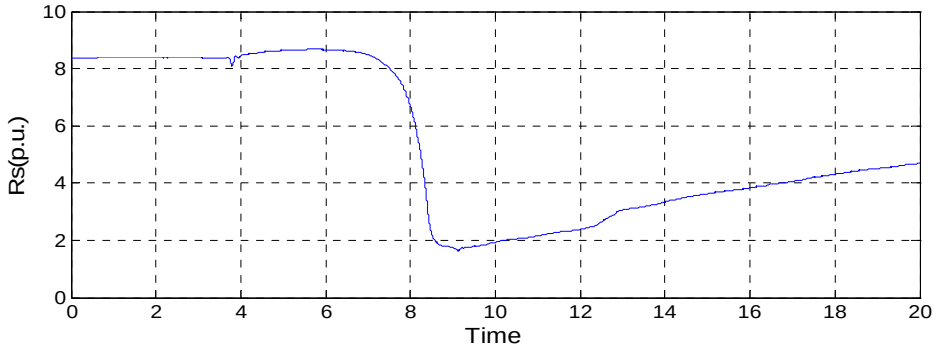

Figure E8 Stator Resistance Variation of 8th Order EKF

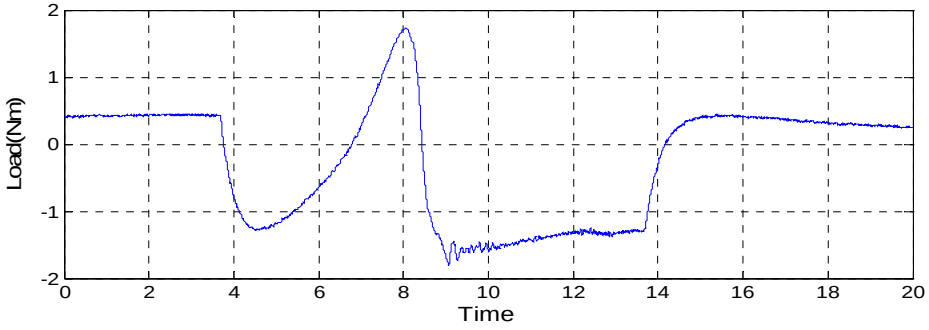

Figure E8 Estimated Load Variation of 8th Order EKF

AUTOBIOGRAPHY

E.Emre ÖZSOY was born in İstanbul in 1980. He graduated from İstanbul Technical University department of Electrical Engineering in 2003. He has been working for Ereğli Iron and Steel Company First Hot Strip Mill as an Electrical Maintanence Engineer since 2003.